PRODUCTION OF GRAPHENE OXIDE AND POLYMER BASED NANOCOMPOSITE MICROSIEVES VIA BREATH FIGURE METHOD

A THESIS SUBMITTED TO
THE GRADUATE SCHOOL OF NATURAL AND APPLIED SCIENCES
OF
MIDDLE EAST TECHNICAL UNIVERSITY

BY

AYŞE ELİF KIRATLI

IN PARTIAL FULFILLMENT OF THE REQUIREMENTS
FOR
THE DEGREE OF MASTER OF SCIENCE
IN
CHEMICAL ENGINEERING

AUGUST 2017

Approval of the thesis:

PRODUCTION OF GRAPHENE OXIDE AND POLYMER BASED NANOCOMPOSITE MICROSIEVES VIA BREATH FIGURE METHOD

submitted by **AYŞE ELİF KIRATLI** in partial fulfillment of the requirements for the degree of **Master of Science in Chemical Engineering Department, Middle East Technical University** by,

Prof. Dr. Gülbin Dural Ünver
Dean, Graduate School of **Natural and Applied Sciences** _____

Prof. Dr. Halil Kalıpçılar
Head of Department, **Chemical Engineering** _____

Asst. Prof. Dr. Erhan Bat
Supervisor, **Chemical Engineering Dept., METU** _____

Assoc. Prof. Dr. P. Zeynep Çulfaz-Emecen
Co-supervisor, **Chemical Engineering Dept., METU** _____

Examining Committee Members:

Prof. Dr. Halil Kalıpçılar _____
Chemical Engineering Dept., METU

Asst. Prof. Dr. Erhan Bat _____
Chemical Engineering Dept., METU

Assoc. Prof. Dr. P. Zeynep Çulfaz-Emecen _____
Chemical Engineering Dept., METU

Prof. Dr. Nihal Aydoğan _____
Chemical Engineering Dept ., Hacettepe University

Assoc. Prof. Dr. İrem Erel Göktepe _____
Chemistry Dept., METU

Date: *18.08.2017*

I hereby declare that all information in this document has been obtained and presented in accordance with academic rules and ethical conduct. I also declare that, as required by these rules and conduct, I have fully cited and referenced all material and results that are not original to this work.

Name, Last name: Ayşe Elif, Kıratlı

Signature:

ABSTRACT

PRODUCTION OF GRAPHENE OXIDE AND POLYMER BASED NANOCOMPOSITE MICROSIEVES VIA BREATH FIGURE METHOD

Kıratlı, Ayşe Elif

M.S., Department of Chemical Engineering

Supervisor: Asst. Prof. Dr. Erhan Bat

Co-Supervisor: Assoc. Prof. Dr. P. Zeynep Çulfaz-Emecen

August 2017, 108 pages

Porous polymer films are used in various different fields such as electronics, sensors, biomedical, catalysis, and separation. Breath figure (BF) is a method of obtaining porous polymers via a self-assembly process based on water condensation. In this process condensed water droplets can be regularly arranged on surface depending on process conditions. They continue to grow or sink until all solvent is evaporated. After complete evaporation, honeycomb shaped porous polymeric films are obtained. Amphiphilic copolymers or end group functionalized polymers are often used for obtaining such structures. It is difficult to form regular honeycomb patterned films via BF method from linear hydrophobic polymers such as polysulfone (PSF). PSF itself is not very effective in stabilizing water droplets during the BF process even though such films could be very useful for membrane based separation applications. In such circumstances, a hydrophilic additive is needed for droplet stabilization. Since

hydrophilic additives reduces the interfacial tension, regular surface morphology can be easily obtained.

In this work, poly(PEGMA) grafted graphene oxide (GO) is proposed as a stabilizer for obtaining porous PSF films via breath figure process. GO sheets were synthesized and then decorated with hydrophilic polymer chains of poly(PEGMA) via atom transfer radical polymerization (ATRP). Obtained product was used as a hydrophilic-hydrophobic additive in order to create PSF based honeycomb structures via BF method. By the optimization of BF experimental parameters, porous PSF films were obtained and their performance for microfiltration applications was assessed. The results showed that poly(PEGMA) grafted GO facilitated regular pore formation during BF process and resulted in highly uniform honeycomb patterned PSF films. Average pore sizes of the obtained porous films could be varied from 2 to 7 microns and the pore depth could be varied 2 to 17 microns depending on process conditions. Filtration performance of the porous films was tested by yeast filtration and percentage rejection was calculated as 88.2 ± 5.7.

Keywords: Graphene oxide, ATRP, breath figure, porous polysulfone films, microfiltration

ÖZ

NEFES FİGÜRÜ YÖNTEMİ İLE GRAFEN OKSİT VE POLİMER BAZLI NANOKOMPOZİT MİKROLEKLERİN ÜRETİMİ

Kıratlı, Ayşe Elif

Yüksek Lisans, Kimya Mühendisliği Bölümü

Tez Yöneticisi: Yrd. Doç. Dr. Erhan Bat

Ortak Tez Yöneticisi: Doç. Dr. P. Zeynep Çulfaz-Emecen

Ağustos 2017, 108 sayfa

Gözenekli polimer filmler elektronik, sensörler, biyomedikal, katalizör ve ayırma teknolojileri gibi çeşitli alanlarda kullanılırlar. Nefes figürü (NF) yöntemi yoğuşan su damlacıklarının kendinden örgütlenme esasına dayanan bir yöntemdir ve gözenekli polimer filmlerin eldesi için kullanılır. Yoğuşan damlacıklar yüzeyde süreç değişkenlerine bağlı olarak düzenli bir biçimde hizalanabilir. Damlacıklar çözücü buharlaşana kadar büyümeye ve polimer yüzeyinde batmaya devam ederler. Çözücünün tamamının buharlaşmasından sonra bal peteği biçiminde dizilmiş gözenekli bir yüzey elde edilir. Amfifilik veya fonksiyonel uçlu polimerler NF yöntemi ile düzenli bir yapı oluşturabilirler. Fakat polisülfon (PSF) gibi doğrusal yapılı hidrofobik polimerler ile NF yönteminde düzenli bir yapı elde etmek zordur. Çünkü PSF yoğuşan su damlacıklarını stabilize edemez. Polisülfon gibi bir

malzemenin gözenekli membran uygulamalarında kullanımı oldukça faydalı olacaktır. Bu yüzden PSF'nin NF yöntemiyle düzenli yapıda gözenekli bir yüzey elde etmek için hidrofilik bir katkıya ihtiyaç duyulmaktadır. Hidrofilik malzemeler yüzey gerilimini düşürdüklerinden dolayı NF yöntemi ile düzenli bir yüzey yapısı kolayca elde edilebilir.

Bu çalışmada grafen oksit (GO) tabakaları sentezlendikten sonra hidrofilik poli(PEGMA) zincirleri Atom Transfer Radikal Polimerizasyon yöntemi ile GO tabakalarının yüzeyine aşılanmıştır. Elde edilen ürün hidrofilik bir katkı olarak nefes figürü yöntemiyle düzenli gözenek dağılımına sahip yüzey eldesi için kullanılmıştır. Gözenekli polimer filmler NF deney süreçlerinin değiştirilmesi ile düşük maliyetli mikroelekler olarak kullanılmıştır. Sonuçlara göre, poli(PEGMA) aşılanmış GO tabaklarının gözenek oluşumunu iyileştirdiği ve sonucunda düzenli yapıda gözenekler elde edilmesinde etkili olduğu görülmüştür. Ortalama gözenek boyutu 2 ile 7 mikron arasında ve gözenek derinliğinin 2 ile 17 mikron arasında değiştiği gözlemlenmiştir. Elde edilen gözenekli polimer filmlerin filtrasyon performansı maya çözeltisi süzülerek test edilmiştir ve yüzde reddetme 88.2 ± 5.7 olarak hesaplanmıştır.

Anahtar kelimeler: Grafen oksit, ATRP, nefes figürü yöntemi, gözenekli polisulfon film, mikrofiltrasyon

To my family…

ACKNOWLEDGMENTS

I would like to express my gratitude to my supervisor, Asst. Prof. Dr. Erhan Bat, for his guidance, encouragement, understanding and continuous support through the learning process of this master thesis. I also present my gratitude to my co-supervisor Assoc. Prof. Dr. Pınar Zeynep Çulfaz-Emecen for her valuable advice and useful comments at all levels of my study.

I would like to give my special thanks to Assoc. Prof. Dr. Bora Maviş for providing access to his laboratory for DLS measurements and his valuable comments on deconvolution of XPS data. I would also like to give my special thanks to Prof. Dr. Pınar Çalık for providing access to her laboratory for UV-Vis spectrophotometry measurements.

I would like to extend my thanks to The Scientific and Technological Research Council of Turkey for providing the funding (project no: 115M635), and to the participants of our research group for their support and friendship. Especially Öznur Doğan who has been shared her precious time and comments on the topic, Zeynep Cansu Özçınar, Gözde Şahin, Cansu Çaylan, Hatice Özyetiş, Cemre Avşar and Seda Sivri. It was great sharing laboratory with all of you during last three years. I would also like to thank Sibel Öztürk, Damla Hüccetoğulları and Yiğit Akgün for their help and friendship.

This thesis would not have been possible without the guidance and the help of several individuals who in one way or another contributed and extended with their valuable assistance. I sincerely thank to METU Chemical Engineering Department staff espicially, Mihrican Açıkgöz and İsa Çağlar for their help and METU Central Laboratory staff especially, Salih Kaan Kirdeciler who has helped in SEM analyses.

I also want to express my gratitude to firstly Assoc. Prof. Dr. Ahmet Yozgatlıgil and all my workmates Sara Banu Akkaş, Ceren Aksoy Güleç, Asuman Özgür Keysan, Sina Shafee, Celal Oğuz Özdemir, Armağan Önder Hergüner and Cihan Tuğrul Çiçek from Office of Sponsored Projects for their understanding, kindness and friendly manner.

I would like to thank my beloved friends, Hilal Anıldı who has been there for me all the time when I needed. Melek Bilgen Özben and Burcu Bozdoğan, they have supported me throughout this master study with their moral speeches and laughter. I will be grateful forever for your love.

I would like to express my special gratitude to Oktay Tüfekçi for encouraging me and cheering me up when I feel down.

Last but not the least, I would like to thank my lovely family my mother, Çiğdem, my father, Mehmet Sadık, and my brother, Ahmet Emre who have provided all kinds of support in my life and understanding throughout my entire study. I am very grateful to have you.

TABLE OF CONTENTS

LIST OF FIGURES

FIGURES

LIST OF TABLES

TABLES

CHAPTER 1

INTRODUCTION

Carbon and carbon-based materials play a very important role in our lives. Depending on the bond structure carbon based materials can have various forms. Development in nano-science and technology involves the preparation of different shapes and sizes nanoparticles and introducing them into polymer host. [1]. Classification of carbon derivatives with respect to their structure can be seen in Figure 1.1.

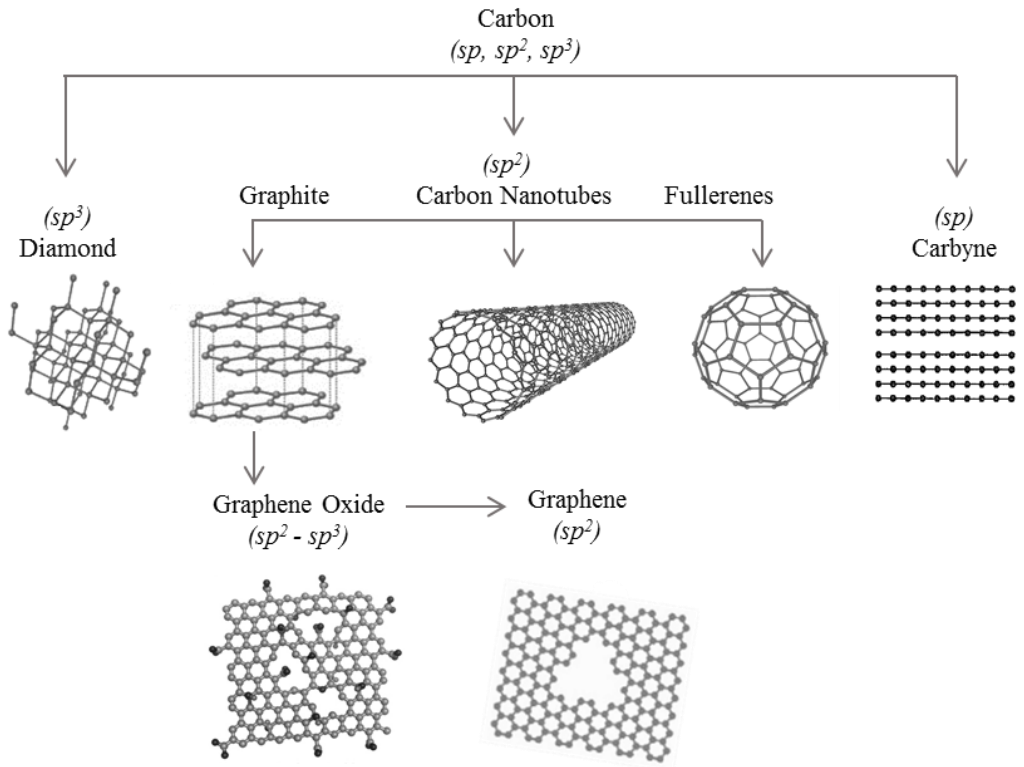

Figure 1.1 Carbon derivatives.

The very first known carbon materials are graphite and diamonds which are naturally occurring minerals. The discovery of structural and physical properties that graphite and diamond have dates back to 19th century, since then, carbon derivatives have been studied and developed. The following discovery of fullerenes (1985), carbon nanotubes (1991), graphene (1987) and its isolation as monolayer (2004), led to promoting applications in various fields of advanced science and technology [2].

Very recently, a great attention has been paid to graphene and its derivatives since the study of Andre Geim and Konstantin Novoselov ‘‘for groundbreaking experiments regarding the two-dimensional material graphene’’ was awarded with Nobel Prize in 2010 [3]. They achieved to isolate one single layer of graphene by micromechanical cleavage for the very first time and demonstrated its outstanding electrical, mechanical, physical and chemical properties. However graphene suffers from being insoluble in aqueous and organic media which inhibit the process-ability. In contrast, graphene oxide (GO) which is obtained by oxidation of natural graphite has the ability of forming good dispersion in aqueous media. The dispersion behavior of GO makes it easily processable: GO can be converted to graphene by reducing the oxygen containing groups or chemically modified for tuning its chemistry. Based on these reasons, a rise in studies on GO has occurred.

Figure 1.2 represents schematically the current growth of publications about GO as a subject and it was plotted by using Web of Science tool. Since 2010 total published articles have reached up to 35,279. And almost half of it was published in 2015 and 2016. In advanced science and technology, GO has found applications in electronic devices [4]–[7], energy storage devices [8]–[11], biosensors and biomedical applications [12] and water purification membranes [13]–[16].

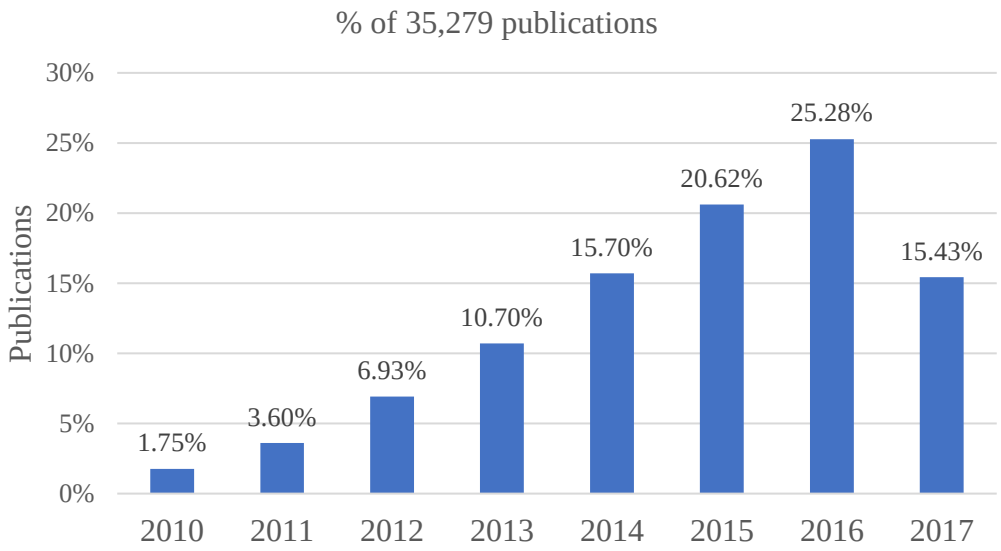

Figure 1.2 Distribution of published studies on graphene oxide into years.

Water purification is an important problem. Because we are living in a populating world and water resources are polluted due to industrialization. At this point, water purification and recycled usage of water became important. Membrane technology is the key for separation of contaminants from polluted water with low energy consumption. Microfiltration, ultrafiltration and reverse osmosis membranes are extensively studied for this purpose and commercial markets have been spreading very rapidly throughout the world. By the help of developing science and technology, improvements and innovations in membrane technology have been ensued especially in morphological design of membranes, chemical tuning of the materials, fabrication methods and module design.

One of the most important problems in membrane technology is membrane fouling. In order to overcome this problem, some surface modification techniques or incorporation of hydrophilic additives are available. GO has hydrophilic oxygen containing functional groups which are bonded to hydrophobic hexagonally close packed carbon basal plane. In virtue of this structural property, GO holds the potential to be used in membrane production for water purification and filtration [16]. GO based

nanocomposite membranes show considerable improved performances in both fouling resistance and mechanical strength [17]–[21].

Another problem within the membrane technology is trade-off limit between high permeability, low selectivity materials and low permeability, high selectivity materials [22]. Due to characteristics of polymeric materials this trade-off limit can be reduced. Polysulfone (PSF) has been widely used as a polymeric membrane material because of outstanding mechanical, thermal and chemical stability [20], [23]. However, as observed for most polymers used for membrane preparation, it suffers from fouling problem due to its hydrophobic nature. Fouling reduces flux through the membrane and increases operation costs by requiring cleaning procedure [19]. In recent years, carbon nanomaterials have been used as a nanoparticle to improve separation performance, mechanical strength, and thermal stability of polymeric membranes. However high cost production of carbon nanotubes with difficulties in scale-up process have decreased their popularity as nanoparticles for membrane production [24], [25].

The good dispersion behavior of GO in water and some polar organic media provides good interface adhesion with the polymer matrix which promotes the preparation of GO based nanocomposites with higher performance. In addition to that, chemical functionalization of GO enables tuning in chemical and physical properties for improved solubility in organic media and compatibility with polymer matrix. GO based PSF membranes showed improved surface hydrophilicity and consequently fouling problem was reduced [17]–[21].

The present study aims at fabrication of GO based nanocomposite microsieves that may be suitable for water purification via breath figure method. Microsieves are special kinds of membranes which have well-defined through pores of 0.1-10 μm and the pores are uniformly cover the surface [22]. The production of microsieves usually involves expensive and complex micro-machinery of lithographic and templating techniques. They need specially designed templates with fixed size and detaching the

membrane from template involves another tedious step. Recently, a self-assembly method called as breath figure (BF) technique has been used for fabrication of microsieves. Compared to other lithographic techniques, BF has following advantages:

- Simple equipment, cost-effective and fast process.
- Condensed water droplets are used for sacrificial template with no fixed pore size. Evaporation of water droplets eliminates the additional detaching step.
- It is versatile: various polymers can be processed into different surface morphologies.

Self-assembly process is the spontaneous arrangement of components into regular and stable structures without any external direction. Building blocks are generally used in self-assembly system to facilitate the process. They are specially designed nanoparticles having different chemistry and shapes. GO sheets were designed to be used as building blocks in BF process. For this purpose, the lateral size of obtained GO sheets were reduced to nano scale. Afterwards, GO was decorated with hydrophilic poly(PEGMA) chains via atom transfer radical polymerization (ATRP). In addition to that, owing to poly(PEGMA) chains GO became soluble in commonly used BF solvents such as chloroform, dichloromethane and toluene.

In brief, the present work involves the preparation of PSF and GO based microsieves via BF method. GO has two main objectives in the present work: being in charge of pore formation during BF process and enhancing surface hydrophilicity for the final PSF nanocomposite microsieve. To achieve this, GO was first modified with poly(PEGMA) chains. It is hypothesized that this polymer modified GO would facilitate the formation of ordered honeycomb patterned polymers and the preferential assembly of poly(PEGMA) chains at the pore surface would increase the hydrophilicity of the membranes. In addition, this modification renders GO dispersible in solvents commonly used in BF method (i.e. chloroform, dichloromethane, and dichloroethane).

CHAPTER 2

BACKGROUND INFORMATION AND LITERATURE SURVEY

2.1. Graphene Oxide

Graphene oxide (GO) is the oxidized form of graphene layers and produced by oxidation of graphite. Oxygen containing groups are covalently attached to hexagonal carbon domain. GO has become a hot topic for scientist and engineers for following reasons [2]:

- Ease in processability enables possible numerous modifications.
- Chemical/physical properties of GO can be tunable by virtue of these modifications.
- The reduction of GO to reduced graphene-like material is an economically viable route toward bulk synthesis of graphene.
- Chemically modified or reduced GO have been used in many applications such as biomedicine, electronic devices, energy storage, polymer composites, paper-like materials, optoelectronics, sensors and environmental.

However, the history of GO can be traced back in 1859 long before being a precursor for graphene production when Brodie oxidized graphite for the very first time. Graphite was reacted with potassium chlorate and fuming nitric acid. It was observed that final weight of graphite was increasing and its appearance changed to light yellow after several repeated purification and oxidizing steps. Brodie also mentioned that yellowish gas released during the oxidation which was toxic gas releasing of NOx. Also formation of explosive chlorine dioxide compound makes the process hazardous [26]. The obtained graphene oxide C/O atomic ratio was reported as 2.19 [27].

After nearly 40 years, Staudenmaier improved Brodie's work by adding concentrated sulfuric acid to oxidizing media and adding potassium chlorate in multiple aliquots. Hence, acidity of the medium was increased and stepwise addition of potassium chlorate favored the oxidation reaction. He achieved graphite oxidation in a single step with a higher yield of C/O atomic ratio, it was nearly 2 [28]. In spite of these improvements, Staudenmaier method was still both time consuming and dangerous: the addition of potassium chlorate lasted over a week and formation of explosive chlorine dioxide and NOx release was still an issue.

Nearly 60 years later Hummers and Offeman modified the graphene oxide synthesis by replacing the oxidizing agent with potassium permanganate and reaction media with water-free solution of sodium nitrate and concentrated sulfuric acid. Reaction was continued for only 2 hours at 45 °C. At the end of 2 hours, oxidation was completed and the resulting product had a higher oxidation degree with a C/O atomic ratio of 2.1-2.9 [29].These adjustments made the process more rapid and relatively safe (eliminating chlorine dioxide formation by replacing $KClO_3$ to $KMnO_4$). However, release of toxic NOx gases was not solved. After these modifications, Hummers method became the most widely applied method for graphene oxide synthesis. In the following years, different versions of Hummers method were developed such as using different ratio of graphite to oxidizing agent ratio or using pre-treated graphite source, changing oxidation conditions and time. Recently in 2010, Marcano *et al.* improved the Hummer's method (Tour method) by using concentrated sulfuric acid and phosphoric acid mixture as oxidizing media. Therefore they eliminated the release of toxic NOx and they claimed H_3PO_4 increased the oxidation degree of the obtained product [30].

Very recently, Peng *et al*. proposed a method which involves of using potassium ferrate as an oxidizing agent and concentrated perchloric acid as a reaction medium. They reported oxidation time became shorter with a higher yield in an eco-friendly way however using ferrates make the process relatively expensive [31]. Today

graphene oxide synthesis is a very popular subject in order to obtain the product with high oxidation degree and minimum defects in a simple and harmless way.

Apparently, synthesis routes for GO are developing day-by-day. However, the detailed understanding of its oxidation and formation mechanisms are still burdensome. Graphene oxide is a large molecule with a complex structure. Its structure depends on many parameters such as oxidation time, temperature, graphite to/oxidizing agent ratio, the source of the used graphite etc. Consequently, it results nonstoichiometric atomic composition for GO and sample-to-sample variability [26]. In the literature, there are some theoretical studies [32], [33] attempting to explain graphene oxide formation mechanism. However, these simulations and methodologies are yet to be verified with experimental data.

Today, with the help of developing technology and characterization techniques, the knowledge regarding GO structure and its formation mechanism is building-up. Accordingly, the number of unanswered questions is being fall out and the big picture is shaping-up. Recently, Dimiev *et. al.* [34] conducted a study which brings a clear vision into oxidation mechanism. When conducted the modified Hummer's method, different aliquots were taken after addition of every certain amount of $KMnO_4$. Oxygen content of taken samples was analyzed by Raman spectroscopy and XRD. They proposed three independent steps regarding to oxidation and they highlighted some important points which are discussed below and Figure 2.1.1 illustrates the all formation mechanism of graphene oxide:

1. Formation of Sulfuric acid-graphite intercalation compound (H_2SO_4-GIC)
2. Formation of pristine graphite oxide (PGO)
3. Formation of graphene oxide (GO)

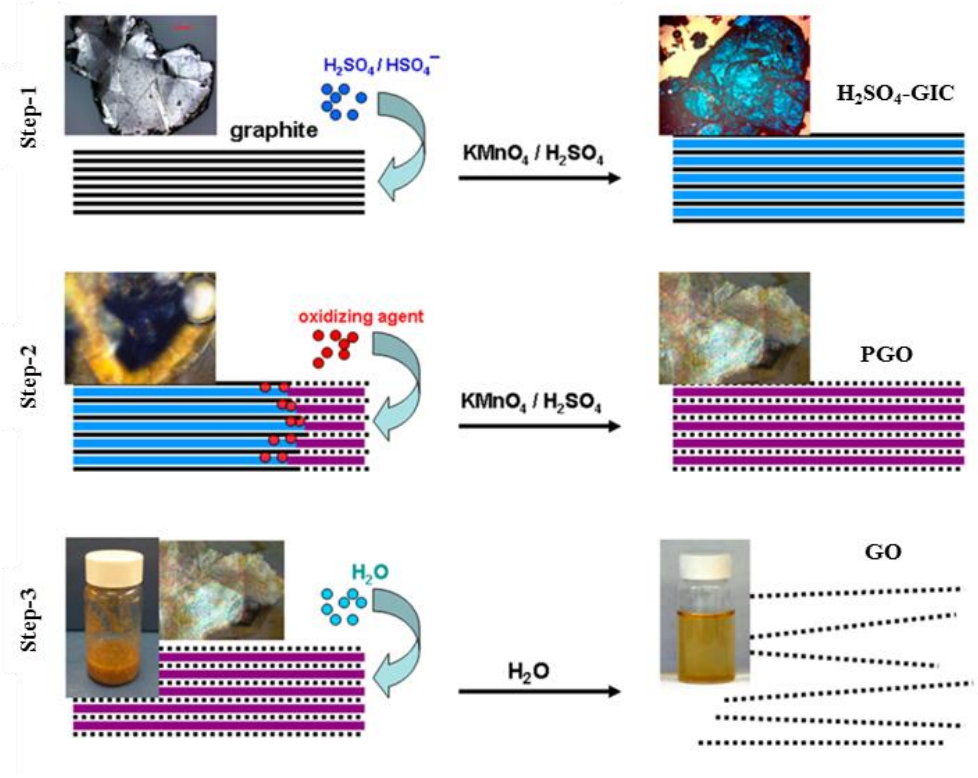

Figure 2.1.1. Micrographic images with schematic representation of three main steps of oxidation mechanism. Sulfur containing intercalate groups were represented with blue lines while purple lines represented oxygen containing groups. Exfoliated single layers of graphene oxide represented with dashed black lines [34].

Firstly, H_2SO_4-GIC intermediate was formed within 5 minutes by attacking H_2SO_4/ HSO_4^- intercalate into C atoms, and this completed step-1. Then the intermediate was transformed to PGO in step-2. This step can take several hours or days. Oxidizing agent attacks to nearest acid intercalate and replaces with it which is a diffusion-controlled mechanism for the formation of C-O/C=O bonds. The rate of formation oxygen containing groups depend on size and morphology of graphite flakes. Smaller graphite flakes were oxidized faster. And similarly, crystalline or thermally expanded graphite flakes were oxidized faster. Higher oxidation yield was achieved in the situation in which after the addition of sufficient amount of $KMnO_4$. Finally PGO was dissolved in water and exfoliated in step-3 and resulting individual GO sheets [34].

The first structural model for GO was proposed by Hofmann in 1939. It involved the idea that GO consisted of only epoxide groups that were spreading across graphitic basal plane. Later in 1946, Ruess introduced the hydroxyl groups onto basal plane and proposed that the basal plane was in the corrugated form and sp^2 hybridization. And more importantly, existence of C-H bond was stated for the first time [26], [35]. After nearly 10 years, C=C bonds, ketone, carboxylic groups and enolic groups were added to GO structure by Clauss and Boehm [36]. In the following years different structures were proposed. In these studies, functional groups were identified by using basic characterization techniques such as elemental analysis, kinetic observations, XRD data, etc. They are not fully qualified for structural analysis of GO, since it has complex, nonstoichiometric and alternative structure of being sample-to-sample variability [26].

One of the most widely cited models of GO was proposed by Anton Lerf and Jacek Klinowski in 1996. They used Solid-State Nuclear Magnetic Resonance for the first time in characterizing structure of GO. According to Lerf-Klinowski model, GO has epoxide, hydroxyl, orgonasulfate carbonyl, carboxyl and ester moieties [37]. The validity of structural geometry of Lerf-Klinowski model was supported by an experimental simulation which was conducted in 2010 [38] and this makes other proposed structures inconsequential. Discussed geometries are illustrated in Figure 2.1.2.

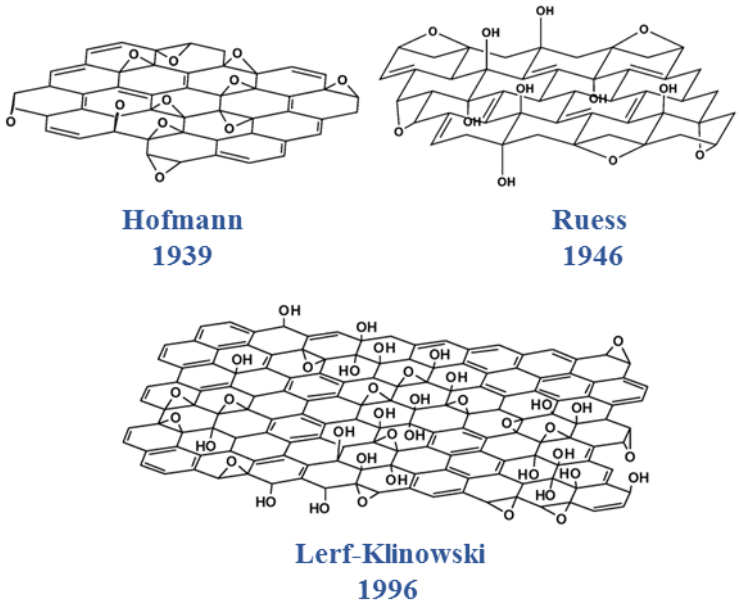

Figure 2.1.2. Proposed structure models for GO [9], [10].

In general, GO has three essential functional groups according to scientific community in which we also are interested;

-COOH carboxylic acid,

-OH hydroxyl,

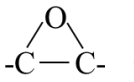 epoxide.

Carboxylic acid moieties are bonded to edge-side carbon atoms while other groups are bonded onto to basal plane. The most abundant groups are hydroxyl and epoxide groups [36]. A representative structure of a single sheet of GO is given in Figure 2.1.3. Having a structure like that provide some exclusive properties to GO.

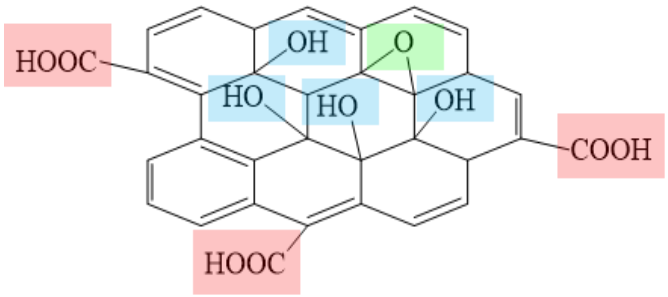

Figure 2.1.3. Representative structure of GO with carboxylic acid, hydroxyl and epoxide moieties.

2.1.1. Properties of Graphene Oxide

Physical features: The appearance of GO looks brownish paper-like sheets. GO is a 2-dimensional soft material which consist of hexagonal carbon basal plane and oxygen containing groups attached onto it. The distance between the GO layers is interchangeable due the media be held in (ambient (dry), water, DMF, etc.). GO layers are one atomic thickness and their lateral size can alter from nano to micro scale. It is possible to change lateral size into nanometer scale by using ultrasonication [39] and freeze-thaw cycles [40].

Chemical reactivity: GO consists of variable ratio of sp^2/sp^3 hybridization network with reactive oxygen functionalities. Controllable functionalization or removal of these oxygen containing groups enables scientist for tailoring numerous possibilities of the chemical structure and properties. Later, GO modification is further explained under following title.

Thermal properties: GO is thermally unstable which provides a route for reduction and resulting graphene production. It loses functional groups up to 600 °C.

Electrical properties: Unlike graphene, the existence of C–O bonds restrains sp^2 hybridization of carbon atoms which resulting GO becomes an insulator [41].

Optical properties: GO shows electron transitions of π-π* (200-400 nm) and n-π* (400-700 nm) in absorbance spectra. π-π* electron transition is seen from existence of

aromatic C=C bonds and n-π* electron transition is seen from existence of C=O bonds [41], [42]. Also GO has photoluminescence property in the visible and near-infrared region [43], [44].

Mechanical properties: mechanical properties of GO depend mainly on intensity of oxygen functionalities and their arrangement in a way of ordered or disordered (amorphous). The changing ratio of functional groups do not have major effect on the mechanical properties [45]. This statement was illustrated in Figure 2.1.4 where R was defined as intensity of functional groups and calculated according to formula: number of sp^3 C (bonded with –O– or –OH)/total number of C atoms x 100%.

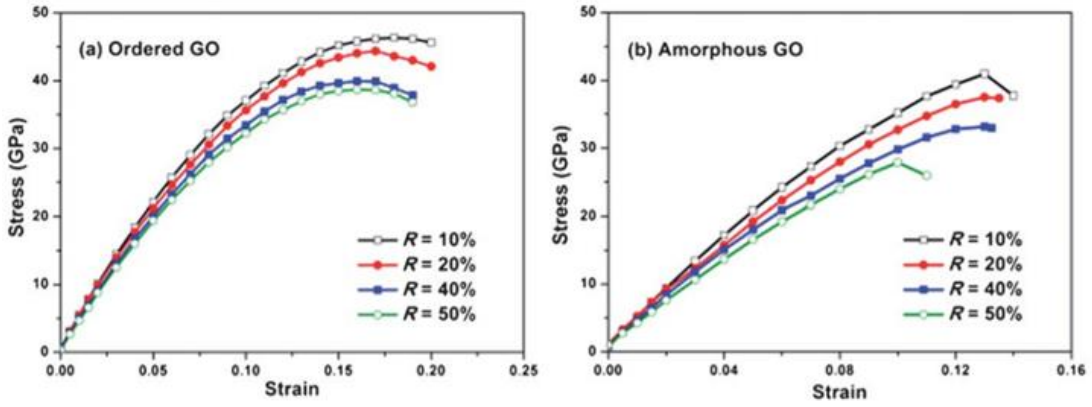

Figure 2.1.4. Strain-stress curves for ordered and disordered GO structures [45].

Dispersability: Unlike graphite and graphene, GO is dispersible in some media such water, DMF, ethylene glycol and THF [46] which provides ease in process-ability.

Amphiphilicity: GO has amphiphilic character which can be self-assembly at interfaces followed by non-covalent inter sheet interactions (van der Waal forces, H-bonding) to form macrostructures [47]. Surfactant or surface-active agent is a material which causes to decrease in interfacial tension between liquid-liquid or liquid-solid mixture systems. Characteristic structure of surfactants is having both a hydrophilic

and a hydrophobic part. Hexagonal packed carbon basal plane is hydrophobic and hydroxyl and carboxylic acid moieties are hydrophilic parts of GO having.

Owing to above mentioned features of GO/modified-GO/reduced-GO have found to be used in many applications in advanced science and technology. Reduced GO can be used in electronic devices since it gained electrical conductivity by removal of oxygen containing groups. Field-effect transistors, optoelectronic devices, transparent conducting film, touch screens, flexible electronic devices, solar cells, and sensors can be exemplified for this area [2]. Chemically modified-GO can be introduced as a nano-additives into polymer matrixes in fabrication of composite materials.

2.2. Modification of Graphene Oxide with Polymer Chains

GO can be modified by means of covalent bonding and non-covalent interactions. The present study covers only modifications that are based on covalent bonding of polymer chains. In recent years, polymer modified GO nanomaterials have been extensively studied for the development of novel, multifunctional nanocomposites. Polymer modified GO sheets show better dispersion behavior in organic media and become more compatible with various polymeric matrices. This polymer modified GO sheets are used as nano-additives to improve engineering properties of polymeric composites. Significant improvements in mechanical, electronic, optical and thermal properties can be achieved by introducing only a small amount of polymer modified-GO loading [48].

Polymer modifications of GO can be conducted in two different methods [49], [50]:

- **Grafting to:** End-functionalized polymer chains are grafted **to** the reactive surface.
- **Grafting from:** Polymer chains are growing **from** the reactive surface.

Figure 2.2.1 illustrates grafting to and grafting from methods. Briefly, in grafting to method pre-synthesized polymer chains with reactive end-groups are attached to

reactive surface. Surface can be activated by plasma treatment, UV- or γ-irradiation, and chemical oxidation [49]. Only a definite portion of pre- polymers can be attached onto substrate due to increasing steric hindrance with the increasing number of grafted polymers [48], [49]. Grafting to method is applicable to a limited range of substrate types and requires pre-synthesized polymer chains with functional end groups.

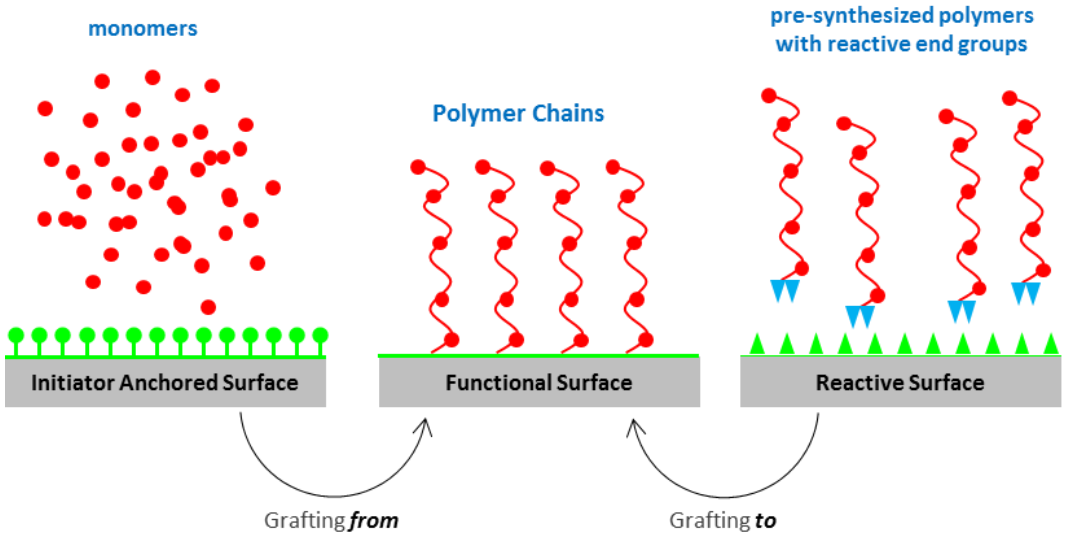

Figure 2.2.1 Schematic illustration of surface functionalization with grafting from and grafting to methods [51].

On the other hand, grafting from method utilizes the polymerization which is initiated from surface -therefore, it is also known as surface-initiated polymerization [49]. Initiation groups are anchored onto surface by the help of chemical reaction. Then polymerization starts with adding monomers to media in the presence of proper catalyst. Active polymer chains continue to grow until all monomers are consumed. Consequently, high molecular weight of grafted polymers on surface can be achieved. Grafting from method has advantageous over grafting to method in terms of high grafting density and being applicable to wide range of substrate and monomers [24], [25]. Grafting from method has been widely used for GO functionalization [48]. The

most followed approach for grafting from is atom transfer radical polymerization (ATRP) in the literature [52].

GO has already a reactive surface covered with hydroxyl, epoxide and carboxylic acid groups. Polymer modification of GO is carried out in two main chemical steps. Firstly, initiation groups are anchored to surface. Afterwards ATRP is performed for growing polymer chains from GO surface.

2.2.1. Attachment of ATRP Initiator on Graphene Oxide

Hydroxyl, carboxylic acid or epoxide groups can be treated with different ATRP initiators to obtain initiator modified-GO (macro initiator) such as GO-Br, GO-Cl, GO-bromoisobutyrate, and GO-bromomethylpropionate for the polymerization of different monomers [52].

Hydroxyl groups on GO can be converted directly initiation groups without any pre-treatment by the reaction with alpha-bromoisobutyryl bromide. Afterwards, polymer chains can be grafted from initiator functionalized GO. The approach was reported by Lee *et al.* [53] in 2010. After immobilization of alpha-bromoisobutyryl bromide to –OH groups following polymerization of styrene, methyl methacrylate, or butyl acrylate were performed. They observed that solubility properties of the resulting materials significantly improved when compared to pristine GO. Mrlík *et al.* performed similar one-step modification of GO with alpha-bromoisobutyryl bromide followed by ATRP of glycidyl methacrylate. Their resulting p(GMA) grafted GO nanocomposite showed tuned electro-responsive properties that can be effectively applied for electrorheological suspensions [54]. Rajender *et al.* and Kumar *et al.* used ATRP to obtain initiator functionalized GO [55], [56].

Carboxylic acid groups can be modified by initiation groups. However they must be converted to amine groups ($-NH_2$). Yang *et al.* converted –COOH groups to $-NH_2$ groups by reacting with diaminopropane in the presence of EDC/NHS. Then –OH and $-NH_2$ groups were treated with ATRP initiator of alpha-bromoisobutyryl bromide.

Finally DMAEMA monomers were polymerized from the surface to obtain GO-p(DMAEMA) with improved dispersity in solvents [57]. Kavitha *et al.* used same modification methodology and grafted poly(acrylic acid) to GO surface. Resulting GO/PAA has found to be a promising application as protein carrier with a feature of being biocompatible and hosted protein drugs [58]. Goncalves *et al.* prepared PMMA grafted GO surface via similar method. The –COOH groups of the GO were first converted to acyl chloride groups by reacting thionyl chloride, then it was treated with ethylene glycol to obtain –OH rich GO. Later, GO was introduced by attachment of ATRP initiator moieties in order to be grafted from PMMA brushes [59].

Initiation groups can be attached by reacting with epoxide groups of GO. In order to accomplish a reaction between epoxide group and initiator, initiator should contain amine groups. Qi *et al.* used an modified ATRP initiator N-(2-aminoethyl)-2-bromo-2-methylpropanamide, and the primary amine groups of the initiator reacted with epoxide groups of GO by means of nucleophilic ring opening reaction to obtain initiator functionalized GO. Resulted final product of PMMA grafted GO nanocomposite was used as corrosion protective coating [60]. Another epoxide group functionalization with ATRP initiator was conducted by Roghani-Mamaqani *et al.* They firstly modified alpha-bromoisobutyryl bromide treating with ethylenediamine to become suitable for reacting epoxide groups. Resulting initiator functionalized GO can graft styrene monomers from its surface [61].

Modification of carboxylic acid and epoxide groups involves more than one chemical reaction. Multi-step modification of GO is not only complex and time consuming procedure but also it may lead to problematic issue of GO stacking which results in obtaining non-dispersible clusters. GO sheets tend to form clusters/agglomerates due to molecular interactions. Yang *et al.* reported that attachment of amine groups effect electrostatic interaction between GO sheets negatively and forming GO agglomerates [57].

2.2.2. Atom Transfer Radical Polymerization of Graphene Oxide

ATRP is one of the most powerful and versatile living radical polymerization techniques which has been widely used to prepare several polymeric functional nanomaterials. It provides [62], [63]:

- Precise control over molecular weight
- Narrow range of molecular weight distribution
- Tailoring structure of polymers (functionality)
- To work with various monomers (MMA, tBA, DMAEMA, GMA, PNIPAM, St, so on) and initiators (linear, flat surface or nanoparticle) (diversity)
- Tunable reaction condition

ATRP was first reported in 1995 by two independent groups: Sawamoto [64] and Matyjaszewski [65]. Sawamoto *et al.* reported the use of ruthenium metal catalysts with aluminum activators while Matyjaszewski used a transition-metal halide and 2,2'-bipyridine as catalyst system with a initiator *et al.* of alkyl halide.

ATRP is controlled by a dynamic equilibrium between propagating active chains and dormant species. The mechanism for ATRP is shown in Figure 2.2.2. There are four main species in the reaction medium:

- GO-Br : as initiator
- Cu(I)/L : as activator which is a transition metal complex in lower oxidation degree
- Cu(II)/L: as deactivator which is a transition metal complex in higher oxidation degree
- GO-R•: as radicals

GO-Br and Cu(I)/L are denoted as dormant species and GO-R• and Cu(II)/L are denoted as propagating active species. The mechanism of ATRP is based on the

persistent radical effect in between propagating active species and dormant species [63], [66], [67].

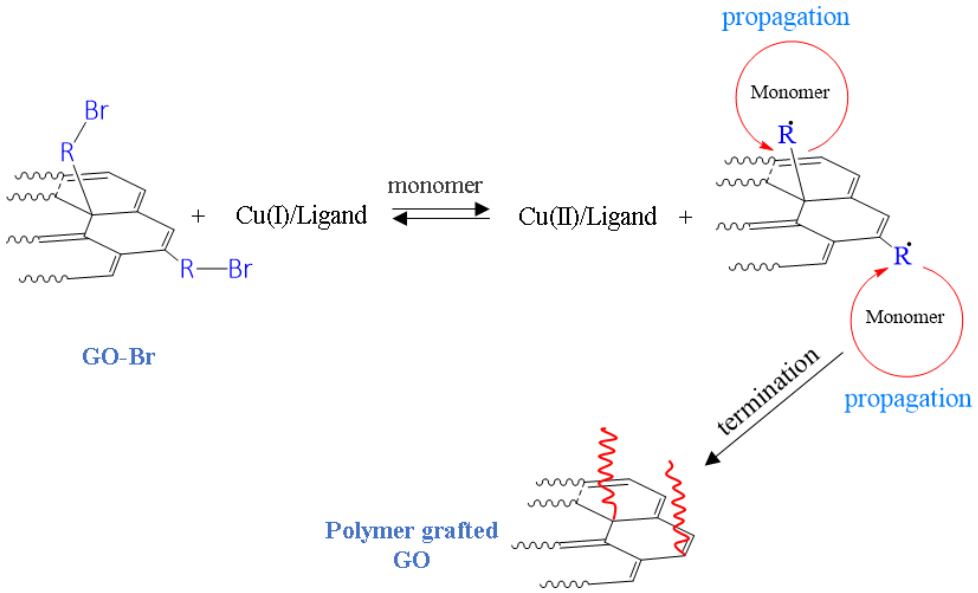

Figure 2.2.2 ATRP mechanism which initiated from GO surface.

Basically it includes, activation of GO-Br by the activator and resulting in the generation of radicals. Monomers are propagating by addition to generated radicals. Then growing radicals are deactivated by the help of the deactivator to form dormant species (Br-capped pre-polymer chains). This cycle are continued until no monomers left in the media or exposed to air [63]. Termination reactions also occur in ATRP which accounted for mainly radical coupling and disproportionation. However, a very small portion of active polymer chains undergo termination in a well-controlled successful ATRP. This phenomena is occurred due to the low concentration of active propagating radicals and higher concentration of dormant species. When the deactivation of propagating radicals into dormant species is fast, the concentration of radicals can be maintained at small amounts. Consequently, it results in minimum termination reactions [63], [66].

The polymer modified-GO can be found in many applications such as optoelectronics, supercapacitors, biomedical engineering and membrane technology [68].

2.3. Graphene Oxide based Membranes

Separation processes are essential elements of our lives from biological level to industrialization. Every cell in our body process a separation on which molecule pass into cell or retain. In industry, products are separated and purified for improved quality and more importantly they provide opportunities for recycling, waste reduction and more efficient use of resources. Among the separation processes membrane separation and technology has stood out with low energy consumption and efficient separation performance.

Membrane is a semi permeable, selective barrier between two phases which allows to some molecules pass while other molecules cannot due to different size of particles or affinity of molecules. Separation processes via membranes can be classified according to their structure, separation mechanisms or separation size range, as it can be seen from Figure 2.3.1.

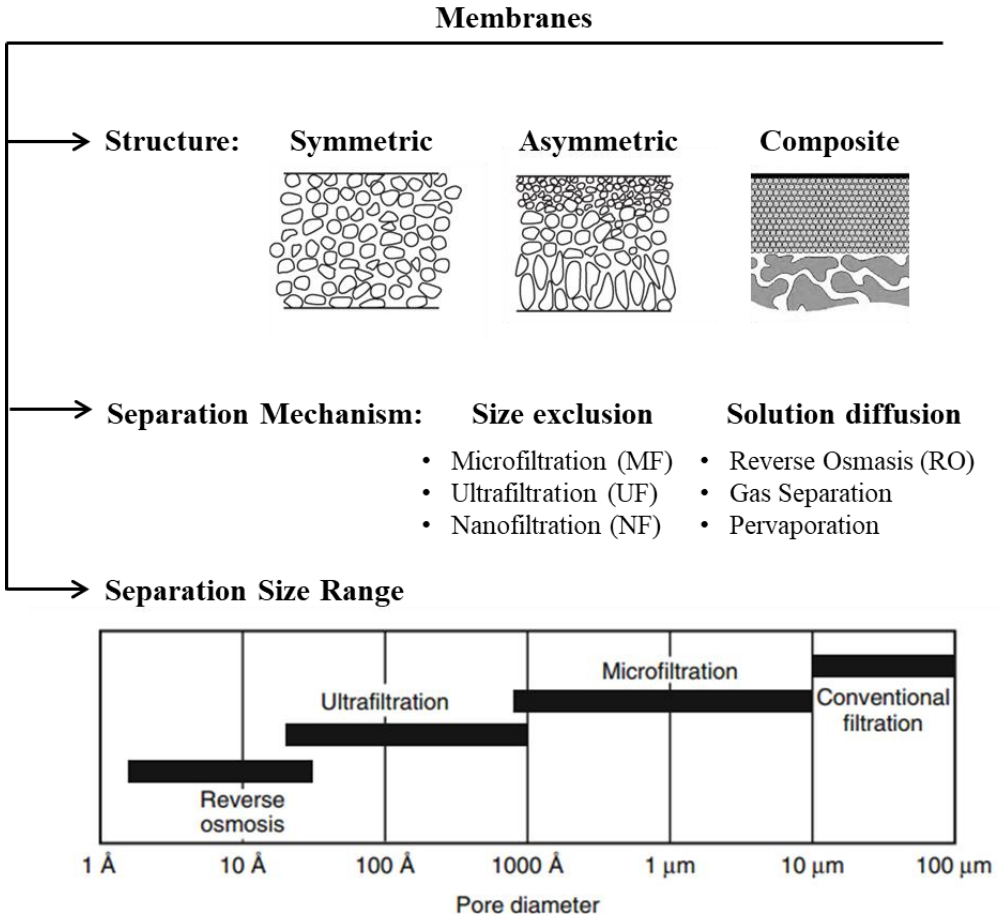

Figure 2.3.1 Membrane classification according to different categories.

Water is the most valuable source in our world and it is rapidly consumed due to urbanization and population growth. Membrane technologies for water purification have been actively pursued for decades. Increasing demand for clean water makes it necessary to make innovations in novel membrane materials, fabrication methods and processes [69]. Researchers are focused on new materials to enhance water purification performance of the current processes. GO holds a great potential to assemble a brand new membrane material for water purification due to high hydrophilicity, unique 2D structure with mono-atom thickness, outstanding mechanical strength and good flexibility as well as facile production [70]. These features provide improved membrane performance in water permeance, selectivity, antifouling property, etc.

GO can be used in membrane applications as:

- A main material to produce vacuum assisted free-standing membranes,
- A selective layer on the top surface of the membranes
- Polymer incorporated composite/nanocomposite membranes.

In the first technique, it is benefited from GO dispersibility in water. The prepared GO aqueous solution was vacuum filtered on a support layer and the thickness of the membranes can be easily tuned. Obtained GO films show a good mechanical strength and flexibility [71]. Another approach is benefited from self-assembled behavior of GO sheets to form free-standing GO membrane [72]. The hydrosol of GO was heated and with the evaporation of hydrosol GO was self-assembled at liquid/air interface to prepare macroscopic GO membranes. Free-standing GO films are feasible candidates for reverse osmosis (RO) membranes to be utilized in desalination. Because they are fully capable of 100% of salt rejection without any loss from water permeation during process [73].

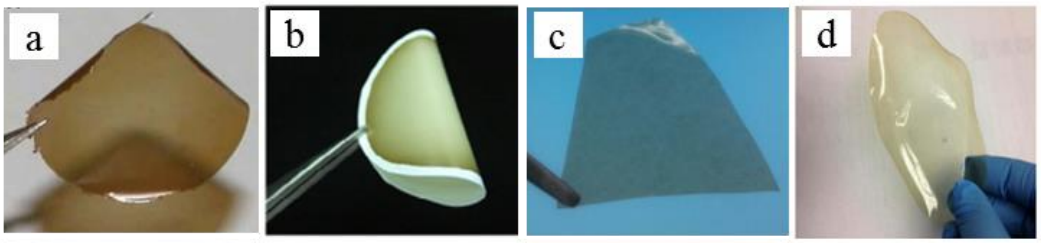

Figure 2.3.2 Sample images of (a) free-standing GO membrane [15], (b) immobilization of GO onto membrane surface [74], (c) and (d) polymer-GO nanocomposite membranes [75], [76].

Membrane surface modification with GO provides improvements in many aspects: antimicrobial effect, chlorine resistant, anti-fouling, higher water permeation and higher selectivity [73]. Due to 2D structure of GO sheets, GO can be deposited on membrane surfaces by means of electrostatical immobilization and act like a selective skin layer. The selective layer of GO provides to reduce surface pore diameter and

narrow the pore size distribution of nanofiltration membranes [68]. High hydrophilic property and fast water transport through the GO sheets enables it as a barrier coating to enhance both fouling and chlorine rejection for desalination membranes. Choi *et al.* produced a polyamide thin-film composite membrane via layer-by-layer deposition of GO sheets for desalination applications [77]. The produced membrane showed a great performance in chlorine rejection and protein foulant. In another study it was observed that the improved water permeation through the GO layered polyacrylonitrile composite membrane and it performed an excellent pervaporation separation of a 70% isopropyl alcohol/water mixture (99.5% water in permeate) [74].

GO can be incorporated with polymer composite. Besides, GO can be further modified in order to enhance compatibility with polymer host as mentioned previously. Modified-GO or pristine GO are added to polymer solutions and then prepared solutions are casted by the common phase-inversion method. GO based composite or nanocomposite membranes show improve water permeance, antimicrobial properties, antifouling properties and mechanical strength.

Isocyanate-treated GO was employed in polysulfone ultrafiltration membrane by Zhao *et al.* in order to improve hydrophilicity, water flux and antifouling property [78]. In literature, there are few studies related to polymer decorated GO incorporated nanocomposite membranes. Mansourpanah *et al.* prepared polyethylene glycol modified GO based polyamide thin film nanocomposite membranes by phase inversion method in order to enhance rejection and antifouling properties of membrane [79]. They resulted that the rejection capability of obtained membranes against NaCl and Na_2SO_4 and contact angle measurements depending on the surface hydrophilicity were increased. The flux recovery ratio, which refers to the antifouling properties of membranes was also increased. Another polymer modified-GO included study was conducted by Kochameshki *et al*. [18]. Poly(diallyldimethylammonium chloride) chains were attached onto GO chains by means of reversible addition fragmentation chain transfer (RAFT) polymerization, and then obtained product was utilized as nano fillers in PSF nanocomposite membrane. Results show that these modified membrane

had better properties including pure water flux, water uptake, hydrophilicity and antifouling.

Using GO-poly(PEGMA) in membrane applications which is also subjected in the present study has been reported to be effective on ati-fouling property and higher water permeance. Very recently, hydrophilic poly(ethylene glycol) methyl ether methacrylate chains grafted on GO sheets were first synthesized via surface-initiated atom transfer radical polymerization method. Afterwards, poly(PEGMA) grafted GO was used as nanofiller in PSF ultrafiltration membrane in order to enhance antifouling property based on the high hydrophilicity of poly(PEGMA) chains. Obtained nanocomposite membrane showed significant improvements in water flux and flux recovery rate. The excellent filtration and antifouling performance were resulted which was attributed to the segregation of GO-g-poly(PEMGA) nanofillers toward the membrane surface and the pore walls [80].

2.4. Microsieves

Membranes can be utilized in a wide range of application due to the versatility of structure and separation performance. Microfiltration holds a very important role in water purification, food industry and biological applications. Microfiltration is a process in which suspended particles in liquid are filtered due to size differences in between 0.1 μm and 10 μm. For this purpose, porous membranes are being used and they are specially named as microsieves.

Microsieves have isoporus surface morphology with open pores throughout the membrane cross-section. They can perform accurate size separation. Their thickness is small and the porosity is high in which resulted in higher fluxes. Their operation involves relatively low transmembrane pressure depending on pore size and membrane thickness.

The liquid flow of through the microsieve can be calculated by using Hagen–Poiseuille equation [22]:

$$J = N.\frac{\pi d^4}{128.\mu.L}.\Delta P$$

$$N = \frac{4.\varepsilon}{\pi.d^2}$$

Where J is flux, d is the diameter of pores, μ is viscosity, ΔP is the transmembrane pressure, L is cross-sectional length, and ε is porosity. N is the number of pores per square centimeter of membrane. The ability of microsieves to separate particles can be expressed by a term which is called the rejection coefficient, R, which is defined as [22]:

$$R = \left(1 - \frac{C_{permeate}}{C_{feed}}\right).100\%$$

For a perfectly selective microsieve the permeate concentration $C_{permeate} = 0$ and R = 100%, and for a completely unselective microsieve the permeate concentration is equal to the feed concentration, and R = 0.

Microsieves can be made of ceramic and polymeric materials by using different fabrication methods which clean room included expensive machinery steps. Different examples of microsieves are given in Figure 2.4.1.

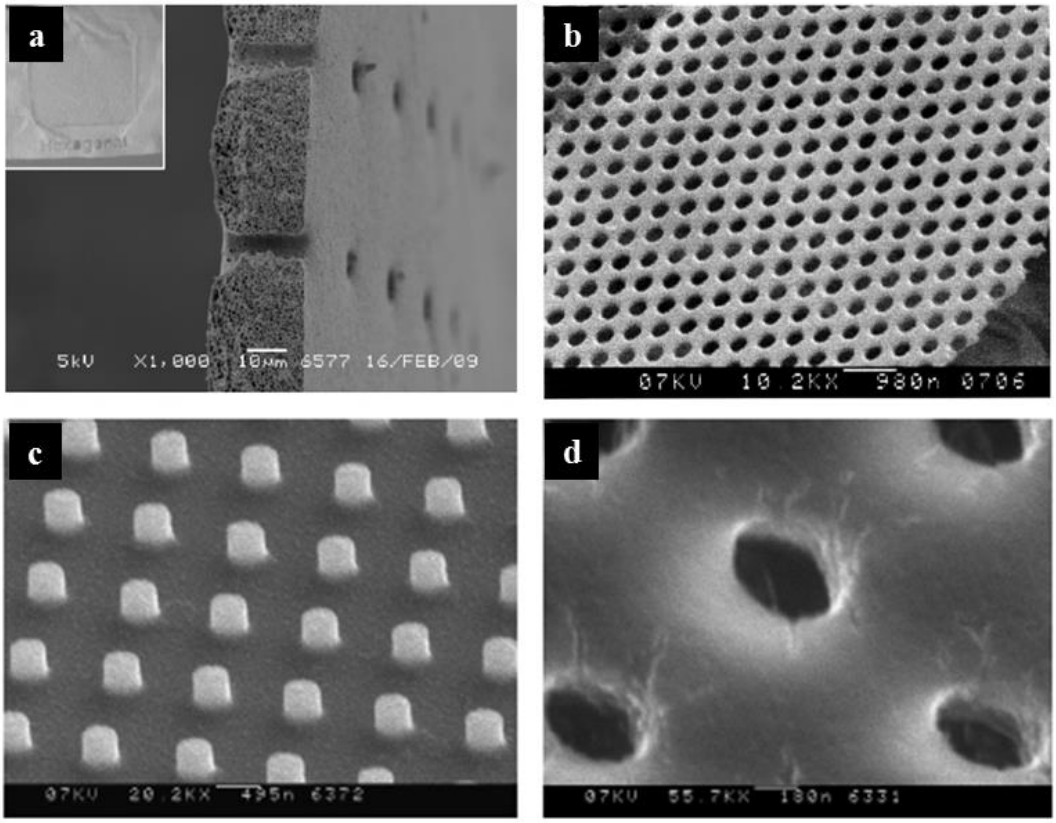

Figure 2.4.1 SEM images of (a) a polymeric microsieve, whereas pore diameter is about 10 µm and the thickness of the microsieve is 30 µm [81], (b) the silicon nitride microsieve, whereas pore diameter is 260 nm and the thickness of the microsieve is 100 nm [82], (c) a mould with 0.4 µm diameter posts and (d) the resulting membrane.

Silicon nitride microfiltration membranes with a definite pore size have been fabricated by using laser-interference lithography and silicon micromachining technology. In these methods, silicon wafer is coated with silicon-rich nitride layer by means of chemical vapor deposition, and then this layer is perforated using photolithography. Finally the silicon substrate is removed by KOH-etching to form a support for obtained microsieve. It is possible to obtain well-defined surface morphology and pore size with these techniques and also they are resistant to extreme chemical conditions. However, they are brittle and expensive. In addition to that, membrane release from the silicon substrate is crucial. Alternatively, polymers are cheaper materials than silicon nitride. These materials can be processed into porous structures by moulding technology or UV-induced photolithographic techniques.

Polymeric membranes may be durable, cheap and disposable but the high cost of fabrication and releasing from the mold still remain as drawbacks.

Recently, Breath Figure method can be utilized for the fabrication of microsieves under proper conditions in a very cost-effective and easy way, which is covered in detailed for the following section.

2.5. Breath Figure Method

Breath Figure (BF) method is basically based on condensation of water vapor on cold surfaces - we observe that phenomenon in our daily life without even noticing it. However, the first scientific observe related to water condensation on solid surfaces was conducted by Aitken in 1893 [83] and later by Rayleigh in 1911 [83]. Until 1994 in which François obtained polymeric porous films with honeycomb structure (see Figure 2.5.1), BF method had not been used in any practical application [84]. The pioneer work of François led up BF method, today it is being used as a producing method of porous polymer films [85].

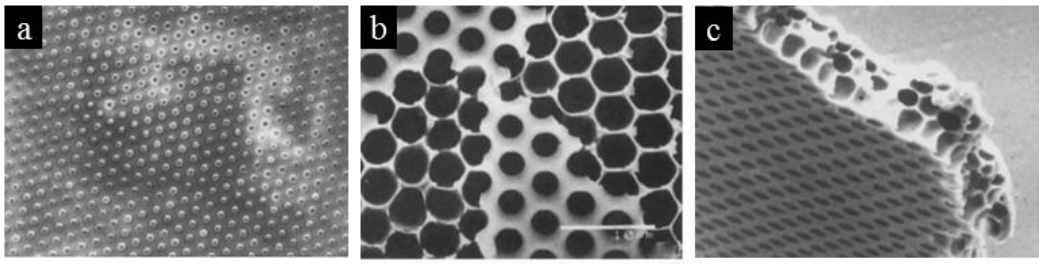

Figure 2.5.1 Hexagonal structured polymeric Bf film obtained by François [85]. A drop of poly(para-phenylene)-block-PS solution in carbon disulfide was exposed to humid air flow (a-b top view, c cross-section of obtained BF films).

BF method is easy to conduct, time and energy saving process which equipped with simple apparatus for the fabrication of strictly ordered pores within the range of nanometer to micro scale. Well-defined micro or nanoscale porous polymeric surfaces are needed in vast range of applications in membrane technology, templating, sensors, photo-electric materials and functional surfaces [86]. Figure 2.5.2 shows BF process.

In general, it includes a substrate, a polymer-solvent system in which solvent is immiscible with water and humid air flow.

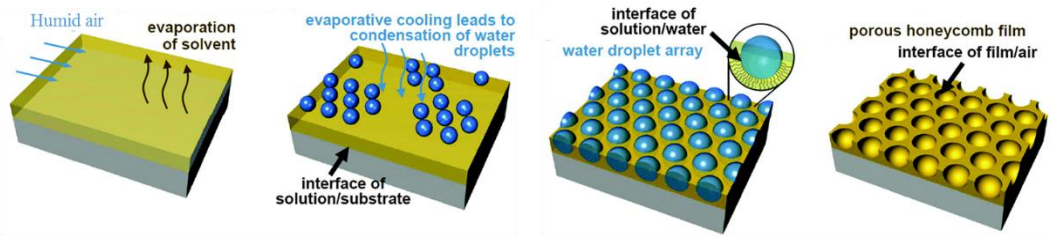

Figure 2.5.2 An illustration of honeycomb porous polymeric film formation mechanism via BF method [87].

BF method is a self-assembly process which is controlled by complex mass and heat transfers processes. In addition to that, stability of condensed water droplets and interactions between the condensed water droplets and both polymer and solvent affect the pore formation mechanism. Therefore the mechanism cannot be explained in terms of thermodynamic and kinetic manner [88]. Hence detailed mechanism of ordered pore formation is still not fully understood. However, generally accepted features of the process involves 4 main steps which were discussed in reviews [84], [86], [88]–[93] and published studies [94]–[99]:

(1) Casting of polymer solution to substrate and it is placed under controlled humid air flow. With the evaporation of volatile organic solvent, the polymer solution surface become colder.
(2) Condensation of water droplets occur on cold polymer/air interface when they contact to it.
(3) Afterwards, droplets are growing and serve as a sacrificial template for shaping on polymer surface in a way to form ordered hexagonal arranged pores
(4) Finally, evaporation of whole volatile organic solvent and water is resulted in obtaining BF porous films.

In order to obtain a hexagonal packing and defect-free surface, water droplets should not coalesce to each other. This phenomenon is explained by Marangoni convection

and thermocapillary flow [100], [101]. Evaporation of solvent ends up with surface getting colder which resulted in local temperature gradient on surface. Due to subsequent temperature gradient, thermocapillary flow of water droplets are occurred. Because colder surface regions hold higher surface tension energy which drives movement of water droplets to minimize the surface energy until the surface is completely covered by water droplets in order. Water is a precipitator for polymer, hence solidified polymer forms a thin protective layer at the air/water interface. Then the protective layer stabilizes the water droplets by attractive interaction and prevent their coalescence. After reaching equilibrium, water droplets start to grow until the time when all solvent is evaporated. Thus, the size of pores is related to growth time which is determined by the evaporation time [84]. Consequently, a highly uniform sized pores that arranged in hexagonal packing on surface is obtained after the water droplets evaporated completely [102], [103]. Stabilization of water droplets and preserving them by a protective layer are directly relating with physical and chemical properties of polymer and solvent. The rate of evaporation and the rate of polymer precipitating should be balanced. The concentration of the protective layer should be high enough to stabilize water droplets without coalesces. Also polymer should be not have hydrophilic character [84]. Many researchers have reported that amphiphilic polymers [104], [105] and polymers with polar groups at the chain ends [106], [107] easily stabilize water droplets and form regular porous films.

BF process is effected by various experimental parameters such as [84], [86], [88]–[93]:

- Temperature and relative humidity of environment, time
- Flow rate of humid air,
- Casting volume
- The physical properties of the solvent (vapor pressure, interfacial tension),
- The physical and chemical properties of the polymer, (structure, molecular weight

- And the hydrophilicity of the substrate.

The nature of BF process is very dynamic which resulted in low repeatability and inconsistent data in literature led to confusion. A slight change of any of these experimental parameters may be resulted in the change of obtained surface properties. Bai *et al.* gave an example for this situation in their review. They noticed that two groups resulted different conclusions on investigating effect of molecular weight on pore diameter [88].

Different kinds of pores in terms of shape, size and length is possible to fabricate by tuning of these parameters. Polysulfone (PSF) is useful as a main component in membrane technology and microfiltration/ultrafiltration applications due to its outstanding properties such as high mechanical, thermal and chemical stability [108], [109]. Fabrication of porous PSF films by conventional BF method are available in literature [94]–[99].

It is difficult to form regular honeycomb patterned PSF films via BF method as PSF itself is not very effective in stabilizing water droplets during BF process even though such films could be very useful for membrane based separation applications. After setting optimal experimental parameters, subsequent evaporation of the volatile organic solvent and water result in various surface morphologies: Some of the obtained surfaces have highly ordered pores, while others changing pore size which formed in irregular pattern. Factors affecting pore size and distribution along the surface are: humidity, concentration of polymer solution, humid air flow rate, polymer molecular weight, storage time of prepared solution. Besides that, regularity of pores can be facilitated by adding surface active agent due to the fact that surface active agents are decrease the surface tension between interfaces (polymer/air or polymer/water). The following Table 2.5.1 summarizes the changing characteristic of porous films with changing parameters.

Table 2.5.1 Response of the surface morhopoloogy due to changing experimental BF parameters [110]–[112].

Parameter	Observation
Solution Concentration ↑	Pore size ↓
Relative humidity ↑	Pore size ↑ ; regularity ↓
Boiling point of solvent ↑	Pore formation ↓ ; pore diameter ↑
Air flow rate ↑	Pore size ↓
Storage time of solution ↑	Pore formation ↑
Surfactant addition [98], [113], [114] ↑	Pore formation and regularity ↑↑

One of the application areas of BF method is a size-selective separation by the utilization of porous media. Literature includes several studies about fabrication of size-selective porous polymer films (Microsieves) by BF method [94], [115]–[119].

Microsieves are special kind of membranes that having ordered through pores within the range of 0.1 to 10 μm pore diameters [23]. Formation of through pores is a prerequisite for fabrication of microsieves. In literature, formation of through pores can be associated with the interaction in between water droplets and substrate. It was reported that using of hydrophilic substrates ended up formation of through pores. Hydrophobic surfaces like glass cannot utilize through pores along with membrane [115], [118].

In order to obtain through pore membranes on various hydrophobic solid substrates, a thin interlayer of water-soluble hydrophilic polymers (poly(acrylic acid) (PAA),

polyvinylpyrrolidone (PVP), polyethyleneimine (PEI), and poly(vinyl alcohol) (PVA)) was introduced by utilizing spin coater. This hydrophilic interlayer can induce the formation of through pores on hydrophobic solid substrates. Furthermore, this water-soluble interlayer makes the microsieve easy to be detached from the substrate and transferred to macro-porous supports to form a composite membrane or separation device. Wu *et al.* prepared microsieves on different interlayered substrates by using an amphiphilic copolymer solution (PS-b-PDMAEMA) [118]. SEM images of both sides of obtained membranes on different hydrophilic surfaces can be seen in Figure 2.5.3.

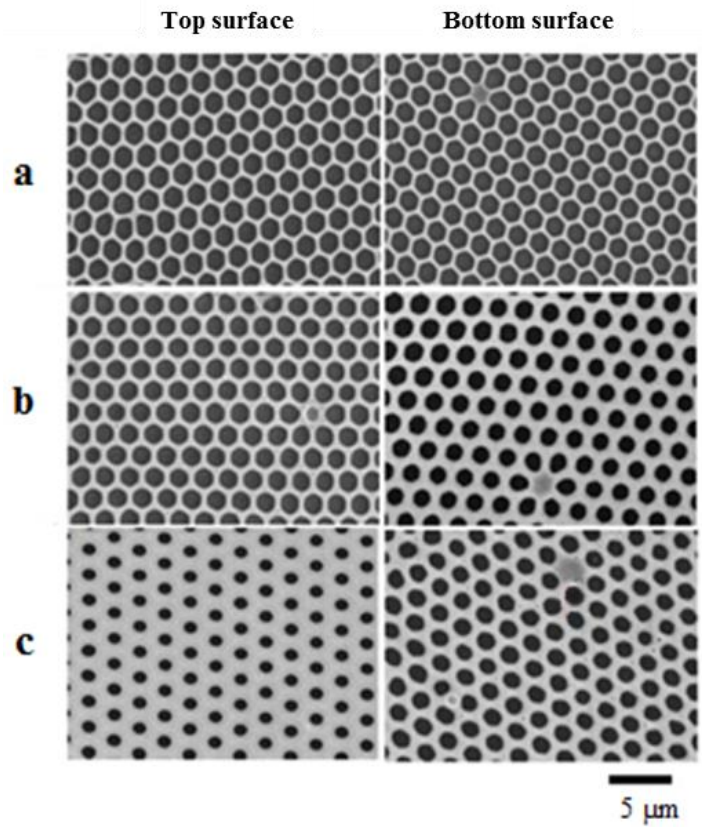

Figure 2.5.3 SEM images of microsieves prepared from 1.5 mg/mL PS-b-PDMAEMA solution on PET substrates coated with (a) PVP, (b) PEI, and (c) PVA [118].

In another study, a highly permeable ordered porous microfiltration membrane of brominated poly(phenylene oxide) (BPPO) was produced by casting on an ice

substrate as illustrated in Figure 2.5.4 [115]. It was concluded that a higher permeability can be achieved by using an ice substrate rather than glass.

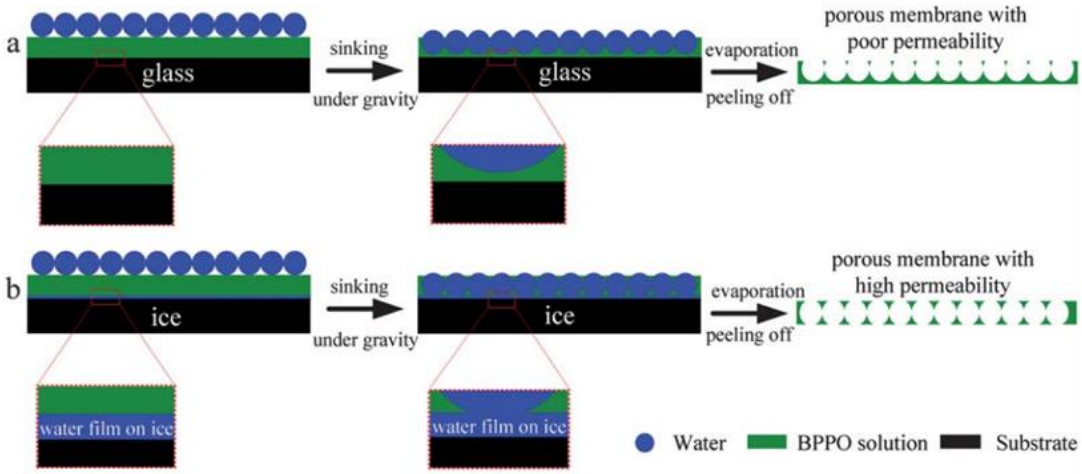

Figure 2.5.4 Schematic illustration of the formation of ordered porous films (a) on glass with lower permeability and (b) ice surface with higher permeability [115].

Water flux of obtained microsieve was calculated by using Hagen–Poiseuille equation Comparison of experimental and theoretical water flux values can be seen from Figure 2.5.5. Experimental results were fitted the Hagen–Poiseuille equation very well [115].

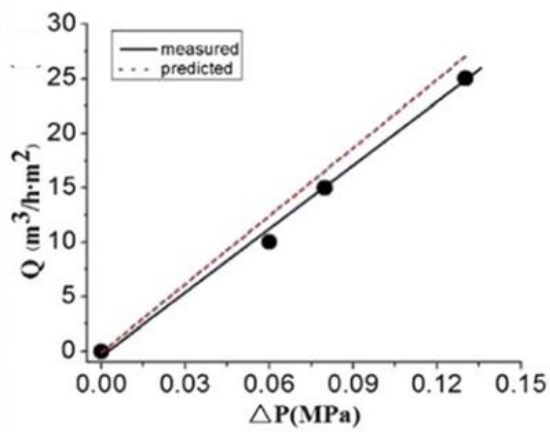

Figure 2.5.5 Relationship between pressure and water flux, the dotted line shows the theoretical prediction according to the Hagen–Poiseuille equation [115].

Wan *et al.* prepared highly uniform ordered membranes with average pore diameter was about at 3 μm for size-selective separation [116]. They used an amphiphilic block copolymer. Polymer solution was cast at an ice substrate and they obtained a membrane with regular patterned through pores which can be seen from Figure 2.5.6-a. Separation performance of obtained membrane was tested by filtration of polystyrene microspheres having diameter of 2-5 μm. Figure 2.5.6-b,c shows size distribution of polystyrene microspheres before and after filtration. It can be seen that larger microspheres than 3 microns were retained.

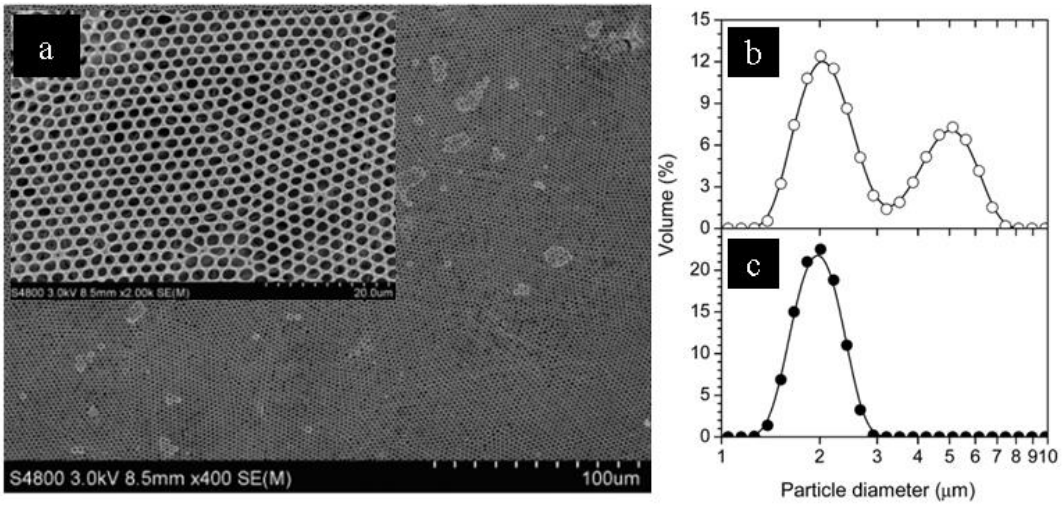

Figure 2.5.6 (a) SEM images of the obtained membrane by Wan *et al.* (b) Size distribution of the feed polystyrene microspheres with bimodal distribution at 2.and 5 μm. (c) Size distribution of the microspheres after filtration by obtained membrane [116].

Another fabrication study of microsieve was conducted by Du *et al.* in 2013 [117]. They modified conventional BF by introducing subsequent cold vulcanization, a representative illustration of modified BF method can be seen in Figure 2.5.7 A commercially available triblock copolymer, polystyrene-b-polyisoprene-b-polystyrene (SIS) was used to fabricate microsieve with pore diameters of from 1 to 7 μm, on glass substrate. In modified Bf method, excess casting of polymer solution was done and then, the excess solution underneath the surface is sucked out from the edge

by a syringe equipped on a microinjection pump in order to provide through pores by sinking of templating water droplets.

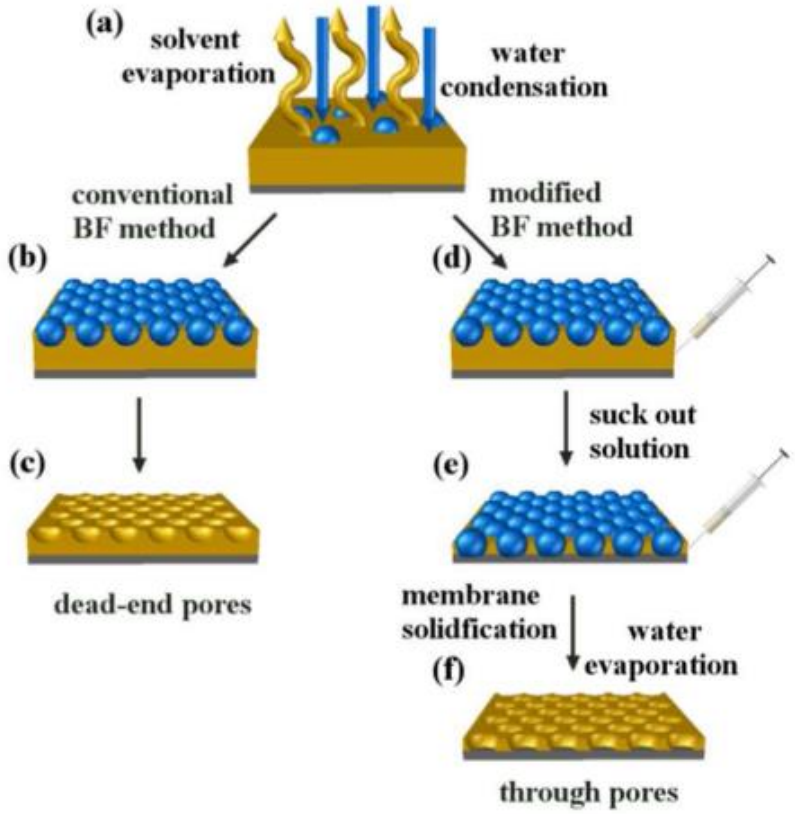

Figure 2.5.7 Illustration of the formation of honeycomb structured polymer films with (a−c) dead-end pores and (d−f) through pores [117].

The separation behavior of obtained microsieve with an average pore diameter of 2 μm were utilized by filtering of aqueous solution mixing of 3 μm and 500 nm polystyrene particles. The results can be seen from Figure 2.5.8. The filtration experiments were carried out without additional pressure. In the following vulcanization, polyisoprene block is cross-linked, endowing the porous membranes with improved mechanical properties and chemical and thermal stability [117].

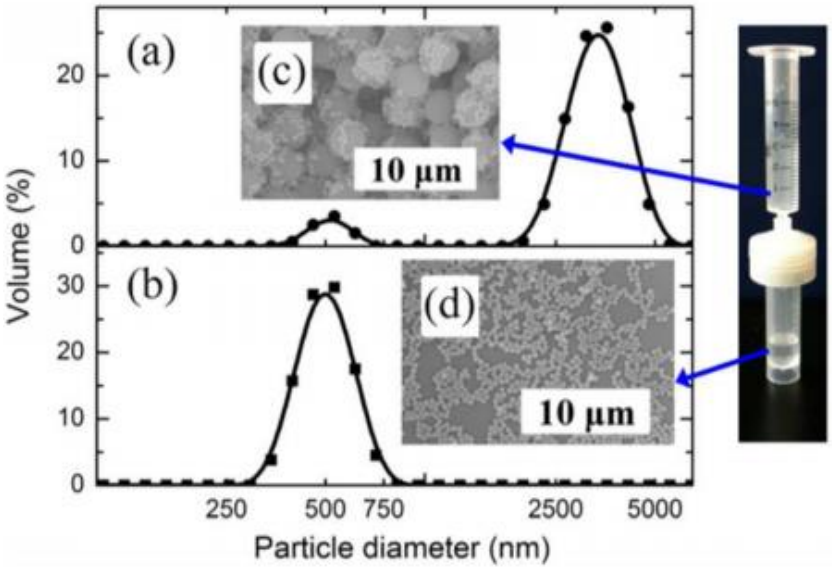

Figure 2.5.8 Size distribution of (a) the feeding particles including of 500 nm and 3 µm PS microspheres and (b) the filtrate obtained by filtering the feeding aqueous dispersion through the SIS microsieve. The corresponding SEM images of the particles (c) before and (d) after filtration [117].

The microsieve production with a large area based on modified BF method was utilized by Tripathi *et al.* in 2014 [94]. Figure 2.5.9 shows top surface image (a) of obtained microsieve and the size of it (c). The pore formation was facilitated by the addition of hydrophilic internal non-solvent in concentrated PSF solutions. Top surface of the obtained microsieve is given in Figure 2.5.9-a. Obtained microsieve with pore size 1.5 µm was capable of retaining all particles above 8 µm. The calculated neat water flux at 35.5 psi trans-membrane-pressure was calculated as 64.38 L/m^2 /min [94].

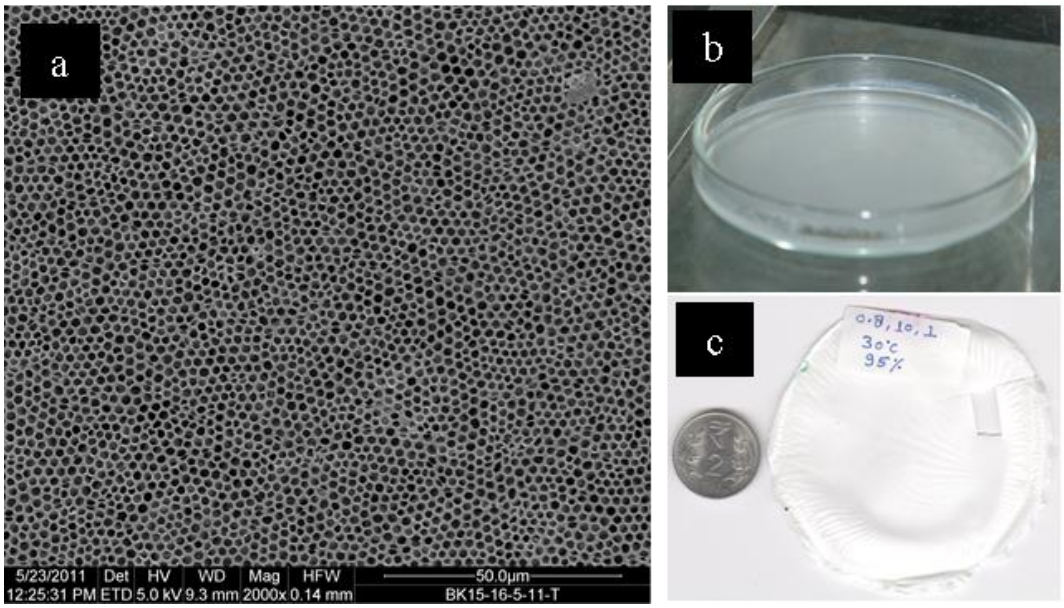

Figure 2.5.9 (a) SEM image of top surface of obtained microsieve, (b) casting polymer solution was appeared cloudy due to exposure of humidity , (c) physical picture of obtained microsieve and the coin has a diameter of 2.4 cm [94].

Hierarchical structure provides a support for enhancement mechanical stability of obtained membrane. Through pore formation was associated with using air/water or air/ice interface which was supported by hierarchical structure of glass beads [119] and TEM grid [120].

CHAPTER 3

MATERIALS AND METHODS

3.1. Materials

Graphite (44 μm of lateral size) was kindly supplied by Asbury Carbons. Potassium permanganate was obtained from Yenilab Kimya San. Tic. Ltd. Şti. Hydrochloric acid (fuming 37%), Hydrogen peroxide (30%) and Toluene were obtained from Merck. Orthophosphoric acid (85%), Acetone (technical grade) were obtained from VWR Chemicals. Sulfuric Acid (95-97%) was obtained from Honeywell. N-Hydroxysuccinimide (98+%), Ethyl 2-bromoisobutyrate (98%), Copper (I) Chloride (97%), 2,2'-Bipyridine (99+%) were obtained from Alfa Aesar. 1,3-Diaminopropane, Poly(ethylene glycol) methyl ether methacrylate (average Mn=300), Triethylamine (99+%), Hexane (95+%), Methanol (99.9+%), Chloroform (99-99.4%), N, N-Dimethylformamide (99+%) were obtained from Sigma-Aldrich. 2-Bromo-2-methylpropionyl bromide (98%) and Polysulfone (pellets, MW 75000) were purchased from Acros Organics.

3.2. Graphene Oxide Synthesis

GO was prepared according to Tour method. Briefly, a mixture of graphite flakes (1 g, 1 wt. equivalent) and $KMnO_4$ (6 g, 6 wt. equivalent) were placed into a reactor flask. An acid mixture containing H_2SO_4 and H_3PO_4 with a volume ratio of 9:1 (120:13.3 ml) was slowly added to the reactor. The used amounts of reactants were decided by considering that the final volume of reaction mixture not to be exceed 250-270 ml which is the maximum volume that can be centrifuged at once. After complete mixing, the reaction flask was placed into an oil bath kept at 50 °C. The reaction mixture was

stirred for 16 h by using a magnetic stirrer. Then, the reaction mixture was let cool to room temperature and ice with the same volume of acid mixture (133.3 ml) was added into reactor. After obtaining a homogeneous mixture, 30% H_2O_2 was added until the color of reaction mixture turned to bright yellow. Finally, reaction mixture was centrifuged and the supernatant was decanted away. Remaining graphite oxide flakes and reactants were washed with hydrochloric acid solution (3.4%) 3 times to remove salts, then washed with acetone for 3 times. Excess acetone was evaporated using rotary evaporator and dried in a vacuum oven. Finally, brownish yellow graphite oxide flakes were obtained. Schematic representation of Tour method is given in Figure 3.2.1.

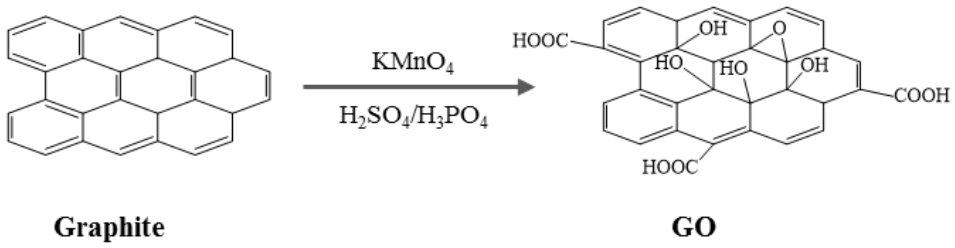

Figure 3.2.1. Schematic representation of graphite oxidation synthesis via Tour method.

3.3. Size Reduction of Graphene Oxide

Dried graphite flakes were dispersed in distilled water at a concentration of 5 mg/ml. A volume of 50 ml GO solution per batch was subjected to ultrasonication (Bandelin Sonopuls HD 2200, 200 W-20 kHz, power value of 37% with 3 cycles) for 2 hours at 0 °C. Then, the dispersion was centrifuged (8000 rpm for 20 minutes) and the precipitated part was decanted away. Exfoliated graphene oxide sheets in the supernatant part were dried by lyophillization. Obtained nano-sized graphene oxide was stored at -20 °C as a precaution against water absorption and reduction due to environmental effects.

3.4. Synthesis of Graphene Oxide Based ATRP Initiators

In this method, ATRP initiators were conjugated to the GO surface by esterification of hydroxyl groups. 100 mg of nano-GO was dispersed in 25 ml dry DMF and ultrasonicated about 20 minutes at 0 °C. Obtained clear solution was placed in an ice bath and kept under Argon atmosphere. Under vigorous mixing, 2.6 ml of TEA was added then, 2 ml of 2-Bromo-2-methylpropionyl bromide was added drop-wise. The reaction mixture was stirred for 2 hours in ice bath under Ar atmosphere. After 24 hours of mixing at room temperature, the reaction was completed and the obtained product (GO-Br) was purified by washing with DI water and EtOH via centrifugation. GO-Br was dried in a vacuum oven for 10-12 hours and stored at 4 °C. Schematic representation of the GO modification can be seen in Figure 3.4.1.

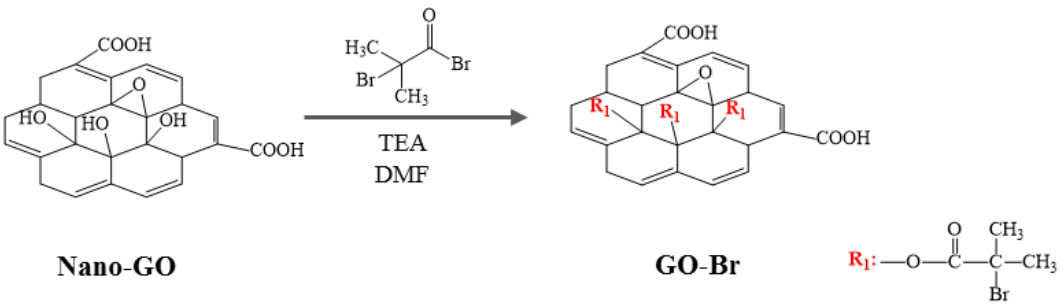

Figure 3.4.1. Synthesis scheme of GO based ATRP initiator.

3.5. Synthesis of poly(PEGMA) Grafted Graphene Oxide by ATRP

Poly(ethylene glycol) methyl ether methacrylate grafted GO was synthesized in the presence of sacrificial initiator. Initiator modified GO was used to perform grafting of polymer chains from GO surface. The procedure for surface initiated ATRP was as follows. 40 mg GOBr and 4 ml of MeOH/H_2O mixture (volume ratio of 4:1) were added into a vial then it was exposed to ultrasonication at 0 °C until obtaining a homogenous solution. PEGMA and sacrificial initiator were added to obtained homogeneous solution. 20 mg CuCl powder and 62 mg 2,2'-Bipyridine were weighed

in another vial. All vials were sealed with a rubber septum and bubbled with Ar gas to evacuate oxygen. 4 ml of MeOH/H_2O mixture was added into CuCl and 2,2'-Bipyridine with a syringe and resulting dark reddishbrown catalyst solution. Finally, polymerization was initiated by the addition of catalyst solution into GO-Br containing vial and it was carried out for 2 hours at 30 °C. The resulting poly(PEGMA) grafted GO was precipitated by centrifuge then it was purified by washing with EtOH. Supernatant part was also purified by dialysis to obtain free poly(PEGMA) chains grown from the sacrificial initiator. Schematic representation of surface initiated ATRP was given in Figure 3.5.1.

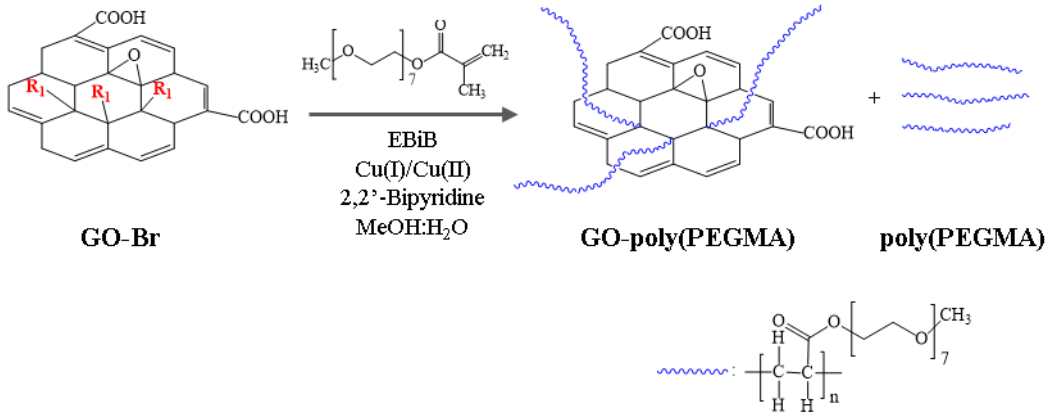

Figure 3.5.1. Synthesis scheme of surface initiated ATRP of GO.

3.6. Production of Graphene Oxide and Polysulfone Based Nanocomposite Microsieves by Breath Figure Method

BF porous films were prepared by using the experimental set-up which is given in Figure 3.6.1. As illustrated in Figure 3.6.1, the relative humidity of the inflowing air is controlled by mixing streams of dry air (< %35 RH) and humid air (>95% RH). The flow rate of air is controlled with two rotameters.

Solutions having different concentrations of PSF (75 kDa), GO-poly(PEGMA) and chloroform were prepared and mixed for at least 24 hours. An aliquot from the

prepared solution was dropped onto the substrate and spread in a way to cover surface of the substrate. During the BF process, the substrate was rotated with the help of a spin coater to enable even distribution of the polymer solution on the substrate surface. Depending on experimental conditions, process time could be varied from 2 to 5 minutes. After evaporation of the solvent, obtained porous films were examined by optical microscopy and scanning electron microscopy.

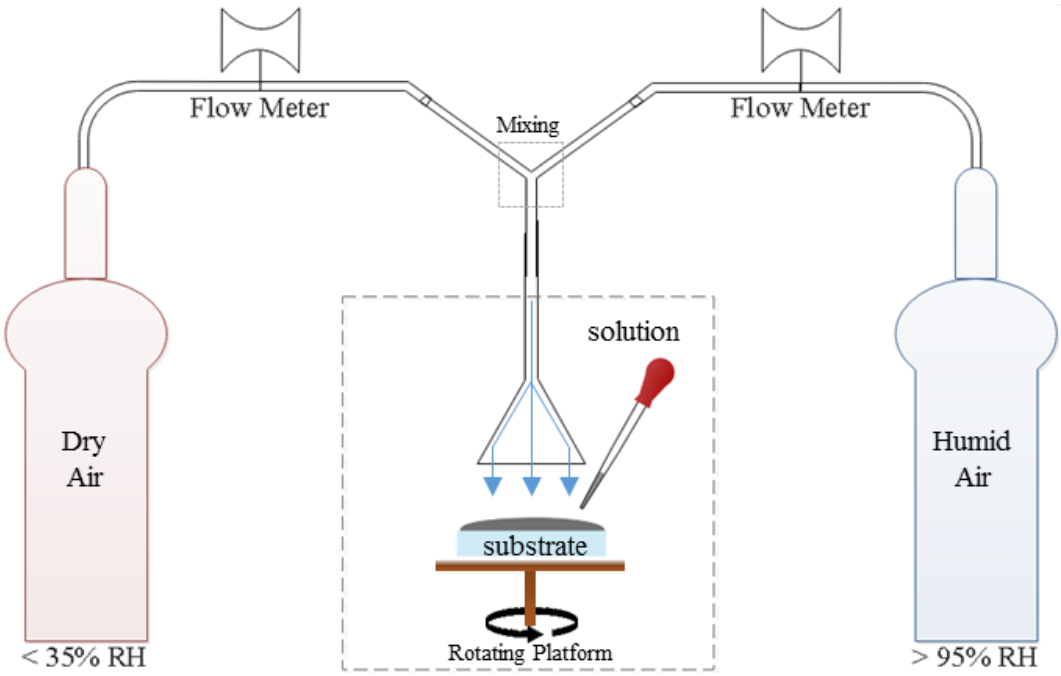

Figure 3.6.1 Schematic illustration of BF experimental set-up.

Investigated experimental parameters of BF process were: Concentration of PSF, concentration of GO-poly(PEGMA), air flow rate, relative humidity, substrate type.

3.7. Water Permeation and Yeast Filtration Tests

Permeation tests of obtained microsieves were measured in a dead end filtration unit. Feed pressure was maintained between 0.5 and 2.5 bars. The permeate volume was measured and the elapsed time was recorded.

A yeast solution of 0.24 mg/ml concentration was prepared and filtrated through the obtained microsieves. The permeate volume was measured and elapsed time was recorded. Absorbance of permeate was also recorded via UV-Vis spectrophotometer Permeate concentration was calculated based on the relationship between absorbance and concentration. The calibration curve can be found in Appendix A.

3.8. Instrumentation

Attenuated total reflection Fourier transform infrared spectroscopy (ATR-FTIR) spectroscopy measurements were done by using Shimadzu IRPrestige-21 spectrophotometer with a scan number of 64 and a range of 550-4000 cm^{-1}. Raman spectroscopy analysis was performed by using Renishaw inVia equipment with a laser wavelength of 532 nm. X-ray photoelectron spectroscopy (XPS) measurements were performed with an overall scan and Al-monochromatic X-ray anode equipped with using monochromatic XPS (SPECS EA 300). Curve fitting of C1s spectrum was performed using Gaussian-Lorentzian correlation after a Shirley background correction by using OriginPro 2016 Peak Fitting software.

UV-Visible spectrophotometry measurements was done by using Shimadzu UV-2550 spectrophotometer. The sample of GO-water solution in quartz cuvette was used for UV-Vis analysis. X- Ray Diffractometer measurements were done with thin films of specimens at 1.54 Å wavelength and equipped with Cu anode. The interlayer spacing for GO can be calculated by using following equation of Bragg's law.

$$\lambda = 2d.sin\theta$$

Where λ is the wavelength of the X-ray beam, d is the distance between layers and θ is the diffraction angle.

Thermal gravimetric analysis (TGA) of samples was done using Shimadzu DTG-60H thermal analyzer and each analysis was performed from room temperature to 600 °C, under nitrogen atmosphere with a scanning rate of 10°C/min.

Size analysis was done with dynamic light scattering (DLS) method and the used equipment was Malvern nanosizer Z series. Solution with the concentration of 0.5 mg/ml GO-DI water was analyzed.

Surface morphology of obtained BF films was examined by field emission scanning electron microscope (FE-SEM, FEI Quanta 400), operated at acceleration voltage of 20 kV. Samples of BF films were coated with a very thin layer of a gold-palladium (Au-Pd) alloy. And surface morphology of GO sheets was examined by FEI Nova NanoSEM 430 Field Emission SEM equipped with a secondary electron detector (Everhart-Thornley detector), operated at acceleration voltage of 10 kV. Atomic Force Microscopy (AFM) analyses of GO sheets were performed with AFM Veeco MultiMode V equipment on tapping mode.

Molecular weight and molecular weight distribution (PDI) were obtained by Gel Permeation Chromatography (GPC) using with Polymer Laboratories-GPC 220. THF was used as the mobile phase (1.0 ml/min), and results were evaluated with triple detection method (UV, refractive index, viscosity). The structural characterization of poly(PEGMA) was performed by Proton Nuclear Magnetic Resonance (^{1}H NMR) with a Bruker Advanced 400 MHz spectrometer at room temperature using deuterated chloroform as solvent. MestReNova NMR Analysis software was used for integral calculations of the results. Based on the integral volume on the NMR spectra, percentage conversion of PEGMA monomer was calculated as follows:

$$\%Conversion: \frac{[polymer]}{[monomer]_0} x100$$

Relative humidity of breath figure chamber was measured by using a hygrometer (Extech Instruments IR Thermometer and Humidity Meter RH101).

CHAPTER 4

RESULTS AND DISCUSSION

This study includes two main steps in fabrication of microfiltration membranes: Firstly, GO based additive was synthesized and later, it was incorporated to membrane fabrication via BF method. There are three main reasons for using poly(PEGMA) grafted GO as follows:

i. It is considered that GO-poly(PEGMA) enhances the pore formation by reducing the surface tension between air/polymer and water/polymer interfaces. Droplet stabilization in BF method using polymer grafted GO has been demonstrated for the very first time within the scope of this study.
ii. In addition to that, using GO-poly(PEGMA) in membrane structure enhances the mechanical stability and integrity of desired membrane due to the interaction between poly(PEGMA)-GO and PSF matrix.
iii. Hydrophilic character of PEG chains improved the anti-fouling property of desired membrane. GO-poly(PEGMA) sheets migrated toward the edge of water droplets during BF process and cover the pore walls which inhibits the attachment of hydrophobic organic molecules and sequent water permeability loss.

The experimental route for this purpose was explained in previous section and, obtained results and observations were given and discussed in detail in this section.

4.1. Synthesis and Size Reduction of Graphene Oxide

GO was prepared via Tour method as described earlier [30]. Graphite was oxidized by $KMnO_4$ in the mixture of H_2SO_4 and H_3PO_4. Graphite has layer structure in which sp^2 bonding of C atoms which are arranged in a hexagonal close-packed lattices. During the reaction, oxidizing agents penetrate between these graphite layers and form C-O bonds. Formation of oxidizing agents are given in following reactions:

$$KMnO_4 + 3H_2SO_4 \rightarrow K^+ + MnO_3^+ + H_3O^+ + 3HSO_4^-$$
$$MnO_3^+ + MnO_4^- \rightarrow \boldsymbol{Mn_2O_7}$$

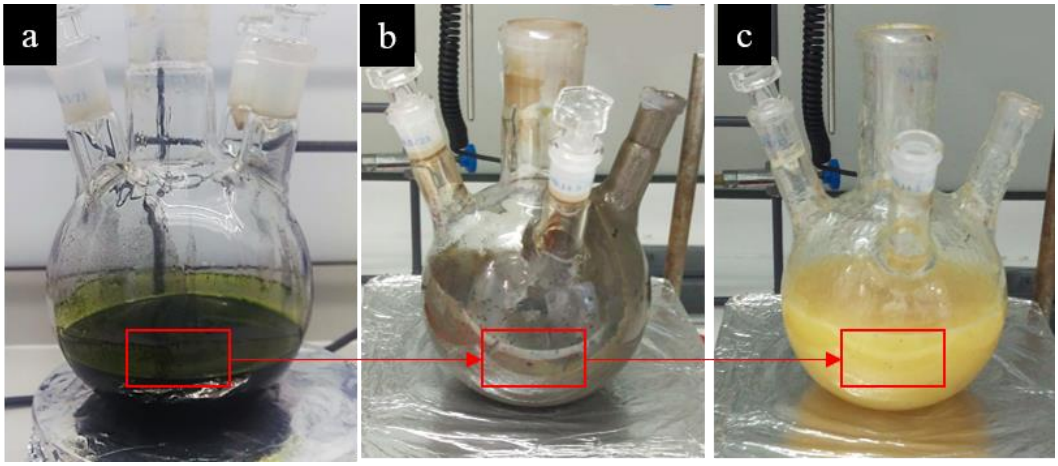

Figure 4.1.1 (a) Graphite/acid and $KMnO_4$ mixture t=0, (b) GO mixture in reaction media t=16 hours, and (c) after addition of water and H_2O_2 to GO mixture.

Photographs of the reaction mixture at different stages of oxidation reaction can be seen from Figure 4.1.1. $KMnO_4$ molecules are dissociated in H_2SO_4 and formed a dark-green colored solution due to the formation of manganese heptoxide (Mn_2O_7). With the consumption of Mn_2O_7, the color of the reaction mixture turned to dark-brown which is an indicator of oxygen containing groups attached onto graphitic layers. In addition to that, the viscosity of the reaction mixture was increased with time due to increase in plane spacing of graphite. The color change and viscosity increment

through the reaction are important observations for the successful completion of reaction. Another physical observation is given in Figure 4.1.2 by dispersing the product in water. Neither graphite nor graphene can be dispersed in water. The complete dispersion of graphene oxide sheets indicate the presence of hydrophilic groups in the structure of the product meaning successful graphene oxide production.

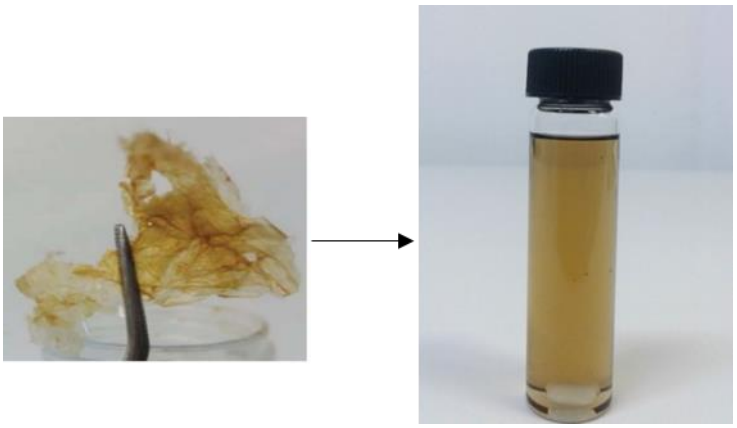

Figure 4.1.2 Obtained GO in the bulk form (left) and an aqueous dispersion of GO (right).

The further chemical analyses were performed in order to investigate oxidation degree of GO and to identify its oxygen containing functional groups. Within this scope, ATR-FTIR, Raman, XPS and XRD spectroscopy analyses were performed.

FTIR spectroscopy is a powerful and easy technique for investigating the structure and functional groups of material. Figure 4.1.3 shows ATR-FTIR spectra of graphite and GO. Graphite is composed of carbon atoms that are arranged in hexagonal lattice and it has no functional groups. Hence, no peaks are visible in its spectrum. Unlike graphite, GO spectrum has different absorption peaks which are assigned to hydroxyl, carboxylic acid and epoxide groups. Detailed examination of functional groups and their corresponding absorption bands are given in Table 4.1.1.

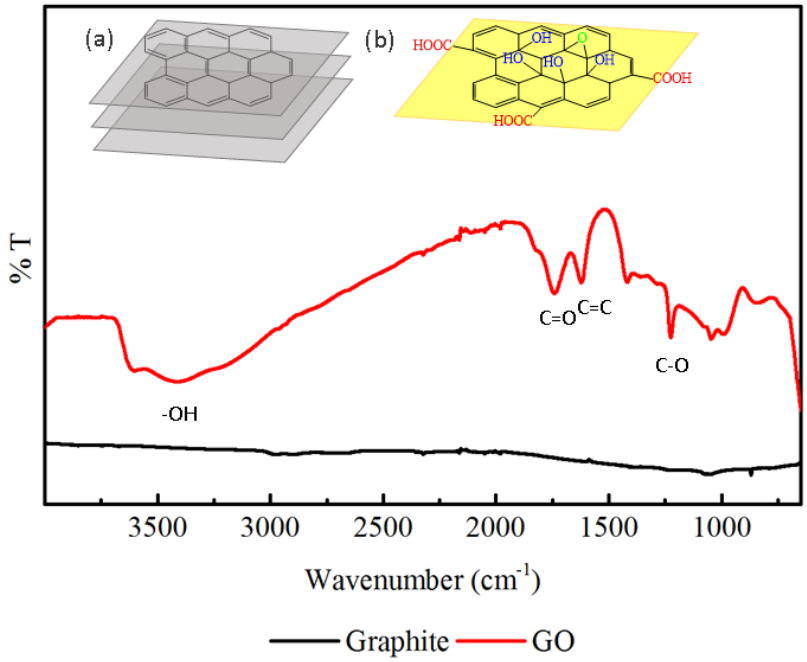

Figure 4.1.3. ATR-FTIR spectra of (a) graphite and (b) obtained GO and their structural representations.

Observed peaks from GO spectrum are in a good agreement with literature according to Table 4.1.1.

Table 4.1.1. FTIR absorption bands of functional groups

Functional Group	**Wavenumber (cm^{-1})**	**Literature (cm^{-1})** [30]
C=C sp^2 vibrations	1620	1590-1620
C=O stretching vibrations	1740	1720-1740
C-O vibrations	1225	1250
-OH stretching vibrations	3000-3690	3420

Raman spectroscopy is a commonly used method for characterization of carbon based materials. It is useful in the analysis of the defects on the graphitic domain. Defects can be naturally occurred disorders on the graphitic domain, misarranged or missing carbon atoms and chemical functionalization of sp^2 carbon atoms. For the case of GO, most defects are due to chemical functionalization by means of oxidation. The typical Raman spectra of GO shows two characteristic peaks D band (1340 cm^{-1}) and G band (1580 cm^{-1}) [42]. D band represents defects, in other words oxidation of C atoms, and G band represents graphitic domain. Figure 4.1.4 shows Raman spectrum of pristine graphite and the obtained GO. Only G band was observed at 1573 cm^{-1} for graphite while both G and D bands were observed at 1588 and 1347 cm^{-1} for GO.

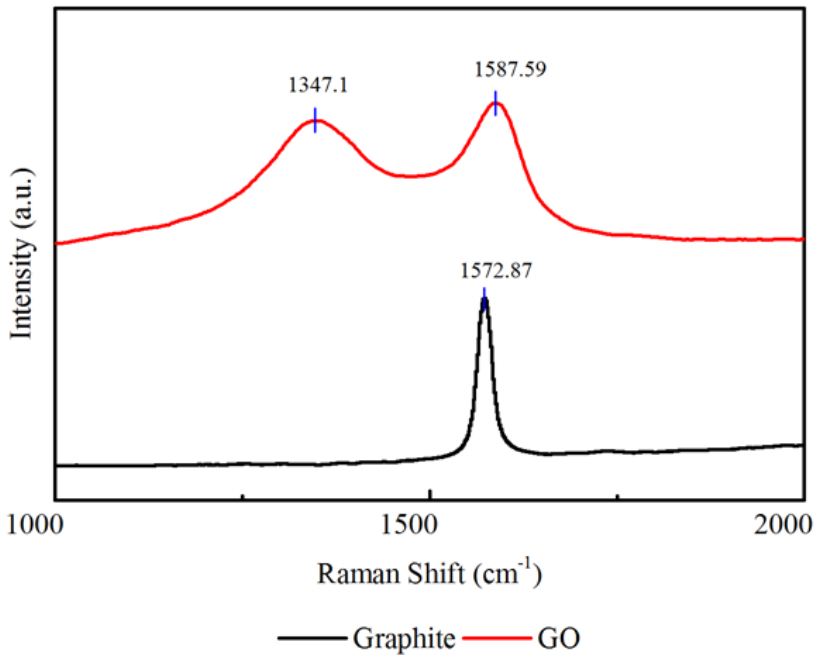

Figure 4.1.4. Raman spectra of graphite and obtained GO.

The intensity ratio of D band to G band (I_D/I_G) indicates the quality of obtained GO. I_D/I_G was calculated as 0.953 where higher values indicate higher oxidation degree since D band has higher intensity than graphite. In literature, I_D/I_G reported as 0.94 for GO and 0.17 for graphite [121].

XPS analysis was performed to further investigate surface chemistry and degree of oxidation of the synthesized GO. XPS is the most widely used surface analysis technique because it reveals elemental content of the material and identifies the relative composition of the present functional groups on the surface. XPS measurements were done for both graphite and GO as seen from Figure 4.1.5.

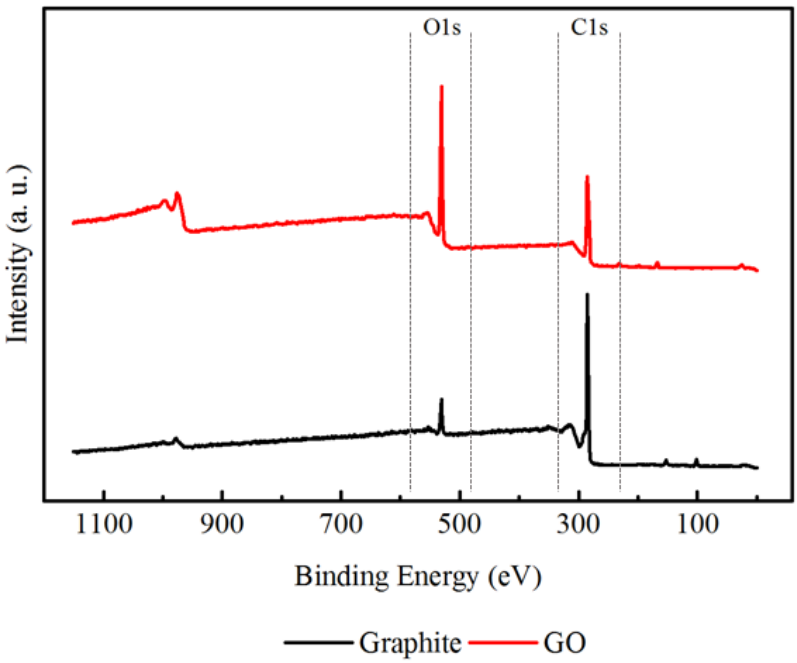

Figure 4.1.5. XPS spectra of graphite and obtained GO

The increased intensity of O1s peak of GO spectrum verifies the existence of gained oxygen containing groups. Detailed quantitative analyses for oxygen containing functional groups was done by examination of C1s core level spectrum of GO and graphite. Curve fitting of C1s spectra of graphite and obtained GO is given in Figure 4.1.6.

There is not a clear agreement how to address functional groups between 284 and 290 eV of C1s core level spectrum in literature. A little shifts can be occurred due to environmental and instrumental variation. The assigned binding energies of different peaks from literature were listed in Table 4.1.2.

Table 4.1.2 Assigned binding energy values of some functional groups.

	C=C	C-O	C=O	O=C-O	Ref.
Binding Energy (eV)	284.8	286.3	287.2	288.4	[122]
	284.6	285.8	287.1	289.1	[123]
	284.8	286.4	287.8	289.9	[124]
	284.8	286.2	287.8	289.0	[125]
	284.4	286.2	286.2	288.0	[126]
	284.6	286.6	287.8	288.9	[127]

Figure 4.1.6 shows C1s core level spectra of GO and graphite. Dashed line represents cumulative peak and it was curve-fitted into two peak components for graphite and four components peaks for GO. Graphite spectra showed a characteristic peak of sp^2 hybridization C bonding at 284.8 eV, as expected. Also a shoulder was observed due to π to π* transition at 209.2 eV.

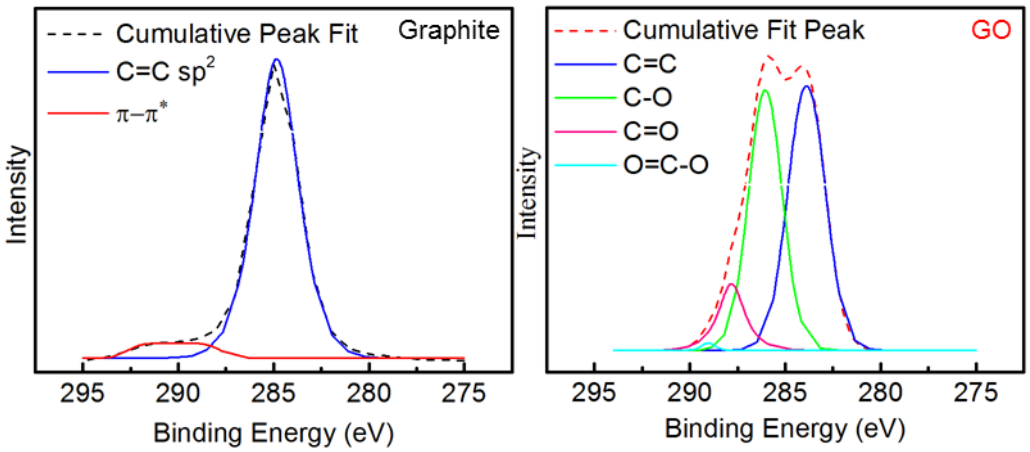

Figure 4.1.6. C1s core level spectra of graphite and GO

For GO spectrum, the binding energy of the C=C bonding was assigned to 284.6 eV and then, hydroxyl group, epoxide groups and carboxylic acid groups were assigned to 286.7 eV, 288.5 eV and 289.7 eV respectively. The area under each curve is proportional to the amount of corresponding bond in the structure. Hence, the most abundant groups in GO structure was found to be hydroxyl groups followed by epoxide groups. Elemental composition and C/O ratio of graphite and GO can be seen from Table 4.1.3 is present. The oxidation degree can be varied according to production method and many other parameters such as oxidant to graphite ratio or time which are discussed earlier. The obtained GO high oxidation degree when compared to literature. The results of XPS are consistent with literature and also they corroborated with FTIR results.

Table 4.1.3 Elemental analysis pristine graphite and obtained GO based on XPS analyses.

	%C	**%O**	**%Other**	**C/O**
Graphite	85.9	10.7	3.4	8.0
GO	60.8	38	1.2	1.6

XRD was performed to measure distance between graphitic layers before and after oxidation. It is expected that an increment at the distance between layers due to the presence of oxygen containing groups. The XRD spectra for graphite and obtained GO can be seen in Figure 4.1.7. It shows a characteristic peak around 24° for graphite. After oxidation this peak disappeared and a new diffraction peak occurred at about 10°. Interlayer spacing was calculated as 0.37 nm for graphite and 0.88 nm for GO. Layer spacing of GO layers increased due to the attachment of oxygen containing groups onto layers as expected. In the literature, the interlayer spacing of GO samples vary from 0.6 nm to 1 nm depending on oxidation degree of graphite [128]. The

interlayer spacing for the obtained GO is consistent with literature with a relatively high interlayer spacing due to good oxidation degree.

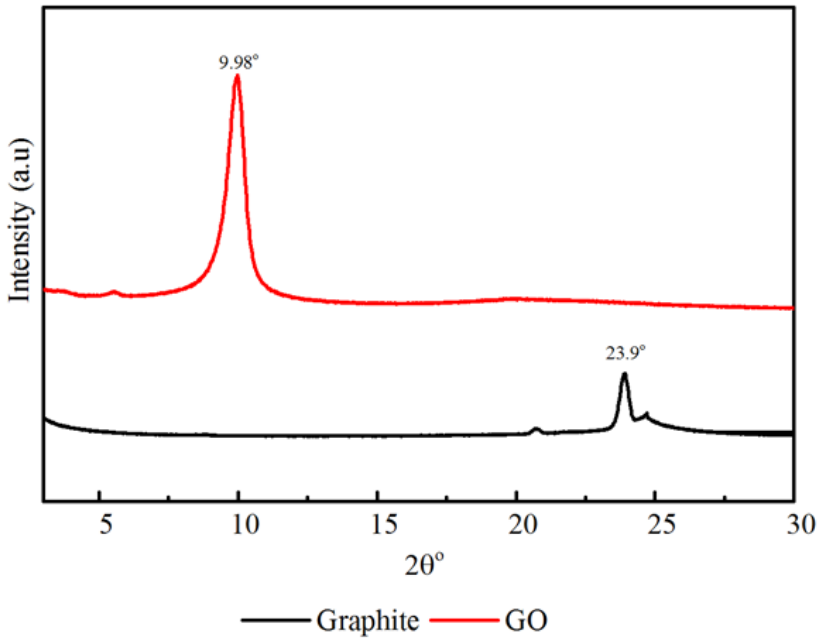

Figure 4.1.7. XRD spectra of graphite and GO

For GO, it is very important to be fully dispersed in polar media (i.e. water, DMF) and to yield a clear dispersion. Obtained graphite oxide can easily be dispersed in water and DMF by the help of mixing. The optical transparency of aqueous dispersion of GO (2.5 mg/ml) can be observed with bare eyes as in Figure 4.1.8. Nonetheless UV-Vis spectrophotometry was performed and characteristic absorbance peaks of GO can be also seen from Figure 4.1.8. The observed maximum peak at 230 nm is attributed to π-π* transition of C-C bonds and the observed shoulder around 300 nm is attributed to n-π* transition of C=O bonds [30].

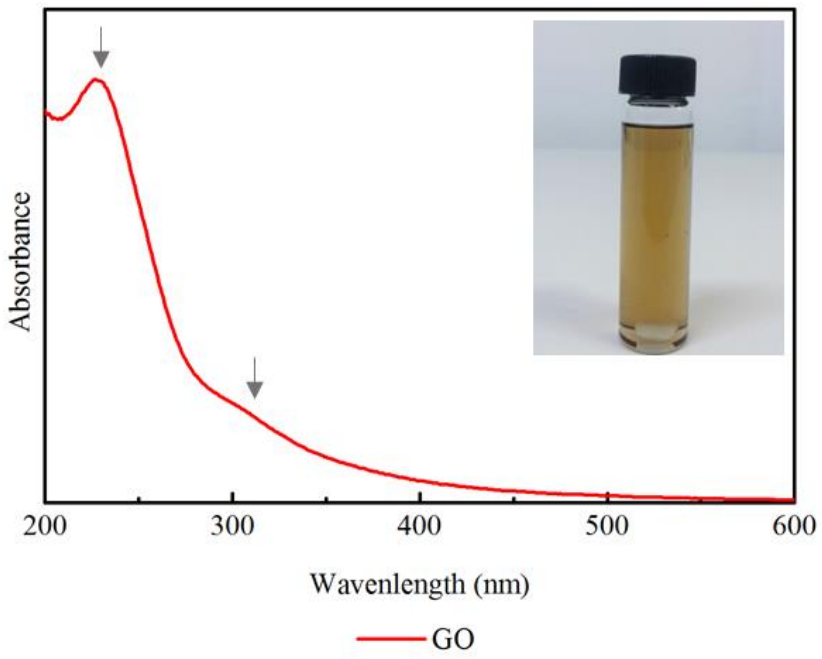

Figure 4.1.8. UV-Vis spectrum of obtained GO (GO solution was diluted to 0.05 mg/ml for UV-Vis measurements).

The behavior of GO upon heating was monitored by TGA which was conducted under N_2 atmosphere. The weight lost occurred in the range of 30-50 °C was likely caused by the evaporation of adsorbed water from environment. GO lost its functional groups and was reduced upon heating. According to Figure 4.1.9, the decomposition temperature was observed at about 200-210 °C which is in good agreement with the literature. Hence, Marcano *et al.* reported in their study decomposition temperature of GO was about at 200 °C [30]. In the end of TGA run, 77% weight lost occurred and remaining 23% of it was referred to graphitic domain. Figure 4.1.9 also shows TGA curve of graphite, it was recorded under the same conditions and no weight loss can be observed since it was composed of only carbon atoms.

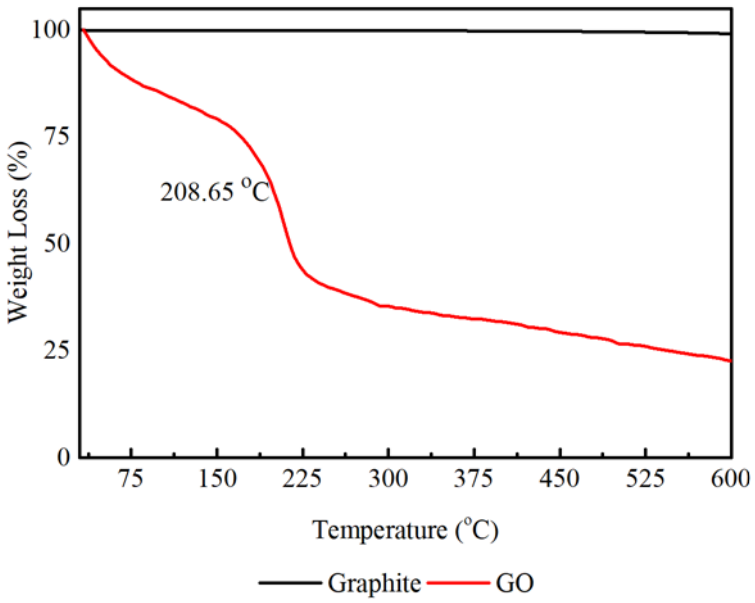

Figure 4.1.9. TGA curve of graphite and obtained GO.

Ultrasonication is a powerful technique for preparing dispersions or for particle size reduction. GO sheets are broken into sub-micron sizes when they are subjected to ultrasonic cavitation. Sound waves propagate pressure cycles that oscillate between high and low pressure points in liquid aqueous media. Between this cycles bubbles form, grow and explode when they reach to their critical sizes. This phenomenon is called as ultrasonic cavitation. Explosion causes to jet flows in liquid media, consequently GO sheets collide at high speeds. Ultrasonic cavitation depends on many parameters such as concentration of the solution, sonication time and ultrasound frequency. Lower frequencies (20-30 kHz) provide more time for bubble growing which results in higher destructiveness to GO sheets. Thus, size reduction process was done with the same concentration of GO solution which was placed in an ice bath.

Size reduction of GO was monitored with DLS measurements. Figure 4.1.10 shows particle size distribution of pristine GO and nano-GO. DLS instrument measure the scattered light from moving suspended particles. It determines mean particle size and particle size distribution in regard to principle of Brownian motion and Doppler shift.

Doppler shift occurs due to the movement of particles and larger values of the shift indicates smaller particles.

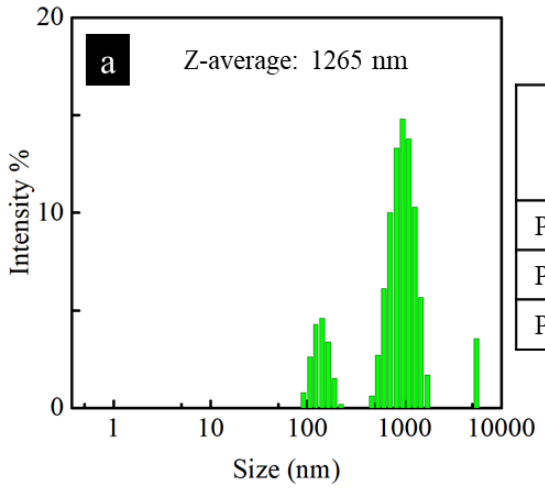

	Size (nm)	Std. Dev. (nm)
Peak 1	981	277
Peak 2	139	27
Peak 3	5560	0

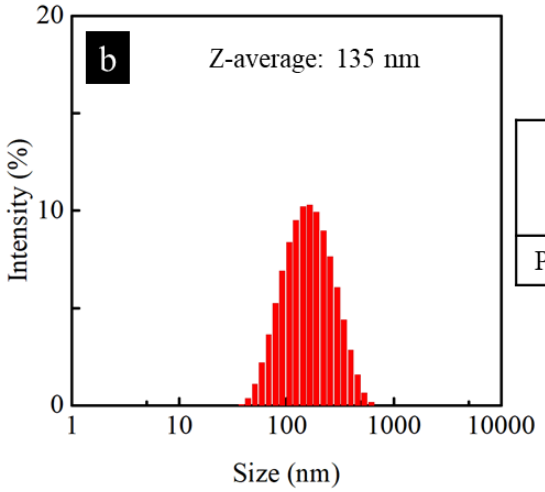

	Size (nm)	Std. Dev. (nm)
Peak 1	181	96

Figure 4.1.10. Particle size distribution of (a) pristine GO and (b) nano-GO.

The same concentration of two aqueous solutions of GO were prepared and one of them was subjected to ultrasonication and then centrifuge processes as described in section 3.2. Figure 4.1.10-a shows the size distribution of pristine GO solution which was dispersed by only few minutes of sonication in an ultrasonic bath. Thus, its distribution was observed in a large scale with a mean particle size of 1265 nm. The mean particle size of used graphite was 44 μm. So it can be said that during oxidation

graphite flakes were violently divided into different sizes and size reduction was occurred in a wide range. Controllable size reduction was achieved by following ultrasonication and centrifuge processes. Dispersed GO sheets were divided into nano-scales under optimum ultrasonication. Afterwards larger particles of GO were decanted away with the help of centrifuge. A uniform distribution of nano-GO sheets with a mean particle size of 135 nm was obtained as seen from Figure 4.1.10-b.

In order to examine surface morphology of GO sheets and further investigate of size analyses, SEM and AFM microcopy imaging techniques were performed. SEM images are given in Figure 4.1.11.

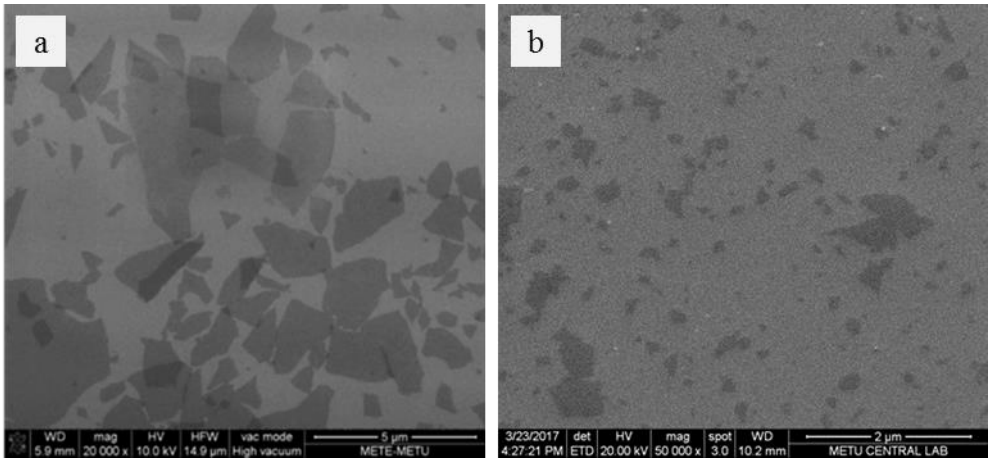

Figure 4.1.11 SEM images of (a) pristine GO at 20000x (b) nano-GO sheets at 50000x.

The sheet-like morhology of GO was verified by SEM images. Figure 4.1.11-a includes wide range of GO sheets from nano scale to >5 micrometers. The diversity in lateral size of GO sheets in SEM images is consistent with DLS multimodal distribution however, in DLS measurements larger particles than 5 micrometers are not detected. Most of GO sheets are presented as single sheets. On the other hand Figure 4.1.11-b shows nano-GO SEM images and the size reduction within the GO sheets can easily be seen. In Figure 4.1.12 AFM results are given.

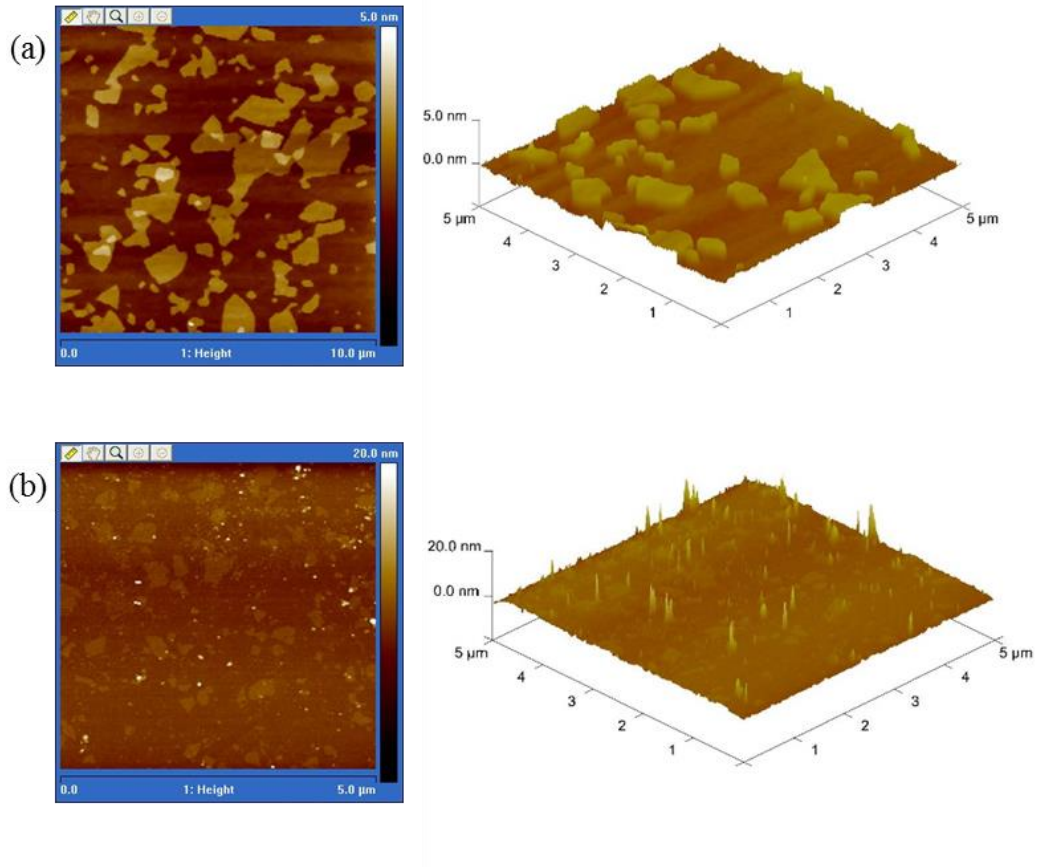

Figure 4.1.12 AFM images of (a) pristine GO at 20000x (b) nano-GO sheets.

According to Figure 4.1.12, morphology and the thickness of obtained pristine GO and nano-GO were verified by AFM analysis. The highlighted areas represent increasing vertical height which indicates imbricated GO sheets. However, for nano-GO images it indicated impurities or agglomerated GO clusters by combining several nano-GO sheets during ultrasonication. And these GO clusters were not precipitated by centrifuge because of their nano dimensions. The further height analyses were done with Image Processing and Analysis software and the results are given in Figure 4.1.13.

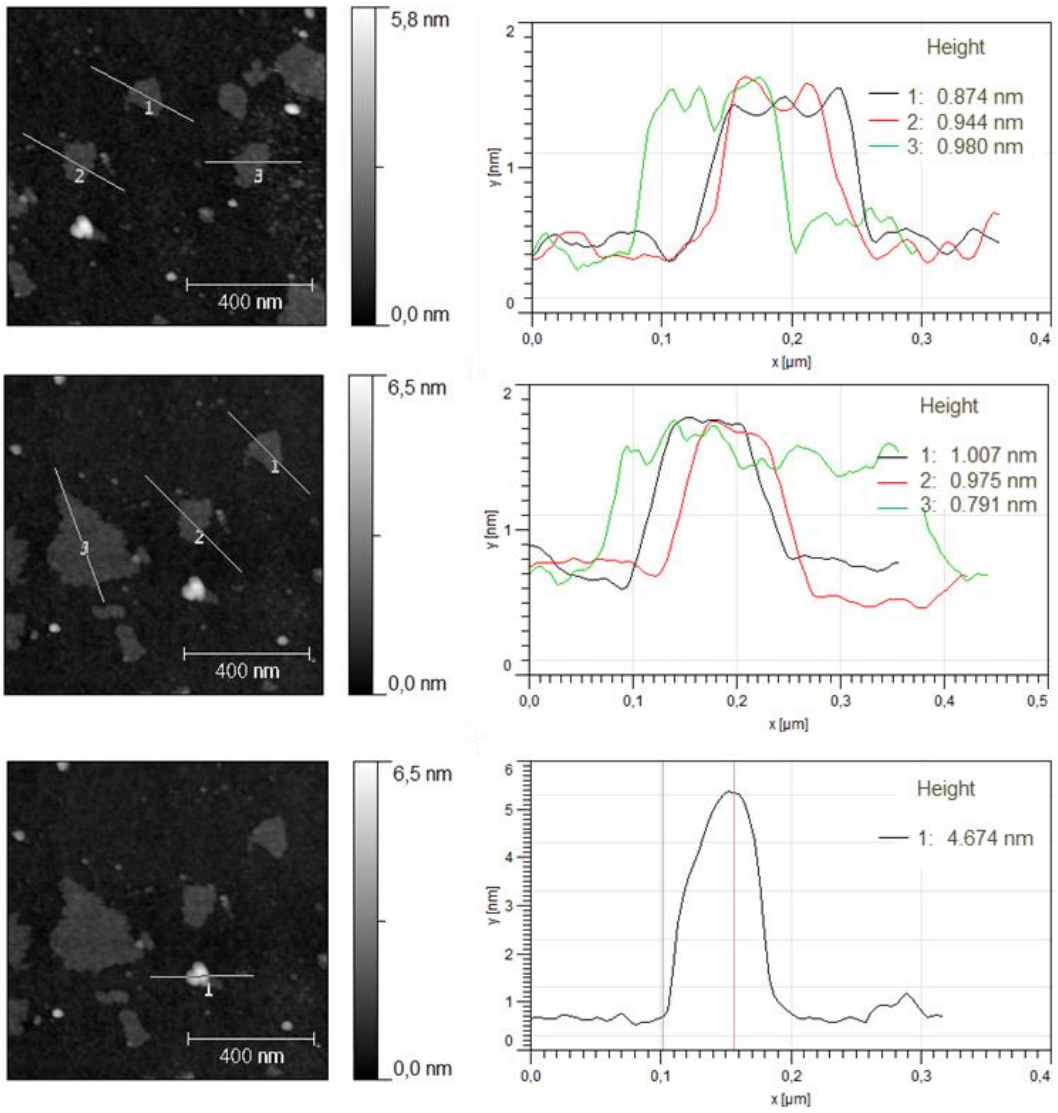

Figure 4.1.13 Height profiles of obtained nano-GO sheets.

As it can be seen from Figure 4.1.13, Majority of nano-GO sheets are present as single sheets and the height of them is changing in a range of 0.7-1.0 nm.

4.2. Modification of Graphene Oxide

After characterizing the obtained GO, the modifications of it were performed in two steps as described in part 3.3. The first one is attachment of ATRP initiator to –OH groups on GO surface. The esterification reaction took place in between Br-C=O

groups of initiator and – OH groups in the presence of excess TEA. TEA was added an acid scavenger to prevent pH changes due to formed HBr. The reaction was conducted under Ar atmosphere and at low temperatures to suppress the side reactions. The obtained black product is abbreviated as GO-Br which is a polymerization initiator for the next step. The schematic representation of the GO-Br synthesis is given in Figure 3.4.1, section 3.4.

For a successful ATRP it is crucial to evacuate all oxygen atoms in the media because the catalyst is sensitive to oxygen. The oxidized level of catalyst (Cu(II)) is not able to convert the dormant polymer chains to active forms. Consequently, the growing chain remains in dormant form and the polymerization stops. The instantaneous color change of the reaction is an important observation for oxygen presence. Used Cu(I)Cl and 2,2'-Bipyridine formed dark red colored solution in MeOH/water mixture, if the media is completely oxygen-free. Otherwise the color of solution turned to vivid green. The sacrificial initiator, EBiB, was added to reactor for characterizing the grafted polymer chains. GO-Br and EBiB are assumed to have same initiation efficiency, consequently the resulting polymer chains that originates by each of them have the comparable length in virtue of ATRP [129]. The schematic representation of surface-initiated polymerization of GO is given in Figure 3.5.1, section 3.5.

The photographs of modified GO derivatives can be seen from Figure 4.2.1. At the end of modifications, GO became fully dispersible in chloroform and the formed dispersions were stable for months. The improved solubility behavior of GO indicated that polymer grafting to GO was accomplished.

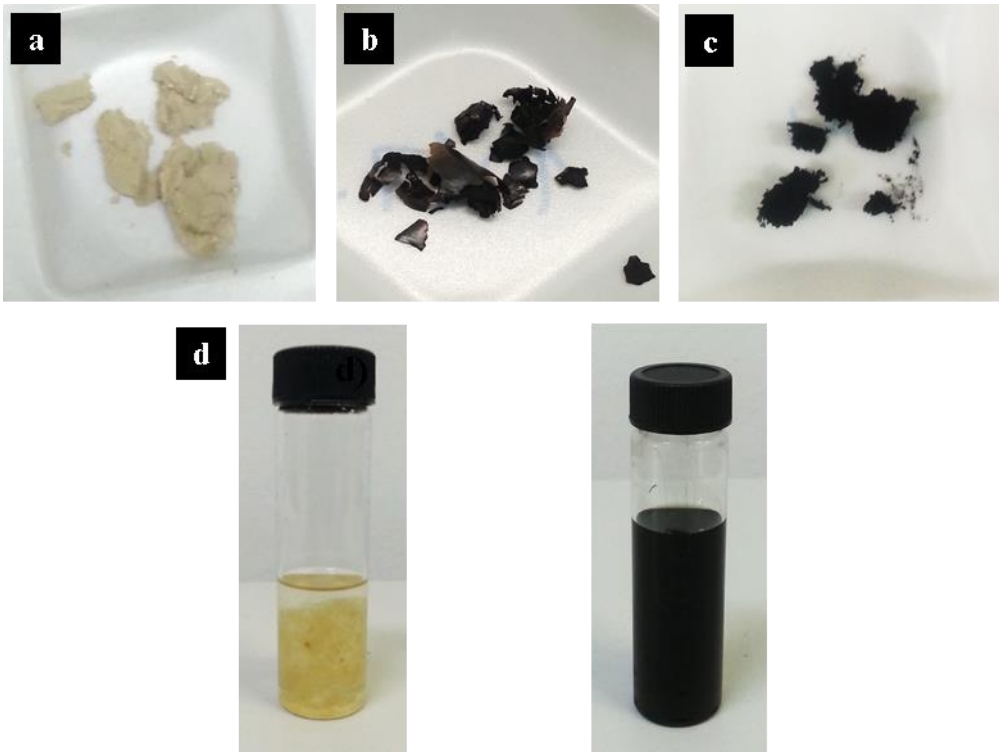

Figure 4.2.1 (a) nano-GO (b) GO-Br, (c) poly(PEGMA) grafted GO, and (d) improved solubility of poly(PEGMA) grafted GO in chloroform.

The chemical characterizations of modified GO derivatives were done by ATR-FTIR, XPS and TGA analyses. The chemical changes that occurred at every step of modifications can be easily seen from Figure 4.2.2. The peak that is caused by the presence of –OH groups was diminished after the esterification reaction in GO-Br spectrum. In this manner, the attachment of ATRP initiator was achieved. However, C-Br peak could not be observed due to the complex and massive structure of GO and low concentration of C-Br bond.

The green curve indicates free chains of poly(PEGMA) that propagated from EBiB, the sacrificial initiator. Therefore, the characteristic peaks of poly(PEGMA) were identified. Three important peaks are available for poly(PEGMA) O-C-O ether peak in 1000-1320 cm^{-1}, -C=O ester peak in 1750-1735 cm^{-1}, and C-H alkyl groups in 2750-3000 cm^{-1}.

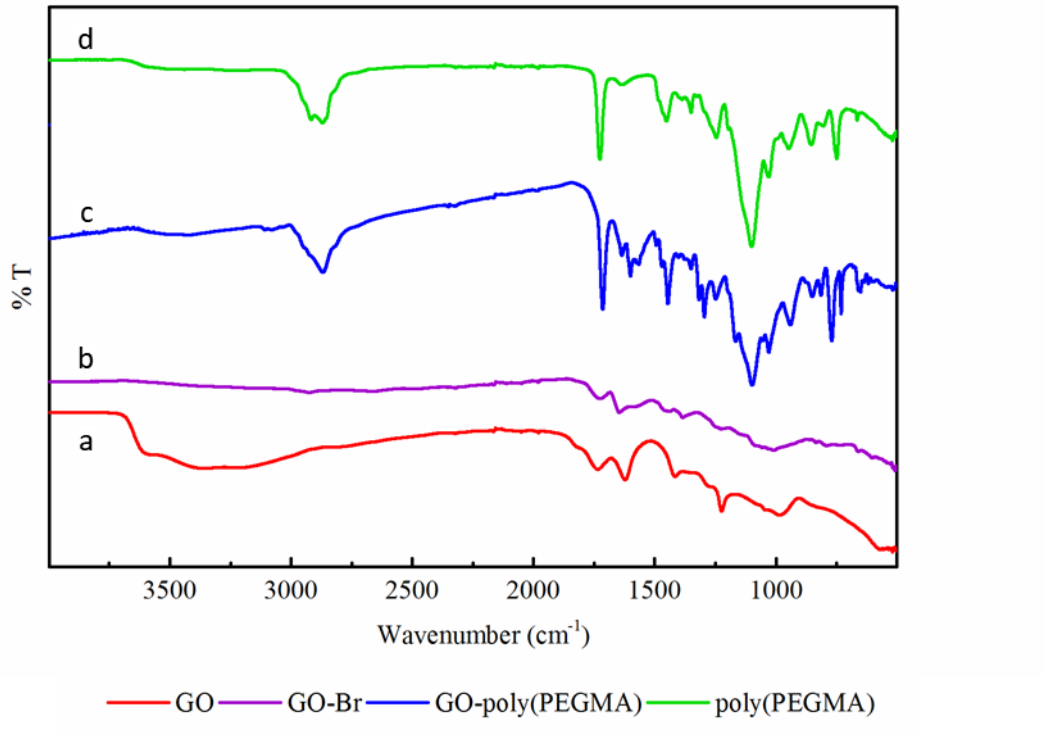

Figure 4.2.2 FTIR spectra of (a) obtained GO, (b) initiator modified GO, (c) poly(PEGMA) grafted GO and (d) free chains of poly(PEGMA).

All mentioned peaks were observed in GO-poly(PEGMA) spectrum (blue line). FTIR analysis confirmed that polymer grafting from GO surface was successful.

In order to investigate Br presence of GO and further chemical characterization, XPS measurements were performed and the results are given in both Figure 4.2.3 and Table 2.5.1. The changing intensities of C1s and O1s for two derivatives of GO can be observed from the given results. The most important point is the presence of Br3d peak which verified attachment of ATRP initiator to GO surface.

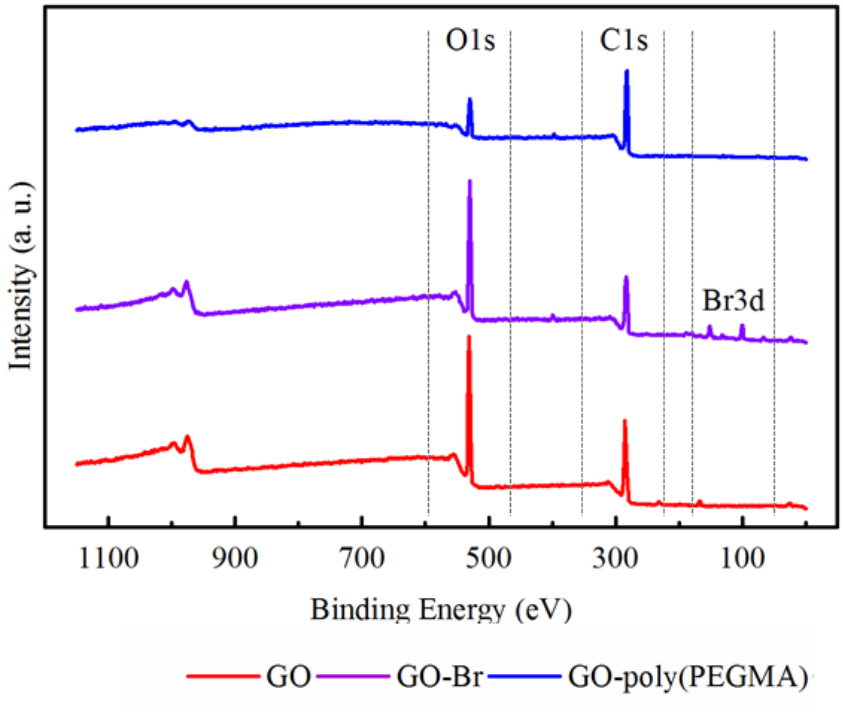

Figure 4.2.3 XPS spectra of obtained GO, initiator modified GO, poly(PEGMA) grafted GO.

Elemental content of related products is given in Table 4.2.1. The nitrogen source is likely due to environmental impurities. The atomic weight percentage of Br was calculated as 0.6. The changing amount of functional groups was also examined by curve fitting of C1s peaks.

Table 4.2.1 Elemental analysis of GO derivatives based ox XPS measurements.

	%C	**%O**	**%N**	**%Br**	**% Other**	**C/O**
GO	60.8	38	-	-	1.2	1.60
GO–Br	51.7	38	2	0.6	7.6	1.36
GO-poly(PEGMA)	81.7	15.7	2.1	-	0.5	5.20

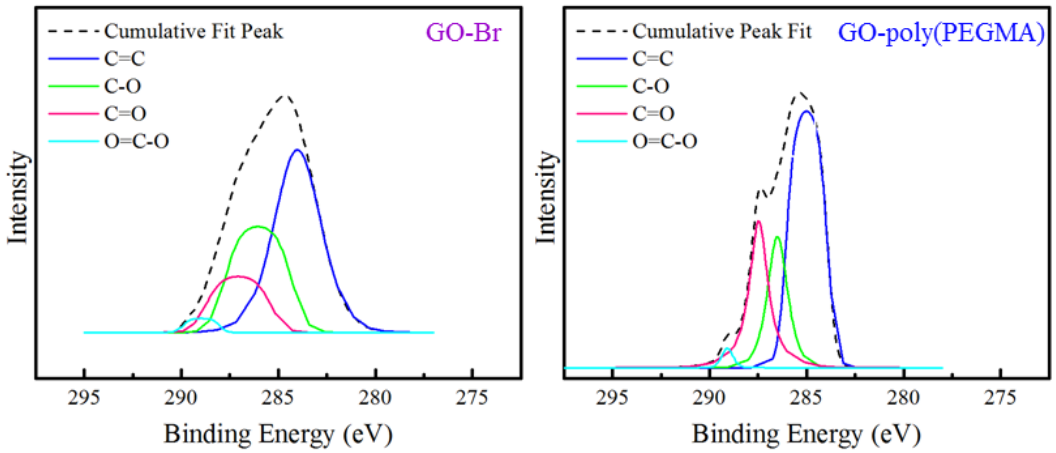

Figure 4.2.4 C1s core level spectra of initiator modified GO and poly(PEGMA) grafted GO

Figure 4.2.4 shows C1s core level spectrum of obtained GO-Br and GO-poly(PEGMA). The obvious decrease can be seen in –OH groups when compared to GO spectra. For poly(PEGMA) grafted GO, an increase can be seen in ester peak which came from poly(PEGMA) chains.

Thermal response of GO-Br and GO-poly(PEGMA) was recorded upon controllable heating of samples by using TGA. The result is given in Figure 4.2.5 and Table 4.2.2. With the additional content of poly(PEGMA), GO gained thermal stability of from 200 °C to about 350 °C decomposition temperatures. In addition to that, the increased weight loss from GO sample to GO-poly(PEGMA) sample is related to increase in percentage weight of carbon content.

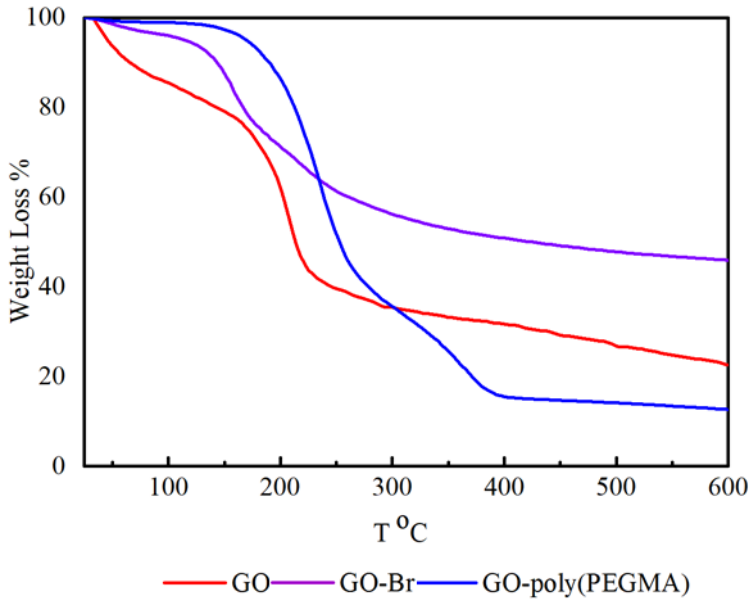

Figure 4.2.5 TGA curves of obtained GO, initiator modified GO, poly(PEGMA) grafted GO.

Table 4.2.2 TGA results for GO, GO-Br and GO-poly(PEGMA)

	GO	**GO-Br**	**GO-poly(PEGMA)**
$T_{decomp.}$, °C	208.65	156.51 218.87	236.62 363.23
% Weight Loss	77	54	87

NMR provides the information about chemical structure. Thus, the structural feature of grafted poly(PEGMA) was verified with ^{1}H-NMR measurement and the results are given in both Figure 4.2.6 and Figure 4.2.7.

Figure 4.2.6 show the results of the solution of monomer and polymer while Figure 4.2.7 includes only polymer solution. %Conversion was calculated based on the ratio of PEGMA concentration to initial PEGMA concentration.

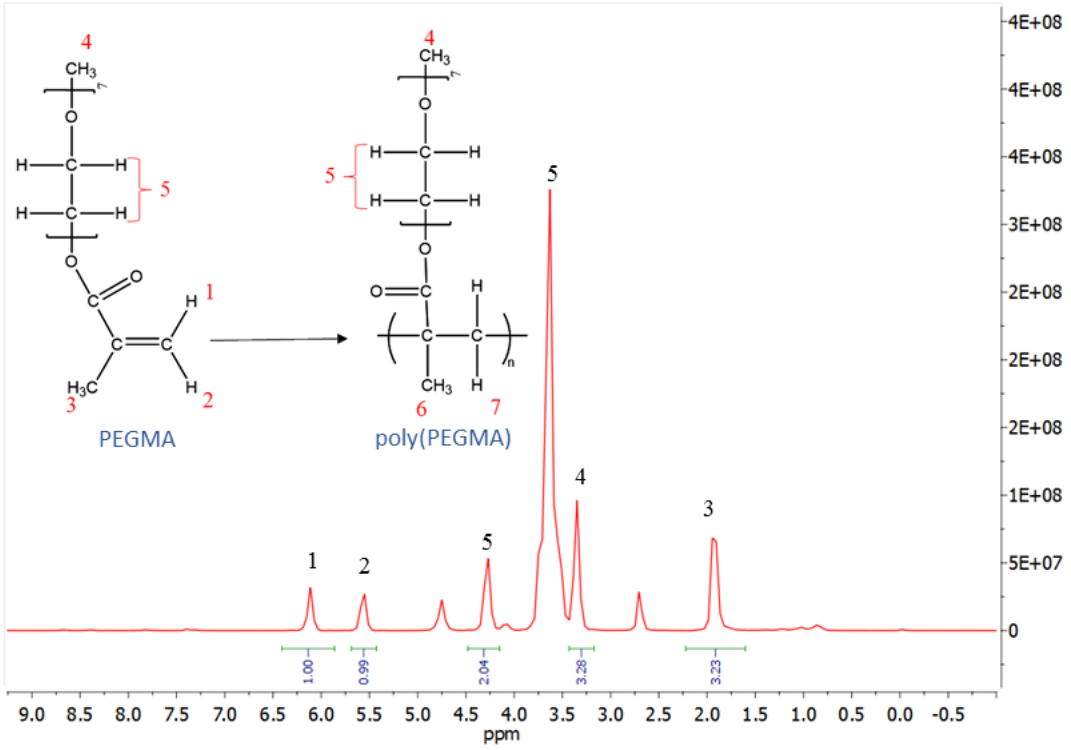

Figure 4.2.6 NMR spectrum of the solution includes poly(PEGMA) and PEGMA

The peaks of caused by vinyl protons (1,2) were observed at 5.8 and 6.15 ppm for only PEGMA monomer. And also, the intense peaks that were observed in between 3.0 and 4.5 ppm were assigned to protons of methylene groups (4,5) for poly(PEGMA). By using the area under the peaks, %conversion of monomer was calculated as about 70%. The ideal conversion is present in the range of %70-80 for terminating the polymerization without losing end group functionality. In this manner, reaction conditions in ATRP is suitable.

When compared to Figure 4.2.7 with Figure 4.2.6, the diminish of peaks 1 and 2 was observed due to polymerization and new peaks (6,7) were arisen at 0.5-2.0 ppm caused by the protons in the polymer backbone. In addition to that, the increased intensity of the peaks in between 3.5-4.5 ppm was observed.

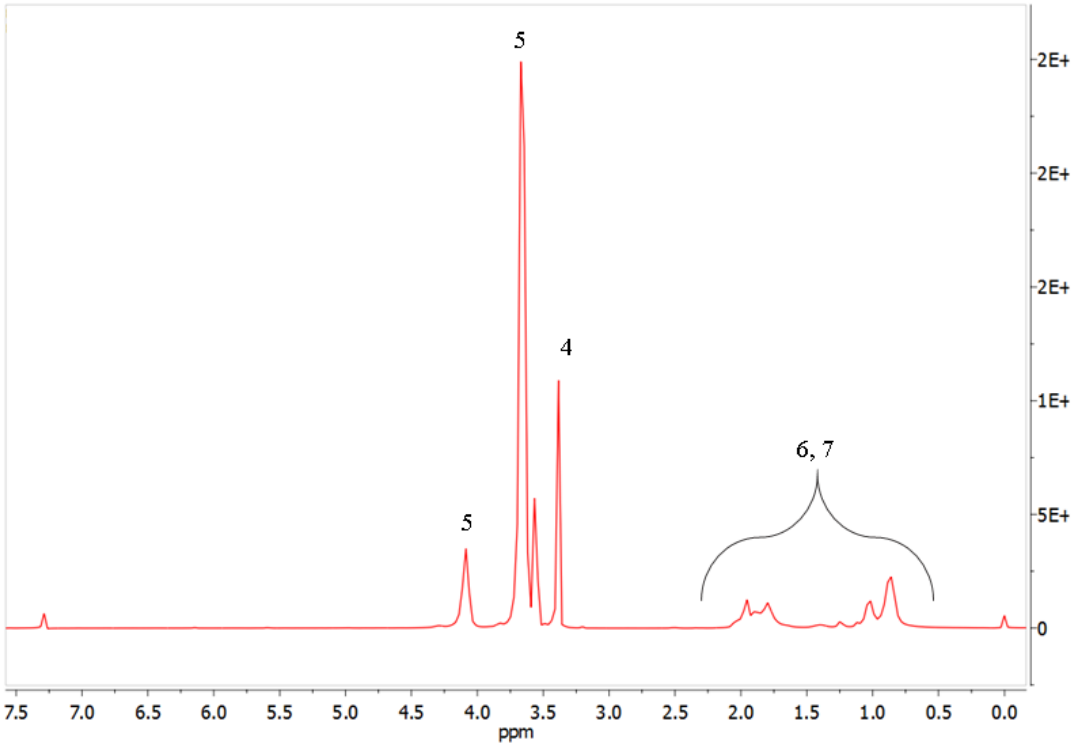

Figure 4.2.7 NMR spectrum of the solution including only poly(PEGMA)

GPC is a powerful instrumental analysis tool for molecular weight determination of polymers. The polymer solution is fed into a packed-column, and polymer chains are moving through the column at different rates according to their chain length (*i.e.* size). Resulting signal is shaped due to molecular weight of polymer chains and its distribution. The molecular weight of obtained poly(PEGMA) was determined using GPC and the result is given in Figure 4.2.8. The output signal is sharp and unimodal due to narrow distribution of molecular weight of polymer chains as expected since ATRP provides higher control over molecular weight compared to conventional free radical polymerization. It was found that $\bar{M}_n$value of poly(PEGMA) was 40000 g/mol and $\bar{M}_w$ was about 45000. The PDI value of obtained poly(PEGMA) was calculated as 1.13. PDI values lower than 1.2 is usually accepted as an indicator of controlled polymerization.

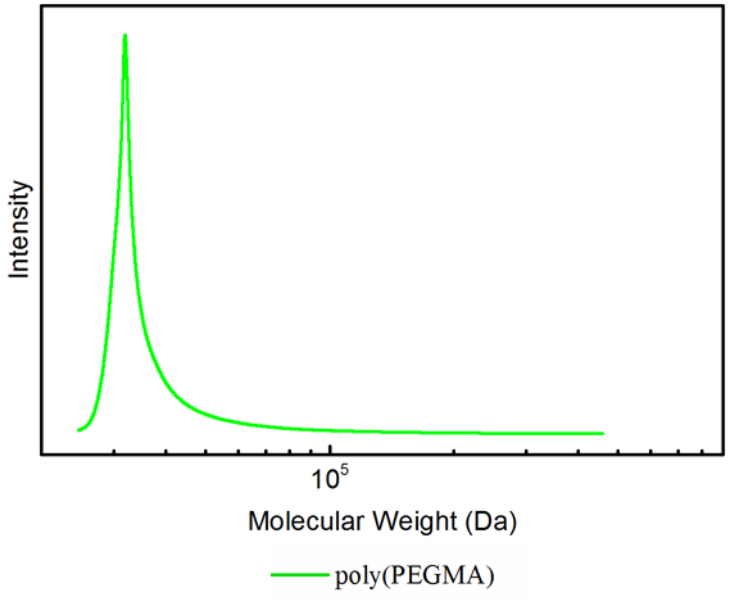

Figure 4.2.8 GPC output signal of obtained poly(PEGMA)

4.3. Development of Microsieve Production by Optimization of Breath Figure Parameters

Chloroform is a proper solvent for PSF and also it is one of most commonly used solvents in the BF process. Hence PSF-Chloroform system was chosen for BF studies. The work flow for the fabrication methodology of microsieves is given in Figure 4.3.1. Firstly, pore formation on the polymer surface was obtained by optimizing concentration of PSF and GO-poly(PEGMA) under suitable evaporation rate. Then adjustment of pore size was achieved by changing relative humidity. Finally, obtained pores were forced to become through pores by the help of interaction between a hydrophilic substrate and water droplets. For this purpose, PVA coated glass, dextran coated glass and water were used as hydrophilic substrates. Besides, it was observed that, the evaporation rate of the solvent is also affected on obtaining through pore structures. Investigated parameters and their effects were discussed in detailed as follows.

PSF concentration in solution (mg/ml), GO-poly(PEGMA) concentration in solution (mg/ml) (or it can be mentioned as the weight ratio of PSF to GO-poly(PEGMA) (mg/mg)), air flow rate of incoming air (LPM) (L/min), relative humidity (%RH), Casting volume (V) and humid air flow time (t) were investigated as parameters on pore formation.

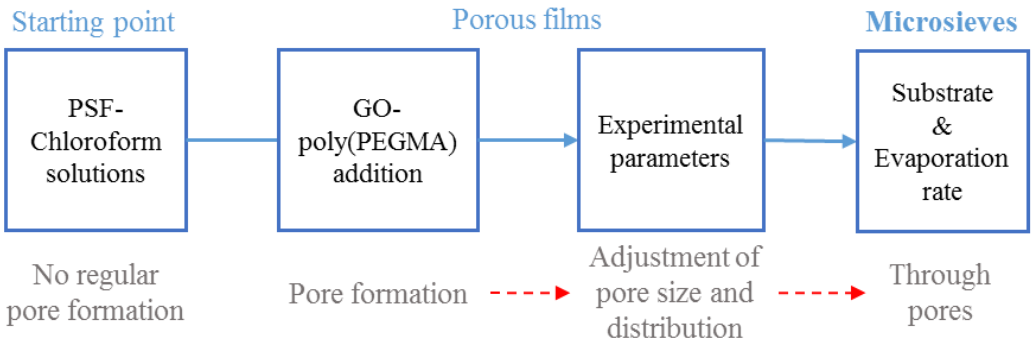

Figure 4.3.1 The methodology for obtaining microsieves via BF method.

Concentration is the most important parameter for the pore formation. Obtained surfaces by using only PSF-Chloroform solution were given in Figure 4.3.2.

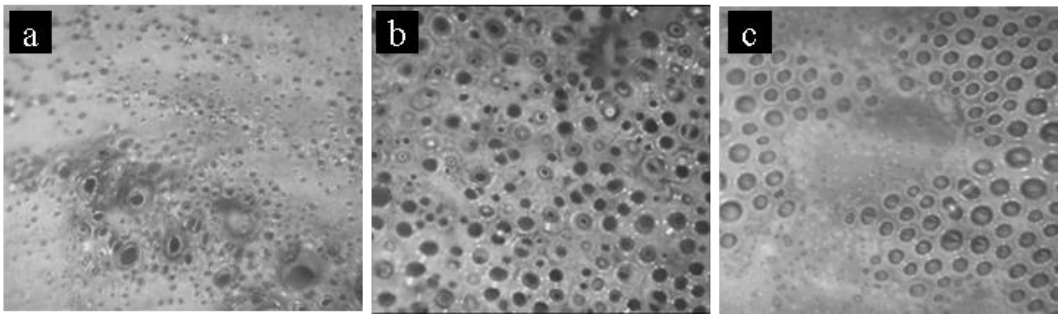

Figure 4.3.2 Microscopic images of PSF films of (a) 20 mg/ml (b) 40 mg/ml and (c) 60 mg/ml PSF-Chloroform solutions. Experimental conditions; RH: 70-75%, LPM: 0.1, V: 200 µl, t: 200 s. (50x magnification).

Only PSF itself was not able to stabilize water droplets and arrange them in order to form regular honeycomb patterns due to its hydrophobic nature and linear structure.

Locally formed pores with different sizes were present in Figure 4.3.2. It was observed that increased concentration of PSF has a little influence on pore formation. On the other hand, after the addition of a little amount of GO-poly(PEGMA) to solution very regular pore structures were obtained under same conditions. The effect of GO-poly(PEGMA) addition can be seen from Figure 4.3.3.

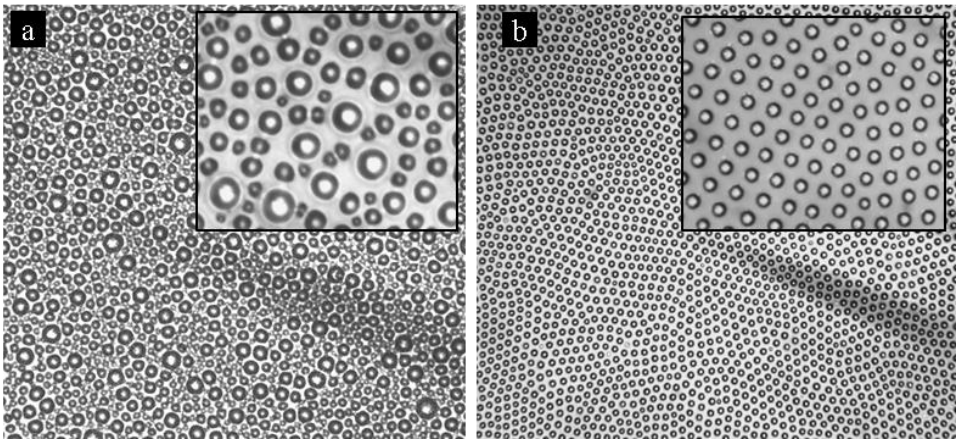

Figure 4.3.3 Microscopic images of polymeric films of GO-poly(PEGMA)-Chloroform with different concentrations of PSF-Chloroform: (a) 20 mg/ml (b) 40 mg/ml. The weight ratio of GO-poly(PEGMA) to PSF was set to 100/1. Experimental conditions; RH: 70-75%, LPM: 0.1, V: 200 µl, t: 200 s. (20x and 100x magnifications).

The same weight ratio of GO-poly(PEGMA) to PSF (100/1) was not enough for obtaining uniform honeycomb BF films in the case of 20 mg/ml concentrated PSF solution. On the contrary, Figure 4.3.3-b shows very regular surface properties for 40 mg/ml PSF-Chloroform solution. Formed pores were uniformly distributed on the surface with an average pore size of 2-2.5 µm. This indicates that the concentration of PSF in the solution is more effective than the weight ratio of PSF to GO-poly(PEGMA) on pore formation.

The effect of GO-poly(PEGMA) concentration for 20 mg/ml solution was examined and the results are given in Figure 4.3.4. It was observed that higher amounts of GO-poly(PEGMA) is needed for lower concentrated solutions of PSF to obtain regular honeycomb patterns.

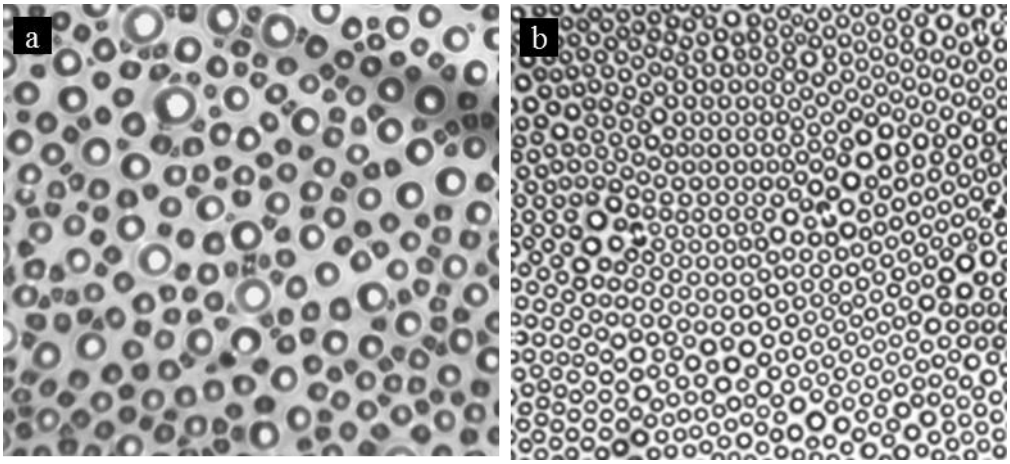

Figure 4.3.4 Effect of GO-poly(PEGMA) amount in 20 mg/ml PSF-Chloroform solution with weight ratio of PSF/GO-poly(PEGMA) (a) 100/1 and (b) 100/5 mg/ml. Experimental conditions: RH: 70-75%, LMP: 0.1, V: 200 µl, t: 200 s (100x magnification).

The regular pattern for 20 mg/ml PSF-Chloroform solution was obtained with GO-poly(PEGMA) having a concentration of 1 mg/ml. The surface which is given in Figure 4.3.4-b shows higher average pore size when compared to Figure 4.3.3-b due to decreasing concentration of PSF.

This situation can be explained with Raoult's law.

$$P_i = P_0.(1 - X_p)$$

Where P_i is the partial pressure of solvent in gas phase, P_0 is the vapor pressure of pure solvent, and X_p is the mole fraction of the polymer. According to that, more concentrated solutions have lower partial pressures. Formation of water droplets on the polymer surface and their merging into bigger droplets are directly related to the temperature difference between the surface temperature and ambient temperature. Since low vapor pressure leads to slow evaporation of the solvent, temperature of the surface remains high which results in obtaining smaller droplets. Evaporation rate of the solvent is a key factor on determining pore morphology.

Air flow rate is the most important parameter for optimizing evaporation rate of the solvent. It provides the necessary time for stabilization of water droplets packed into regular structures. The higher flow rates facilitate fast evaporation and consequently, polymer solidifies in a way to form irregular surface properties in both macroscopic and microscopic levels.

Figure 4.3.5 and Figure 4.3.6 show the effects of air flow rate on surface morphology. Figure 4.3.5 -a,b represent the samples of fast evaporation (above 0.5 L/min). Polymer solidified before pore formation and resulted in white opaque polymer films. Conversely, Figure 4.3.5 -c shows a slowly evaporated sample which formed a transparent film that was well dried without leaving evaporation marks. Besides, addition of GO-poly(PEGMA) enhances the homogeneous film formation with well coverage behavior. Figure 4.3.5-d shows a sample which includes GO-poly(PEGMA). Appearance of the film (d) looks more homogeneous and fully covered on substrate

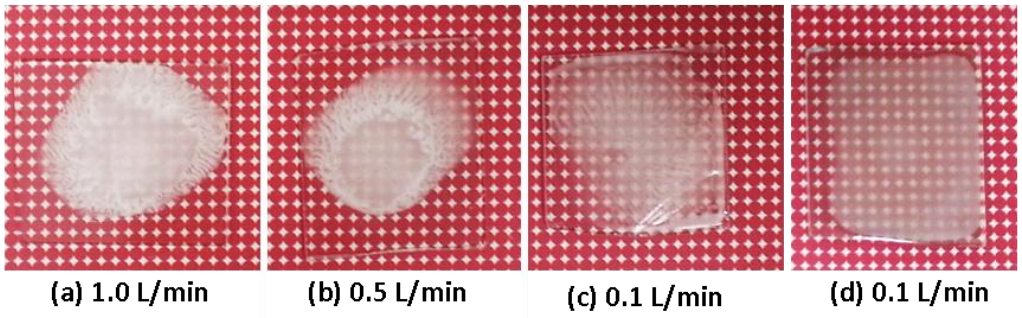

Figure 4.3.5 Effect of air flow rate on physical properties of surface. Only sample (d) includes GO-poly(PEGMA) with a concentration of 0.4 mg /ml. (Casting volume was 200 µl).

Figure 4.3.6 shows the effect of evaporation rate on pore formation. The regular structure was only obtained under the slow evaporation rate. Therefore, 0.1 L/min was chosen as optimal humid air flow rate of the current system.

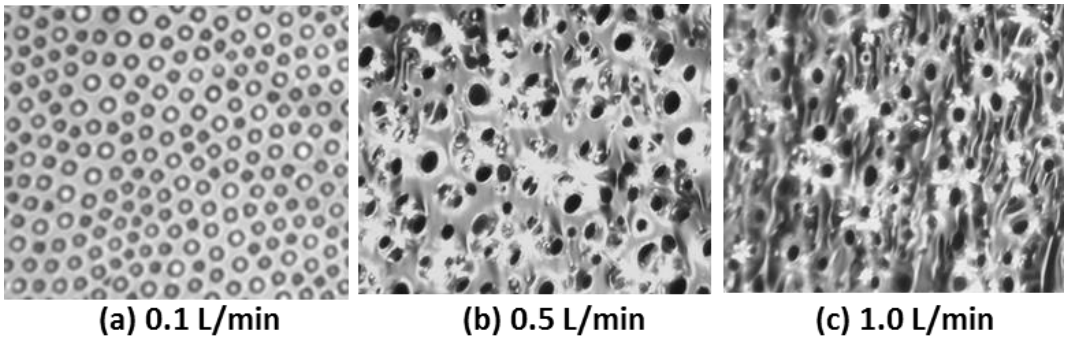

Figure 4.3.6 Effect of air flow rate on pore formation (casting volume was 200 µl).

So far, the effects of concentration and air flow rate (*i.e.* evaporation rate) on pore formation and homogeneous film formation were investigated. Based on the results, the following observations have been made and conclusions were drawn:

- Polymer concentrations lower than 40 mg/ml of PSF were not able to fully cover the substrate surface after evaporation process, which resulted in obtaining insufficient membrane area for the module. Higher casting volumes than 200 µl of diluted solutions led to irregular surface properties. Therefore, it can be said that there exists a tradeoff between surface morphology and the membrane surface area.
- For microsieve applications, it is considered that having small average pore size is the best for getting efficient filtration performance. Therefore, 40 mg/ml concentration of PSF-Chloroform which includes GO-poly(PEGMA) concentration of 0.4 mg/ml was chosen for microsieve production. Besides that, best coverage performance while drying of polymer film was observed with that solution.

In the literature, the relation between relative humidity and pore diameter have been shown in several studies [109]–[112]. Higher amount of relative humidity resulted in surfaces covered with larger pores due to the higher content of water in the environment. Figure 4.3.7 shows the change in average pore sizes by increasing relative humidity.

As previously mentioned, considering the filtration performance of microsieve, the smallest average pore size is preferred. By holding the relative humidity between 70-75% the smallest possible average pore size was obtained. It is possible to obtain larger average pore size by increasing humidity for different applications. Average pore size of 4-4.5 micrometers was obtained under 80-85% relative humidity while average pore size of 6-6.5 micrometers was obtained under 90-95% relative humidity.

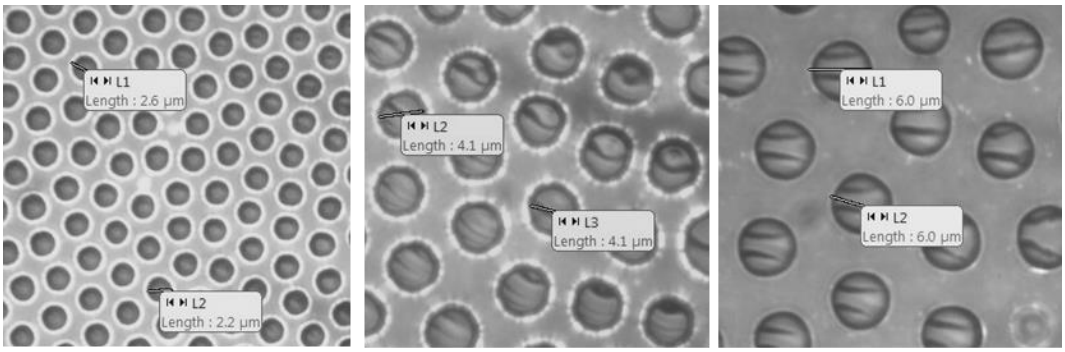

Figure 4.3.7 Effect of relative humidity on average pore size: (a) 2-2.5 µm at RH=70-75%, (b) 4-4.5 µm µm at RH=80-85%, and (c) 6-6.5 µm µm at RH=90-95%.

The final step for the fabrication of microsieves is converting the formed pores into open pores throughout the membrane cross-section. Hydrophilicity of the used substrate is directly related to pore shape as previously mentioned. Condensed water droplets on the polymer surface are attracted by hydrophilic surface and it facilities the movement of water droplets downward through the membrane. Besides, evaporation rate of the solvent is also a decisive parameter for resulting through pores. Water droplets can be move downward before polymer solidifies. 40 mg/ml PSF-Chloroform solution which includes 0.4 mg/ml concentrated GO-poly(PEGMA) solution was casted onto PVA coated glass, dextran coated glass and water with 200 µl aliquots under 70-75% relative humidity and with air flow rate of 0.1 L/min. Prepared membranes are listed on Table 4.3.1 according to different used substrates. Afterwards, surface and cross section area of obtained membranes were examined by

SEM analysis. Filtration performances were tested with water and yeast solution (0.24 mg/ml).

Table 4.3.1 List of prepared microfiltration membranes

Membrane	% Conc. (wt/v) PsF-Chloroform	Weight ration of Psf/GO-poly(PEGMA) (wt/wt)	Substrate
A	4	100/1	PVA-Glass
B	4	100/1	Dextran-Glass
C	4	100/1	Water

Figure 4.3.8 shows the physical appearance of obtained membranes and they were able to easily be transferred into filtration module.

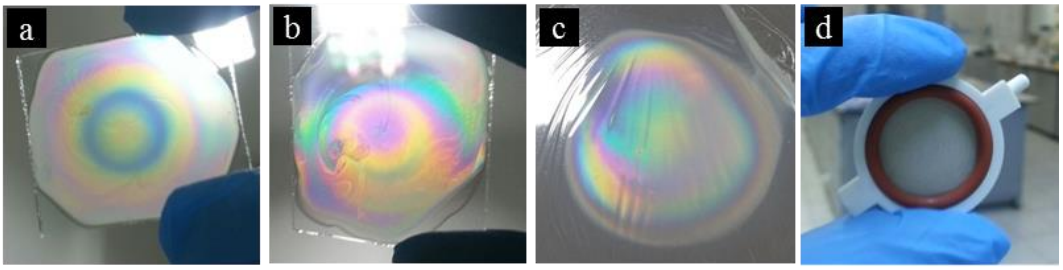

Figure 4.3.8 Photographs of obtained membranes from casted on (a) PVA coated, (b) dextran coated glasses and (c) water. (d) Membrane was transferred into filtration module.

Figure 4.3.9 illustrates the SEM images of obtained Membrane-A from casted on PVA coated glass with a 200 µl casting volume. The surface morphology shows a very regular structure which has well-arranged pores with uniformly distributed through the surface area. The average pore diameter was approximately 2.5 µm and the film thickness was 10 µm. Formed pores on the top surface could not reached through the bottom surface. The depth of the pores was almost 2.5 µm. Bottom surface of the film looks like a non-porous surface. Although Membrane-A has a dead-end pore structure according to SEM images, in the present case, water permeation and yeast filtration experiments could not be performed with these membranes due to very low flux.

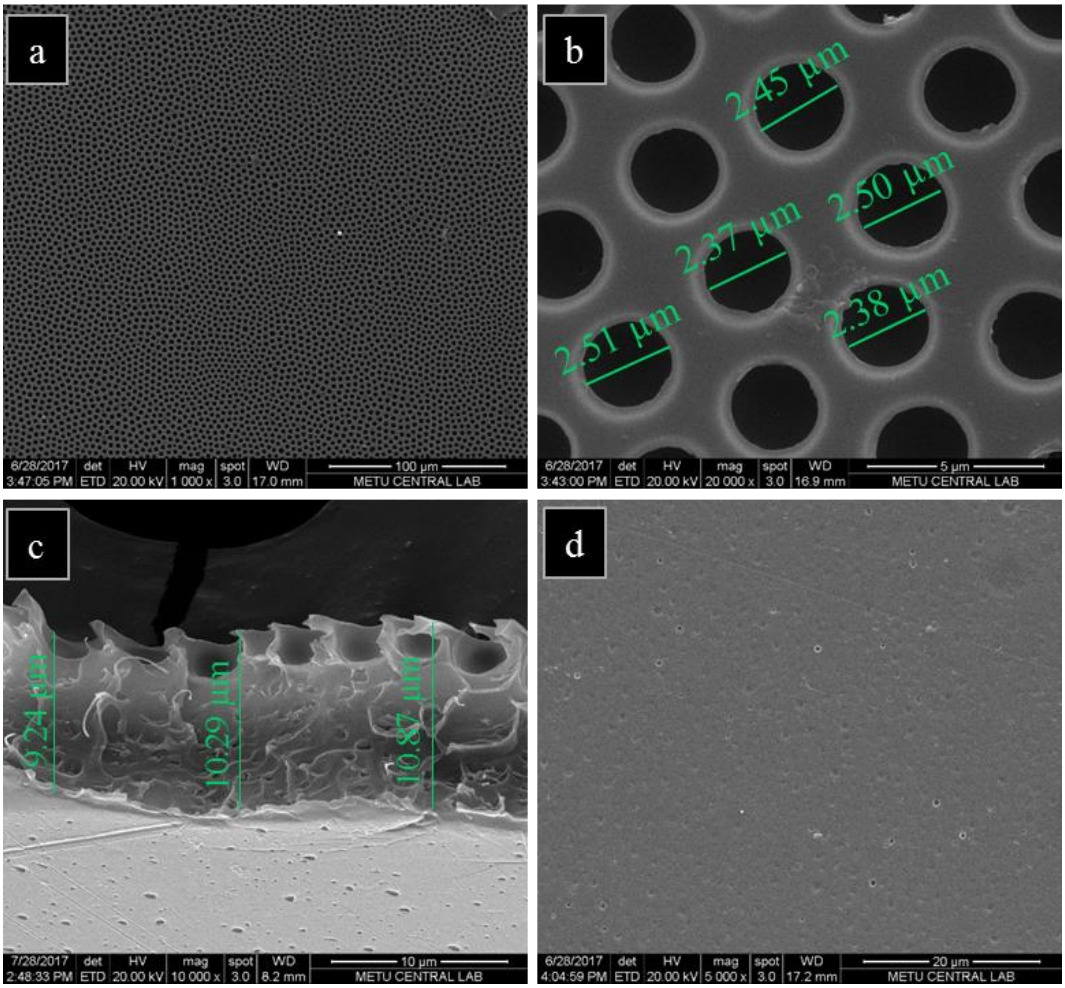

Figure 4.3.9 SEM images of (a), (b) top surface, (c) cross-section and (d) bottom surface of Membrane-A which was casted on PVA coated glass with a volume of 200 µl SEM images.

A similar situation was observed for the case of dextran coated glass as it can be seen from Figure 4.3.10.

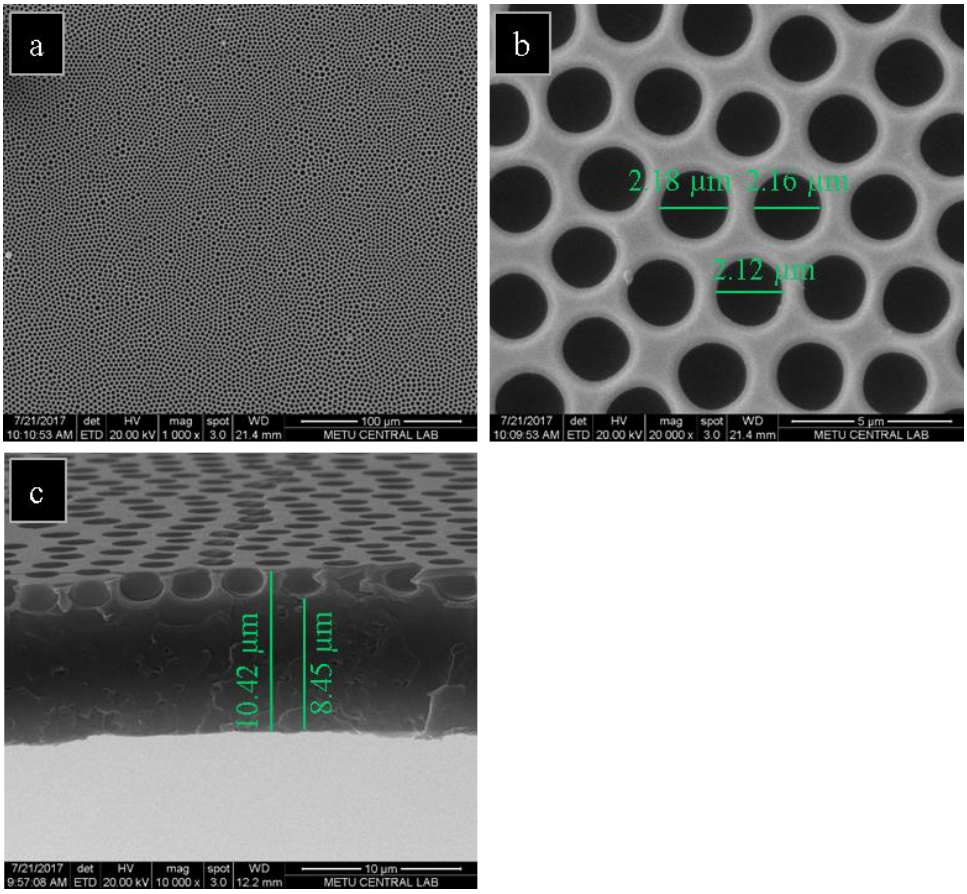

Figure 4.3.10 SEM images of (a), (b) top surface and (c) cross-section of Membrane-B which was casted on dextran coated glass with a volume of 200 µl SEM images.

Using water as substrate was considered for obtaining better results. However, it was harder to cast on water and spread the solution than glass surface. Since chloroform has higher density than water and hydrophobic nature of PSF. A volume of 200 µl of the solution was dropped on water, it immediately soaked into water and formed a bubble. Then the excess water was sucked which led to bubble popped out and spread. It was considered that a very thin layer of water was remained underneath of the casted solution. SEM images of the obtained membrane is given in Figure 4.3.11. Membrane-C shows varying pore size from 6 micrometer to 8 micrometer and a lower thickness. The water permeance of Membrane-C has been improved. However, the yeast filtration through the Membrane-C resulted with very low rejection.

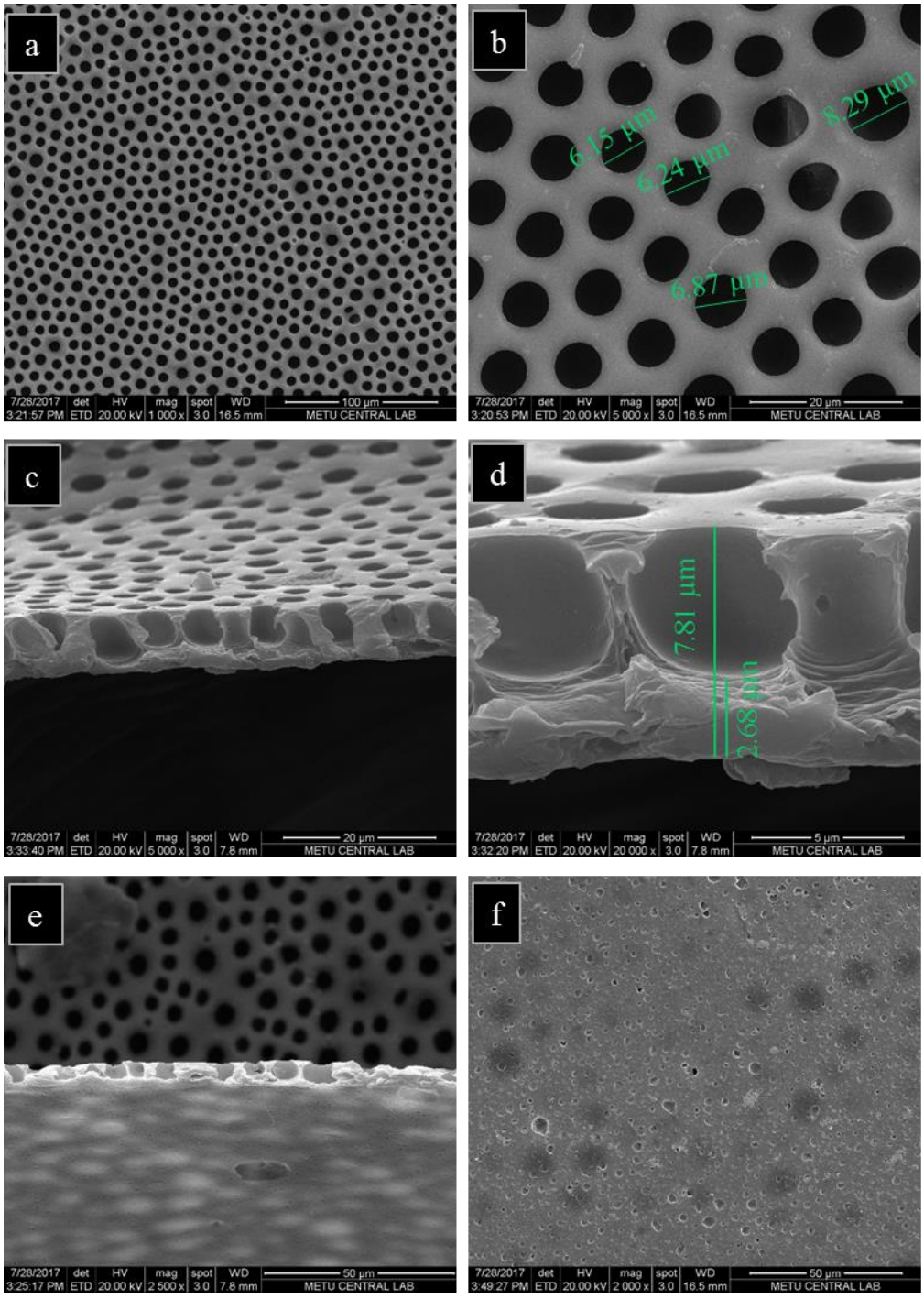

Figure 4.3.11 SEM images of (a), (b) top surface, (c), (d) cross-section and (e), (f) bottom surface of Membrane-C which was casted on water with a volume of 200 µl.

When the results of Membrane-A, Membrane-B and Membrane-C were taking into consideration, two different routes could be followed to obtain through pore structure:

- Film thickness can be decreased by decreasing concentration of the solution or reducing casting volume. However, these suggestions lead to obtaining films having small surface area as mentioned earlier. And changing concentration of PSF would lead to readjustment of all decided parameters.

- Evaporation rate of the solvent can be slowed down by decreasing air flow rate or decreasing the vapor pressure of the solvent. But the lower values of air flow rate also influence the relative humidity adversely. Therefore, it was decided to decrease the vapor pressure of solvent to slow down the evaporation.

Hence, 1,2-Dichloroethane (T_{bp}= 83.5 °C) which has higher boiling point than chloroform (T_{bp}= 61.2 °C) was added to solution with a volume ratio of 1:1. Obtained membrane was named as Membrane-D and the surface morphology and the cross section were examined by SEM. Water permeation and yeast filtration were also performed. The results related to Membrane-D were given in Figure 4.3.12.

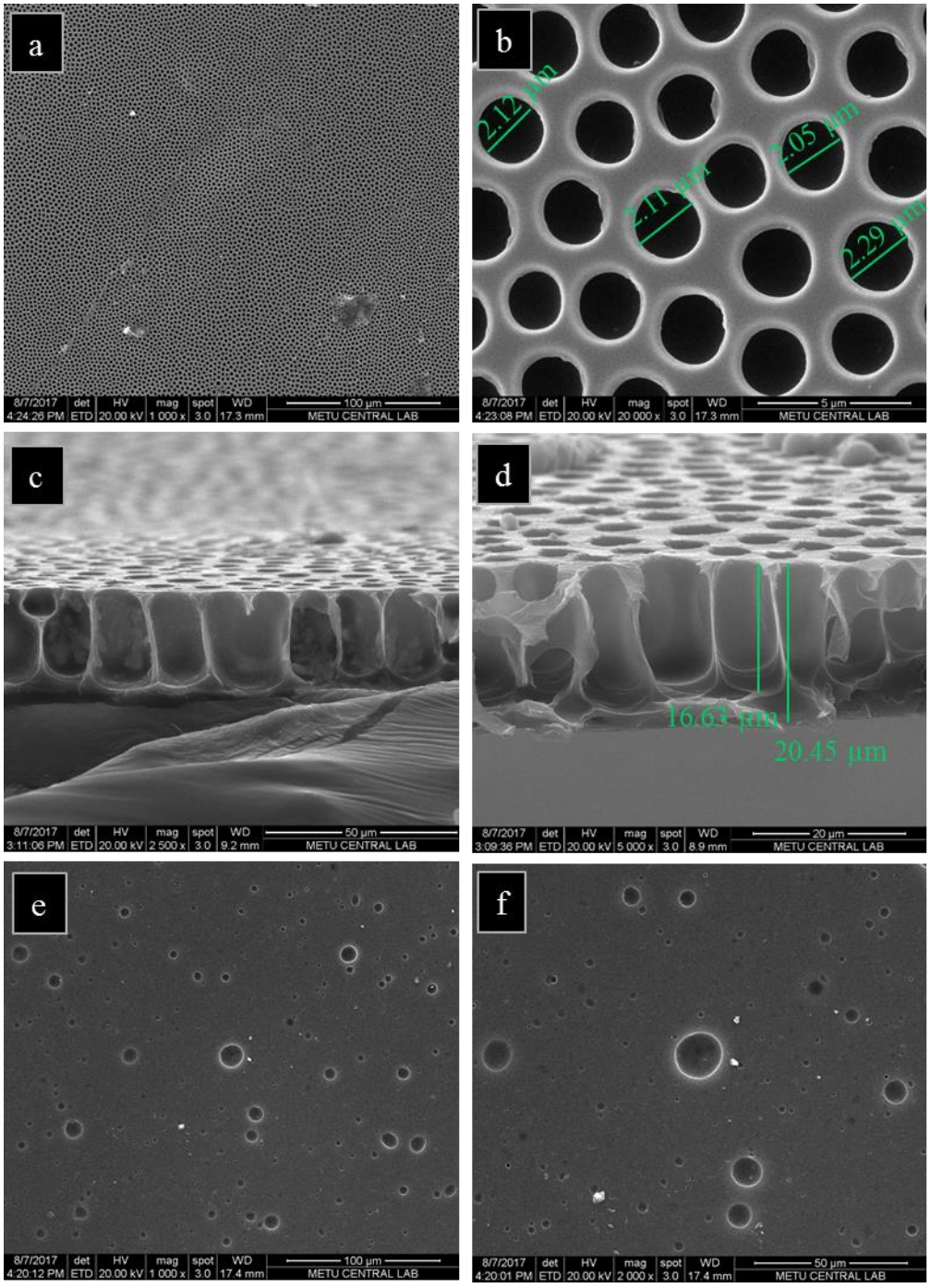

Figure 4.3.12 SEM images of (a), (b) top surface, (c), (d) cross-section and (e), (f) bottom surface of Membrane-D which was casted on water with a volume of 200 µl.

From Figure 4.3.12, average pore size for Membrane-D was about 2.1-2.3 μm. Pore depth increased from 2-3 micrometers to about 17 micrometers due to slow evaporation of solvent. Water droplets were able to move downward through the cross-section of membrane before PSF solidifies. The huge increment in thickness may be explained with increasing pore depth per unit area within the membrane. A great improvement was obtained on larger pore depth which resulted better water permeation performance and yeast filtration through the membrane was achieved.

Table 4.3.2 contains the theoretical and measured water permeance results and Table 4.3.3 contains yeast filtration performance by calculating percentage rejection for both Membrane-C and Membrane-D.

Table 4.3.2 Measured and calculated water permeance values for membrane C and D.

	($L/h.m^2.bar$)		
	Water Permeance (measured)	Water Permeance (calculated)	Yeast Permeance
Membrane C	27681 ± 7830	51.8×10^6	235 ± 177
Membrane D	305 ± 277	1.9×10^6	4.3 ± 2.2

According to measured and theoretical water permeance results, Membrane-C has higher permeability due to smaller thickness and bigger average pore size than Membrane-D. For both membranes, theoretical permeance is much larger than experimental ones which is caused by all formed pores were not in through pore structure.

Table 4.3.3 Yeast filtration performance and percentage rejection for membrane C and D.

		Permeate Concentration (mg/ml)				
	Feed Concentration (mg/ml)	#1	#2	#3	#4	%R
Membrane C	0.24	0.195	0.208	0.192	0.184	18.9 ± 4.2
Membrane D	0.24	0.01	0.028	0.043	0.032	88.2 ± 5.7

Four different membranes were produced in the same way for both Membrane-C and Membrane-D. They were tested by filtering 0.24 mg/ml yeast solution. Figure 4.3.13 shows the filtration performance of Membrane-D. Collected permeate was a quite clear solution due to high rejection to yeast. Membrane-C was not effective for yeast filtering due to larger average pore size than yeast particles. Table 4.3.3 shows concentration of collected permeates for each test. A calibration curve was drawn to illustrate the relation between yeast concentration and absorbance at 600 nm which can be found in Appendix A.

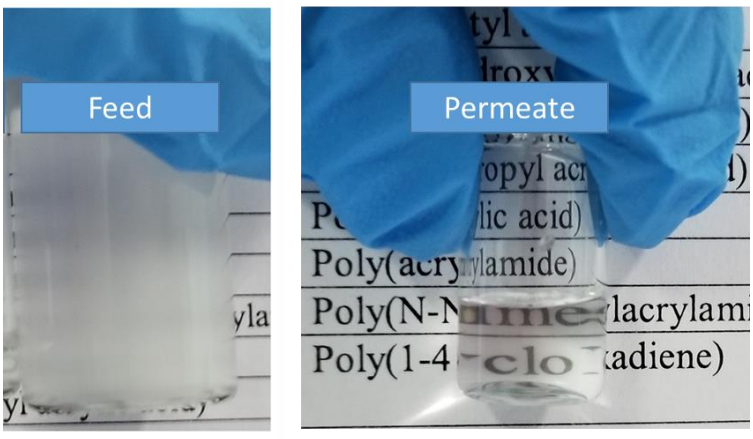

Figure 4.3.13 Digital photographs of feed yeast solution to be filtered and collected permeate with Membrane-D.

CHAPTER 5

CONCLUSION

In this study, it is intended to fabricate PSF microsieves via breath figure self-assembly method by using poly(PEGMA) grafted GO as a droplet stabilizer in the breath figure process.

To achieve this, first GO was synthesized and performed spectroscopic characterizations confirmed that GO has three main functional groups of hydroxyl, epoxide and carboxylic acid. Nano-sized GO sheets were obtained by the utilization of ultrasonication and centrifuge processes. It was observed that ultrasonication and followed by centrifuge is an efficient method for reducing lateral size of GO sheets in nano-scale with a unimodal distribution.

Nano-sized GO sheets were decorated with hydrophilic poly(PEGMA) chains for improved solubility and hydrophilicity by means of ATRP. Obtained GO-poly(PEGMA) product showed high dispersibility in chloroform. No precipitation was observed for months indicating that the dispersions were highly stable. Benefiting from its hydrophilic nature, poly(PEGMA) grafted GO sheets were used as a hydrophilic additive for the stabilization of water condensation during BF method. It was observed that the addition of GO-poly(PEGMA) into PSF solution resulted in obtaining highly uniform porous structures. Decreasing PSF concentration or increasing relative humidity resulted in obtaining larger average pore size. Besides using a hydrophilic substrate, slower evaporation rates of the solvent affected obtaining open pore structures. Increasing boiling point of used solvent by the addition of 1,2-Dichloroethane resulted in larger pore depth.

As a conclusion, GO based nanocomposite PSF microfiltration membranes were obtained via BF self-assembly method. Their filtration performance was measured by filtering a yeast solution. Results showed that obtained membranes can be used for yeast filtration. It was observed that Membrane-D has a great potential in microfiltration applications with a percentage rejection of 88. It can be further improved by decreasing the film thickness. More importantly this study holds a great potential to fabricate cost effective and efficient microsieves by further optimizing the experimental parameters.

REFERENCES

[1] R. Shah, A. Kausar, B. Muhammad, and S. Shah, “Progression from Graphene and Graphene Oxide to High Performance Polymer-Based Nanocomposite: A Review,” *Polym. Plast. Technol. Eng.*, vol. 54, no. 2, pp. 173–183, Jan. 2015.

[2] R. B. Mathur, B. P. Singh, and S. Pande, *Carbon Nanomaterials: Synthesis, Structure, Properties and Applications*. CRC Press, 2017.

[3] I. V. G. and A. A. F. K. S. Novoselov, A. K. Geim, S. V. Morozov, D. Jiang, Y. Zhang, S. V. Dubonos, “Electric Field Effect in Atomically Thin Carbon Films,” *Science (80-.).*, vol. 306, no. 5696, pp. 666–669, 2004.

[4] C.-Y. Su *et al.*, “Highly Efficient Restoration of Graphitic Structure in Graphene Oxide Using Alcohol Vapors,” *ACS Nano*, vol. 4, no. 9, pp. 5285–5292, Sep. 2010.

[5] S. Wang, P. K. Ang, Z. Wang, A. L. L. Tang, J. T. L. Thong, and K. P. Loh, “High Mobility, Printable, and Solution-Processed Graphene Electronics,” *Nano Lett.*, vol. 10, no. 1, pp. 92–98, Jan. 2010.

[6] S. K. Saha *et al.*, “Solution-Processed Reduced Graphene Oxide in Light-Emitting Diodes and Photovoltaic Devices with the Same Pair of Active Materials,” *RSC Adv.*, vol. 4, no. 67, pp. 35493–35499, Aug. 2014.

[7] D. Song, A. Mahajan, E. B. Secor, M. C. Hersam, L. F. Francis, and C. D. Frisbie, “High-Resolution Transfer Printing of Graphene Lines for Fully Printed, Flexible Electronics,” *ACS Nano*, p. acsnano.7b03795, Jul. 2017.

[8] Y. Zhu, S. Murali, M. D. Stoller, A. Velamakanni, R. D. Piner, and R. S. Ruoff,

Microwave Assisted Exfoliation and Reduction of Graphite Oxide for Ultracapacitors, vol. 48, no. 7. 2010, pp. 2118–2122.

[9] G. Zhou *et al.*, "Graphene-Wrapped Fe3O4 Anode Material with Improved Reversible Capacity and Cyclic Stability for Lithium Ion Batteries," *Chem. Mater.*, vol. 22, no. 18, pp. 5306–5313, Sep. 2010.

[10] Z. Bo *et al.*, "Green Preparation of Reduced Graphene Oxide for Sensing and Energy Storage Applications," *Sci. Rep.*, vol. 4, no. 4684, 2014.

[11] Y. Chen, X. Zhang, D. Zhang, P. Yu, and Y. Ma, "High Performance Supercapacitors Based On Reduced Graphene Oxide in Aqueous and Ionic Liquid Electrolytes," *Carbon N. Y.*, vol. 49, no. 2, pp. 573–580, Feb. 2011.

[12] J. Lee, J. Kim, S. Kim, and D.-H. Min, "Biosensors Based On Graphene Oxide and Its Biomedical Application," *Adv. Drug Deliv. Rev.*, vol. 105, pp. 275–287, Oct. 2016.

[13] Y. P. Tang, D. R. Paul, and T. S. Chung, "Free-Standing Graphene Oxide Thin Films Assembled By a Pressurized Ultrafiltration Method for Dehydration of Ethanol," *J. Memb. Sci.*, vol. 458, pp. 199–208, May 2014.

[14] M. Hu and B. Mi, "Enabling Graphene Oxide Nanosheets as Water Separation Membranes," *Environ. Sci. Technol.*, vol. 47, no. 8, pp. 3715–3723, Apr. 2013.

[15] K. A. Mahmoud, B. Mansoor, A. Mansour, and M. Khraisheh, "Functional Graphene Nanosheets: The Next Generation Membranes for Water Desalination," *Desalination*, vol. 356, pp. 208–225, Jan. 2015.

[16] H. Huang, Y. Ying, and X. Peng, "Graphene Oxide Nanosheet: An Emerging Star Material for Novel Separation Membranes," *J. Mater. Chem. A*, vol. 2, pp. 13772–13782, 2014.

[17] M. Ionita, A. M. Pandele, L. Crica, and L. Pilan, “Improving the Thermal and Mechanical Properties of Polysulfone by Incorporation of Graphene Oxide,” *Compos. Part B Eng.*, vol. 59, pp. 133–139, Mar. 2014.

[18] M. G. Kochameshki, A. Marjani, M. Mahmoudian, and K. Farhadi, “Grafting of Diallyldimethylammonium Chloride on Graphene Oxide by RAFT Polymerization for Modification of Nanocomposite Polysulfone Membranes Using in Water Treatment,” *Chem. Eng. J.*, vol. 309, pp. 206–221, Feb. 2017.

[19] T. Hwang *et al.*, “Ultrafiltration Using Graphene Oxide Surface-Embedded Polysulfone Membranes,” *Sep. Purif. Technol.*, vol. 166, pp. 41–47, Jun. 2016.

[20] B. M. Ganesh, A. M. Isloor, and A. F. Ismail, “Enhanced Hydrophilicity and Salt Rejection Study of Graphene Oxide-Polysulfone Mixed Matrix Membrane,” *Desalination*, vol. 313, pp. 199–207, Mar. 2013.

[21] M. Ionita *et al.*, “Synthesis, Characterization and in vitro Studies of Polysulfone/Graphene Oxide Composite Membranes,” *Compos. Part B Eng.*, vol. 72, pp. 108–115, Apr. 2015.

[22] R. W. Baker, *Membrane Technology and Applications*. Chichester, UK: John Wiley & Sons, Ltd, 2004.

[23] M. Mulder, *Basic Principles of Membrane Technology*. Dordrecht: Springer Netherlands, 1996.

[24] S. Kim, L. Chen, J. K. Johnson, and E. Marand, “Polysulfone and Functionalized Carbon Nanotube Mixed Matrix Membranes for Gas Separation: Theory and Experiment,” *J. Memb. Sci.*, vol. 294, no. 1–2, pp. 147–158, May 2007.

[25] D. Wu, L. Wu, W. Zhou, T. Yang, and M. Zhang, “Study on Physical Properties of Multiwalled Carbon Nanotube/Poly(Phenylene Sulfide) Composites,”

Polym. Eng. Sci., vol. 49, no. 9, pp. 1727–1735, Sep. 2009.

[26] D. R. Dreyer *et al.*, "The Chemistry of Graphene Oxide," *Chem. Soc. Rev.*, vol. 39, no. 1, pp. 228–240, Dec. 2010.

[27] B. C. Brodie, "On the Atomic Weight of Graphite," *R. Soc.*, vol. 149, no. 1859, pp. 249–259, 1859.

[28] L. Staudenmaier, "Verfahren zur Darstellung der Graphitsäure," *Ber. Dtsch. Chem. Ges.*, vol. 31, no. 2, pp. 1481–1487, May 1898.

[29] W. S. Hummers and R. E. Offeman, "Preparation of Graphitic Oxide," *J. Am. Chem. Soc.*, vol. 80, no. 6, pp. 1339–1339, 1958.

[30] D. C. Marcano *et al.*, "Improved Synthesis of Graphene Oxide," *ACS Nano*, vol. 4, no. 8, pp. 4806–4814, 2010.

[31] H. Yu, B. Zhang, C. Bulin, R. Li, and R. Xing, "High-Efficient Synthesis of Graphene Oxide Based on Improved Hummers Method," *Sci. Rep.*, vol. 6, no. 1, p. 36143, 2016.

[32] G. Shao, Y. Lu, F. Wu, C. Yang, F. Zeng, and Q. Wu, "Graphene oxide: The Mechanisms of Oxidation and Exfoliation," *J. Mater. Sci.*, vol. 47, no. 10, pp. 4400–4409, May 2012.

[33] D. W. Boukhvalov, "Oxidation of a Graphite Surface: The Role of Water," *J. Phys. Chem. C*, vol. 118, no. 47, pp. 27594–27598, Nov. 2014.

[34] A. M. Dimiev and J. M. Tour, "Mechanism of Graphene Oxide Formation," *ACS Nano*, vol. 8, no. 3, pp. 3060–3068, Mar. 2014.

[35] Z. U. Khan, A. Kausar, H. Ullah, A. Badshah, and W. U. Khan, "A review of graphene oxide, graphene buckypaper, and polymer/graphene composites:

Properties and fabrication techniques," *J. Plast. Film Sheeting*, vol. 32, no. 4, pp. 336–379, Oct. 2016.

[36] J. H. H. Gao Wei, Matthew P. McDonald, Yurii Morozov and G. W. Kuno, Zhiping Xu and Masaru, *Graphene Oxide: Reduction Recipes, Spectroscopy, and Applications*. Cham: Springer International Publishing, 2015.

[37] H. He, T. Riedl, A. Anton Lerf, and Jacek Klinowski, "Solid-State NMR Studies of the Structure of Graphite Oxide," *J. Phys. Chem.*, vol. 100, no. 51, pp. 19954–19958, 1996.

[38] L. B. Casabianca *et al.*, "NMR-Based Structural Modeling of Graphite Oxide Using Multidimensional 13 C Solid-State NMR and ab Initio Chemical Shift Calculations," *J. Am. Chem. Soc.*, vol. 132, no. 16, pp. 5672–5676, 2010.

[39] U. Sierra, P. Álvarez, R. Santamaría, M. Granda, C. Blanco, and R. Menéndez, "A Multi-Step Exfoliation Approach to Maintain the Lateral Size of Graphene Oxide Sheets," *Carbon N. Y.*, vol. 80, pp. 830–832, Dec. 2014.

[40] I. Ogino, Y. Yokoyama, and S. R. Mukai, "Sonication-Free Exfoliation of Graphite Oxide via Rapid Phase Change of Water," *Top. Catal.*, vol. 58, no. 7–9, pp. 522–528, May 2015.

[41] K. P. Loh, Q. Bao, G. Eda, and M. Chhowalla, "Graphene Oxide as a Chemically Tunable Platform for Optical Applications," *Nat. Chem.*, vol. 2, no. 12, pp. 1015–1024, 2010.

[42] A. M. Dimiev and S. Eigler, *Graphene Oxide: Fundamentals and Applications*. 2017.

[43] A. Kundu, R. K. Layek, A. Kuila, and A. K. Nandi, "Highly Fluorescent Graphene Oxide-Poly(vinyl alcohol) Hybrid: An Effective Material for Specific Au3+ Ion Sensors," *ACS Appl. Mater. Interfaces*, vol. 4, no. 10, pp.

5576–5582, Oct. 2012.

[44] A. Kundu *et al.*, “Enhanced Fluorescent Intensity of Graphene Oxide–Methyl Cellulose Hybrid in Acidic Medium: Sensing of Nitro-Aromatics,” *J. Mater. Chem.*, vol. 22, no. 16, p. 8139, Mar. 2012.

[45] L. Liu, J. Zhang, J. Zhao, and F. Liu, “Mechanical Properties of Graphene Oxides,” *Nanoscale*, vol. 4, no. 19, pp. 5910–5916, 2012.

[46] J. I. Paredes, S. Villar-Rodil, A. Martinez-Alonso, and J. M. D. Tascon, “Graphene Oxide Dispersions in Organic Solvents,” *Langmuir*, vol. 24, no. 19, pp. 10560–10564, Oct. 2008.

[47] J.-J. Shao, W. Lv, Q.-H. Yang, W. L. J.-J. Shao, and and Q.-H. Yang, “Self-Assembly of Graphene Oxide at Interfaces,” *Adv. Mater.*, vol. 26, no. 32, pp. 5586–5612, Aug. 2014.

[48] R. K. Layek and A. K. Nandi, “A Review on Synthesis and Properties of Polymer Functionalized Graphene,” *Polymer (Guildf).*, vol. 54, no. 19, pp. 5087–5103, Aug. 2013.

[49] S. Minko, “Grafting on Solid Surfaces: ‘Grafting to’ and ‘Grafting from’ Methods,” in *Polymer Surfaces and Interfaces*, Berlin, Heidelberg: Springer Berlin Heidelberg, 2008, pp. 215–234.

[50] A. Badri, M. R. Whittaker, and P. B. Zetterlund, “Modification of Graphene Graphene Oxide with Polymer Brushes Using Controlled/Living Radical Polymerization,” *J. Polym. Sci. Part A Polym. Chem.*, vol. 50, no. 15, pp. 2981–2992, Aug. 2012.

[51] M. Kim, S. Schmitt, J. Choi, J. Krutty, and P. Gopalan, “From Self-Assembled Monolayers to Coatings: Advances in the Synthesis and Nanobio Applications of Polymer Brushes,” *Polymers (Basel).*, vol. 7, no. 7, pp. 1346–1378, Jul.

2015.

[52] P. (Prithu) Mukhopadhyay and R. K. (Rakesh K. Gupta, *Graphite, Graphene, and Their Polymer Nanocomposites*, First. CRC Press, 2013.

[53] S. H. Lee *et al.*, “Polymer Brushes via Controlled, Surface-Initiated Atom Transfer Radical Polymerization (ATRP) from Graphene Oxide,” *Macromol. Rapid Commun.*, vol. 31, no. 3, pp. 281–288, Feb. 2010.

[54] M. Mrlík, M. Ilčíková, T. Plachý, V. Pavlínek, Z. Špitalský, and J. Mosnáček, “Graphene Oxide Reduction during Surface-Initiated Atom Transfer Radical Polymerization of Glycidyl Methacrylate: Controlling Electro-Responsive Properties,” *Chem. Eng. J.*, vol. 283, pp. 717–720, Jan. 2016.

[55] N. Rajender and K. I. Suresh, “Surface-Initiated Atom Transfer Radical Polymerization (SI-ATRP) From Graphene Oxide: Effect of Functionalized Graphene Sheet (FGS) on the Synthesis and Material Properties of PMMA Nanocomposites,” *Macromol. Mater. Eng.*, vol. 301, no. 1, pp. 81–92, Jan. 2016.

[56] A. Kumar, B. Behera, G. D. Thakre, and S. S. Ray, “Covalently Grafted Graphene Oxide/Poly(Cn-acrylate) Nanocomposites by Surface-Initiated ATRP: An Efficient Antifriction, Antiwear, and Pour-Point-Depressant Lubricating Additive in Oil Media,” *Ind. Eng. Chem. Res.*, vol. 55, no. 31, pp. 8491–8500, Aug. 2016.

[57] Y. Yang, J. Wang, J. Zhang, J. Liu, X. Yang, and H. Zhao, “Exfoliated Graphite Oxide Decorated by PDMAEMA Chains and Polymer Particles,” *Langmuir*, vol. 25, no. 19, pp. 11808–11814, Oct. 2009.

[58] T. Kavitha, I.-K. Kang, and S.-Y. Park, “Poly(acrylic acid)-Grafted Graphene Oxide as an Intracellular Protein Carrier,” *Langmuir*, vol. 30, no. 1, pp. 402–

409, Jan. 2014.

[59] G. Gonçalves *et al.*, "Graphene Oxide Modified with PMMA via ATRP as a Reinforcement Filler," *J. Mater. Chem.*, vol. 20, no. 44, p. 9927, Nov. 2010.

[60] K. Qi, Y. Sun, H. Duan, and X. Guo, "A Corrosion-Protective Coating Based on a Solution-Processable Polymer-Grafted Graphene Oxide Nanocomposite," *Corros. Sci.*, vol. 98, pp. 500–506, Sep. 2015.

[61] H. Roghani-Mamaqani *et al.*, "Surface-Initiated ATRP of Styrene from Epoxy Groups of Graphene Nanolayers: Twofold Polystyrene Chains and Various Graft Densities," *RSC Adv.*, vol. 5, no. 66, pp. 53357–53368, Jun. 2015.

[62] D. J. Siegwart, J. K. Oh, and K. Matyjaszewski, "ATRP in the Design of Functional Materials for Biomedical Applications," *Prog. Polym. Sci.*, vol. 37, no. 1, pp. 18–37, Jan. 2012.

[63] W. Hadasha and B. Klumperman, "Atom Transfer Radical Polymerization as a Powerful Tool in the Synthesis of Molecular Brushes," *Polym. Int.*, vol. 63, no. 5, pp. 824–834, May 2014.

[64] M. Kato, M. Kamigaito, M. Sawamoto, and T. Higashimura, "Polymerization of Methyl Methacrylate with the Carbon Tetrachloride/Dichlorotris-(triphenylphosphine)ruthenium(II)/Methylaluminum Bis(2,6-di-tert-butylphenoxide) Initiating System: Possibility of Living Radical Polymerization," *Macromolecules*, vol. 28, no. 5, pp. 1721–1723, Sep. 1995.

[65] J.-S. Wang and K. Matyjaszewski, "Controlled/Living Radical Polymerization Atom Transfer Radical Polymerization in the Presence of Transition-Metal Complexes," *J. Am. Chem. Soc.*, vol. 117, no. 20, pp. 5614–5615, May 1995.

[66] P. Król and P. Chmielarz, "Recent Advances in ATRP Methods in Relation to the Synthesis of Copolymer Coating Materials," *Prog. Org. Coatings*, vol. 77,

no. 5, pp. 913–948, May 2014.

[67] K. Matyjaszewski, “Atom Transfer Radical Polymerization (ATRP): Current Status and Future Perspectives,” *Macromolecules*, vol. 45, no. 10, pp. 4015–4039, May 2012.

[68] H. W. Yoon, Y. H. Cho, and H. B. Park, “Graphene-Based Membranes: Status and Prospects,” *Philos. Trans. R. Soc. London A Math. Phys. Eng. Sci.*, vol. 374, no. 2060, 2015.

[69] A. Lee *et al.*, “Membrane materials for water purification: design, development, and application,” *Environ. Sci. Water Res. Technol.*, vol. 2, no. 1, pp. 17–42, Jan. 2016.

[70] R. K. Joshi *et al.*, “Precise and Ultrafast Molecular Sieving Through Graphene Oxide Membranes,” *Science (80-.).*, vol. 343, no. 6172, pp. 752–754, Jan. 2014.

[71] D. A. Dikin *et al.*, “Preparation and Characterization of Graphene Oxide Paper,” *Nature*, vol. 448, no. 7152, pp. 457–460, Jul. 2007.

[72] C. Chen *et al.*, “Self-Assembled Free-Standing Graphite Oxide Membrane,” *Adv. Mater.*, vol. 21, no. 29, pp. 3007–3011, Aug. 2009.

[73] H. M. Hegab and L. Zou, “Graphene Oxide-Assisted Membranes: Fabrication and Potential Applications in Desalination and Water Purification,” *J. Memb. Sci.*, vol. 484, pp. 95–106, Jun. 2015.

[74] W.-S. Hung *et al.*, “Pressure-Assisted Self-Assembly Technique for Fabricating Composite Membranes Consisting Of Highly Ordered Selective Laminate Layers of Amphiphilic Graphene Oxide,” *Carbon N. Y.*, vol. 68, pp. 670–677, Mar. 2014.

[75] J. Liu *et al.*, “Covalently Functionalized Graphene Oxide and Quaternized Polysulfone Nanocomposite Membranes for Fuel Cells,” *RSC Adv.*, vol. 6, no. 75, pp. 71305–71310, Jul. 2016.

[76] O. Movil, L. Frank, and J. A. Staser, “Graphene Oxide-Polymer Nanocomposite Anion-Exchange Membranes,” *J. Electrochem. Soc.*, vol. 162, no. 4, pp. F419–F426, Jan. 2015.

[77] W. Choi, J. Choi, J. Bang, and J.-H. Lee, “Layer-by-Layer Assembly of Graphene Oxide Nanosheets on Polyamide Membranes for Durable Reverse-Osmosis Applications,” *ACS Appl. Mater. Interfaces*, vol. 5, pp. 12510–12519, 2013.

[78] H. Zhao *et al.*, “Improving the Antifouling Property of Polysulfone Ultrafiltration Membrane by Incorporation of Isocyanate-treated Graphene Oxide,” *Phys. Chem. Chem. Phys.*, vol. 15, no. 23, p. 9084, May 2013.

[79] Y. Mansourpanah, H. Shahebrahimi, and E. Kolvari, “PEG-modified GO Nanosheets, a Desired Additive to Increase the Rejection and Antifouling Characteristics of Polyamide Thin Layer Membranes,” *Chem. Eng. Res. Des.*, vol. 104, pp. 530–540, Dec. 2015.

[80] H. Wang, X. Lu, X. Lu, Z. Wang, J. Ma, and P. Wang, “Improved Surface Hydrophilicity and Antifouling Property of Polysulfone Ultrafiltration Membrane with Poly(ethylene glycol) Methyl Ether Methacrylate Grafted Graphene Oxide Nanofillers,” *Appl. Surf. Sci.*, vol. 425, pp. 603–613, Dec. 2017.

[81] M. Bikel, P. Z. Çulfaz, L. A. M. Bolhuis-Versteeg, J. G. Pérez, R. G. H. Lammertink, and M. Wessling, “Polymeric Microsieves via Phase Separation Micro Fabrication: Process and Design Optimization,” *J. Memb. Sci.*, vol. 347, no. 1–2, pp. 93–100, Feb. 2010.

[82] S. Kuiper, C. J. . van Rijn, W. Nijdam, and M. . Elwenspoek, “Development and Applications of Very High Flux Microfiltration Membranes,” *J. Memb. Sci.*, vol. 150, no. 1, pp. 1–8, Nov. 1998.

[83] Rayleigh and A. John, “Breath Figures,” *Nature*, vol. 86, no. 2172, pp. 516–517, 1911.

[84] A. Zhang, H. Bai, and L. Li, “Breath Figure: A Nature-Inspired Preparation Method for Ordered Porous Films,” *Chem. Rev.*, vol. 115, no. 18, pp. 9801–9868, Sep. 2015.

[85] G. Widawski, M. Rawiso, and B. François, “Self-Organized Honeycomb Morphology of Star-Polymer Polystyrene Films,” *Nature*, vol. 369, no. 6479, pp. 387–389, Jun. 1994.

[86] D. Wu, F. Xu, B. Sun, R. Fu, H. He, and K. Matyjaszewski, “Design and Preparation of Porous Polymers,” *Chem. Rev.*, vol. 112, no. 7, pp. 3959–4015, Jul. 2012.

[87] L.-S. Wan, L.-W. Zhu, Y. Ou, and Z.-K. Xu, “Multiple Interfaces in Self-assembled Breath Figures,” *Chem. Commun.*, vol. 50, no. 31, pp. 4024–4039, Mar. 2014.

[88] H. Bai, C. Du, A. Zhang, and L. Li, “Breath Figure Arrays: Unconventional Fabrications, Functionalizations, and Applications,” *Angew. Chemie Int. Ed.*, vol. 52, no. 47, pp. 12240–12255, Nov. 2013.

[89] Q. Liu *et al.*, “Design, Preparation, and Application of Ordered Porous Polymer Materials,” *Mater. Chem. Phys.*, vol. 144, no. 3, pp. 213–225, Apr. 2014.

[90] Y. Dou, M. Jin, G. Zhou, and L. Shui, “Breath Figure Method for Construction of Honeycomb Films,” *Membranes (Basel).*, vol. 5, no. 3, pp. 399–424, Aug. 2015.

[91] L. Heng, B. Wang, M. Li, Y. Zhang, and L. Jiang, “Advances in Fabrication Materials of Honeycomb Structure Films by the Breath-Figure Method,” *Materials (Basel).*, vol. 6, no. 2, pp. 460–482, Feb. 2013.

[92] M. Hernández-Guerrero *et al.*, “Honeycomb Structured Polymer Films via Breath Figures,” *Polym. Chem.*, vol. 3, no. 3, pp. 563–577, Feb. 2012.

[93] U. H. F. Bunz, “Breath Figures as a Dynamic Templating Method for Polymers and Nanomaterials,” *Adv. Mater.*, vol. 18, no. 8, pp. 973–989, Apr. 2006.

[94] B. K. Tripathi and P. Pandey, “Breath Figure Templating for Fabrication of Polysulfone Microporous Membranes with Highly Ordered Monodispersed Porosity,” *J. Memb. Sci.*, vol. 471, pp. 201–210, Dec. 2014.

[95] Y. Xu, B. Zhu, and Y. Xu, “A Study on Formation of Regular Honeycomb Pattern in Polysulfone Film,” *Polymer (Guildf).*, vol. 46, no. 3, pp. 713–717, Jan. 2005.

[96] Y. Lu *et al.*, “Fabrication of Conducting Polyaniline Composite Film Using Honeycomb Ordered Sulfonated Polysulfone Film as Template,” *Thin Solid Films*, vol. 516, no. 18, pp. 6365–6370, Jul. 2008.

[97] Y. Yun, W. Xiang, L. Wang, and Y. Hua, “Formation of Honeycomb Structure Films from Polysulfone in a Highly Humid Atmosphere,” *Desalin. Water Treat.*, vol. 34, no. 1–3, pp. 136–140, Oct. 2011.

[98] J. Mansouri, E. Yapit, and V. Chen, “Polysulfone Filtration Membranes with Isoporous Structures Prepared By a Combination of Dip-Coating and Breath Figure Approach,” *J. Memb. Sci.*, vol. 444, pp. 237–251, Oct. 2013.

[99] E. Bormashenko, S. Balter, A. Malkin, and D. Aurbach, “Polysulfone Membranes Demonstrating Asymmetric Diode-like Water Permeability and Their Applications,” *Macromol. Mater. Eng.*, vol. 299, no. 1, pp. 27–30, Jan.

2014.

[100] P. Dell'Aversana, V. Tontodonato, and L. Carotenuto, "Suppression of Coalescence and of Wetting: The Shape of the Interstitial Film," *Phys. Fluids*, vol. 9, no. 9, p. 2475−2485, Jun. 1997.

[101] P. Dell'Aversana, J. R. Banavar, and J. Koplik, "Suppression of Coalescence by Shear and Temperature Gradients," *Phys. Fluids*, vol. 8, p. 15−28, Sep. 1996.

[102] E. Servoli, G. A. Ruffo, and C. Migliaresi, "Interplay of Kinetics and Interfacial Interactions in Breath Figure Templating – A Phenomenological Interpretation," *Polymer (Guildf).*, vol. 51, no. 11, pp. 2337–2344, May 2010.

[103] J. Peng, Y. Han, J. Fu, Y. Yang, and B. Li, "Formation of Regular Hole Pattern in Polymer Films," *Macromol. Chem. Phys.*, vol. 204, no. 1, pp. 125–130, Jan. 2003.

[104] C. Wang *et al.*, "Fabrication of Highly Ordered Microporous Thin Films by PS-b-PAA Self-assembly and Investigation of Their Tunable Surface Properties," *J. Mater. Chem.*, vol. 18, no. 6, p. 683, Jan. 2008.

[105] † Danelle Beattie *et al.*, "Honeycomb-Structured Porous Films from Polypyrrole-Containing Block Copolymers Prepared via RAFT Polymerization as a Scaffold for Cell Growth," *Biomacromolecules*, vol. 7, no. 4, pp. 1072–1082, 2007.

[106] A. Bolognesi, A. C. Mercogliano, S. Yunus, M. Civardi, A. D. Comoretto, and A. Turturro, "Self-Organization of Polystyrenes into Ordered Microstructured Films and Their Replication by Soft Lithography," *Langmuir*, vol. 21, no. 8, pp. 3480–3485, 2005.

[107] L. Ghannam *et al.*, "A Versatile Route to Functional Biomimetic

Coatings:Ionomers for Honeycomb-Like Structures," *Soft Matter*, vol. 3, no. 12, p. 1492, Nov. 2007.

[108] K. Majewska-Nowak, "Synthesis and Properties of Polysulfone Membranes," *Desalination*, vol. 71, no. 2, pp. 83–95, Jan. 1989.

[109] H.-L. Huang and S. Yang, "Filtration Characteristics of Polysulfone Membrane Filters," *J. Aerosol Sci.*, vol. 37, no. 10, pp. 1198–1208, Oct. 2006.

[110] X. Jiang, J. Gu, Y. Shen, S. Wang, and X. Tian, "Formation of Honeycomb-Patterned Microporous Films Based on a Fluorinated Poly(Siloxane Imide) Segmented Copolymer," *J. Appl. Polym. Sci.*, vol. 119, no. 6, pp. 3329–3337, Mar. 2011.

[111] Y. Liu, L. Wang, and X. Han, "Self-Assembly Fabrication of Ordered Microporous Films from a Soluble Polyimide Modified By Methyl Groups Based On Breath Figures," *Desalin. Water Treat.*, vol. 51, no. 25–27, pp. 5107–5112, Jul. 2013.

[112] Z. Wang, W. Cheng, J. Ma, and P. Wang, "Condensed Solute Droplets Templated Honeycomb Pattern on Polymer Films," *J. Colloid Interface Sci.*, vol. 436, pp. 16–18, Dec. 2014.

[113] X. Xu *et al.*, "Multiscale Bio-Inspired Honeycomb Structure Material with High Mechanical Strength and Low Density," *J. Mater. Chem.*, vol. 22, no. 21, p. 10883, May 2012.

[114] Y. Liu, H. Ma, Y. Tian, F. Xie, and X. Wang, "Fabrication of Durable Honeycomb-Patterned Films of Poly(ether sulfone)s via Breath Figures," *Macromol. Chem. Phys.*, vol. 215, no. 15, pp. 1446–1455, Aug. 2014.

[115] H. Cong *et al.*, "Preparation of a Highly Permeable Ordered Porous Microfiltration Membrane of Brominated Poly(Phenylene Oxide) on an Ice

Substrate by the Breath Figure Method," *Soft Matter*, vol. 8, no. 34, p. 8835, Aug. 2012.

[116] L.-S. Wan, J.-W. Li, B.-B. Ke, and Z.-K. Xu, "Ordered Microporous Membranes Templated by Breath Figures for Size-Selective Separation," *J. Am. Chem. Soc.*, vol. 134, no. 1, pp. 95–98, Jan. 2012.

[117] C. Du, A. Zhang, H. Bai, and L. Li, "Robust Microsieves with Excellent Solvent Resistance: Cross-Linkage of Perforated Polymer Films with Honeycomb Structure," *ACS Macro Lett.*, vol. 2, no. 1, pp. 27–30, Jan. 2013.

[118] L.-W. Wu, L.-S. Wan, Y. Ou, L.-W. Zhu, and Z.-K. Xu, "Fabrication of Transferable Perforated Isoporous Membranes on Versatile Solid Substrates via the Breath Figure Method," *Adv. Mater. Interfaces*, vol. 2, no. 16, p. 1500285, Nov. 2015.

[119] Claudia Greiser, A. Susann Ebert, and W. A. Goedel*, "Using Breath Figure Patterns on Structured Substrates for the Preparation of Hierarchically Structured Microsieves," *Langmuir*, vol. 24, no. 3, pp. 617–620, 2008.

[120] Y. Ou, C.-J. Lv, W. Yu, Z.-W. Mao, L.-S. Wan, and Z.-K. Xu, "Fabrication of Perforated Isoporous Membranes via a Transfer-Free Strategy: Enabling High-Resolution Separation of Cells," *ACS Appl. Mater. Interfaces*, vol. 6, no. 24, pp. 22400–22407, Dec. 2014.

[121] Z. Tang, L. Zhang, C. Zeng, T. Lin, and B. Guo, "General Route to Graphene with Liquid-like Behavior by Non-covalent Modification," *Soft Matter*, vol. 8, no. 35, p. 9214, Aug. 2012.

[122] P. F. Li, Y. Xu, and X.-H. Cheng, "Chemisorption of Thermal Reduced Graphene Oxide Nano-Layer Film on TNTZ Surface and Its Tribological Behavior," *Surf. Coatings Technol.*, vol. 232, pp. 331–339, Oct. 2013.

[123] J. Ou *et al.*, “Tribology Study of Reduced Graphene Oxide Sheets on Silicon Substrate Synthesized via Covalent Assembly,” *Langmuir*, vol. 26, no. 20, pp. 15830–15836, Oct. 2010.

[124] D. Yang *et al.*, “Chemical Analysis of Graphene Oxide Films after Heat and Chemical Treatments by X-Ray Photoelectron and Micro-Raman Spectroscopy,” *Carbon N. Y.*, vol. 47, no. 1, pp. 145–152, Jan. 2009.

[125] S. Stankovich *et al.*, “Stable Aqueous Dispersions of Graphitic Nanoplatelets via The Reduction of Exfoliated Graphite Oxide in the Presence of Poly(Sodium 4-Styrenesulfonate),” *J. Mater. Chem.*, vol. 16, no. 2, pp. 155–158, Dec. 2006.

[126] P. Ramesh, S. Bhagyalakshmi, and S. Sampath, “Preparation and Physicochemical and Electrochemical Characterization of Exfoliated Graphite Oxide,” *J. Colloid Interface Sci.*, vol. 274, no. 1, pp. 95–102, Jun. 2004.

[127] G. Zhang, S. Sun, D. Yang, J.-P. Dodelet, and E. Sacher, “The Surface Analytical Characterization of Carbon Fibers Functionalized By H2SO4/HNO3 Treatment,” *Carbon N. Y.*, vol. 46, no. 2, pp. 196–205, Feb. 2008.

[128] N. Morimoto, T. Kubo, and Y. Nishina, “Tailoring the Oxygen Content of Graphite and Reduced Graphene Oxide for Specific Applications,” *Nat. Publ. Gr.*, 2016.

[129] Y. Liu, V. Klep, B. Zdyrko, and I. Luzinov, “Polymer Grafting via ATRP Initiated from Macroinitiator Synthesized on Surface,” *Langmuir*, vol. 20, pp. 6710–6718, 2004.

APPENDIX A

Raw Data for Water Permeation and Yeast Filtration Tests

Pure water permeation test results were tabulated in Table A-1 and Table A-3 while yeast filtration results were tabulated in Table A-3 and Table A-4 for Membrane-C and Membrane-D, respectively.

Table A-1 Pure water permeation test results for 3 different Membrane-C

Transmembrane pressure (bar)	Permeate volume (ml)	Elapsed time (s)
0.01	4.4	110
0.01	2.2	68
0.01	2.0	90

Table A-2 Yeast filtration test results for 3 different Membrane-C

Transmembrane pressure (bar)	Permeate volume (ml)	Elapsed time (s)
1.25	1.5	278
1.0	2.6	60
1.5	2.1	43

Table A-3 Pure water permeation test results for 3 different Membrane-D

Transmembrane pressure (bar)	Permeate volume (ml)	Elapsed time (s)
0.69	2.9	60
1.5	2.2	60
1.3	1.5	120

Table A-4 Yeast filtration test results for 3 different Membrane -D

Transmembrane pressure (bar)	Permeate volume (ml)	Elapsed time (s)
1.6	1.0	817
1.7	0.9	1200
1.7	1.0	2364

Figure A-1 shows the calibration curve for yeast solution at 600 nm. Measurements were done in between 0.2 and 0.8 absorbance values. Interferences may occur due to dilution or concentration issues at out of the given absorbance range.

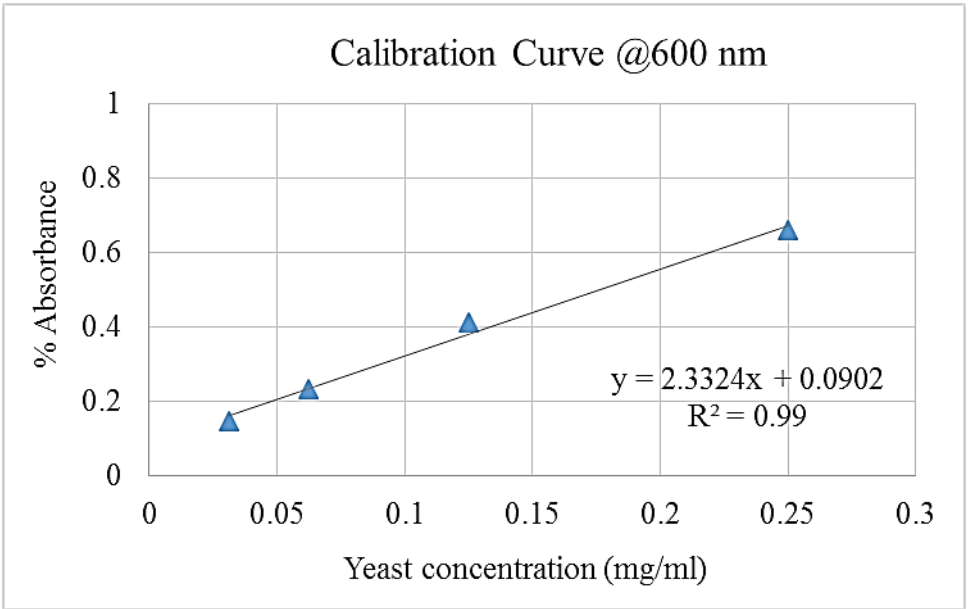

Figure A-1 Calibration curve showing yeast concentration vs. absorbance for yeast filtration studies

Table A-5 shows UV absorbance values for collected permeate solutions for Membrane-C and Membrane-D. With the help of Figure A-1, corresponding concentrations can be calculated at measured absorbance value.

Table A-5 Measured absorbance values for collected permeate (Yeast concentration of the feed solution= 0.24 mg/ml).

		Permeate Absorbance			
	Feed Absorbance	#1	#2	#3	#4
Membrane-C	0.65	0.544	0.573	0.538	0.518
Membrane-D	0.65	0.114	0.156	0.190	0.164

APPENDIX B

TGA Thermograms for GO, GO-Br and GO-poly(PEGMA))

The raw data that were collected from TGA software are given in Figure B-1, Figure B-2 and Figure B-3 for GO, GO-Br and GO-poly(PEGMA).

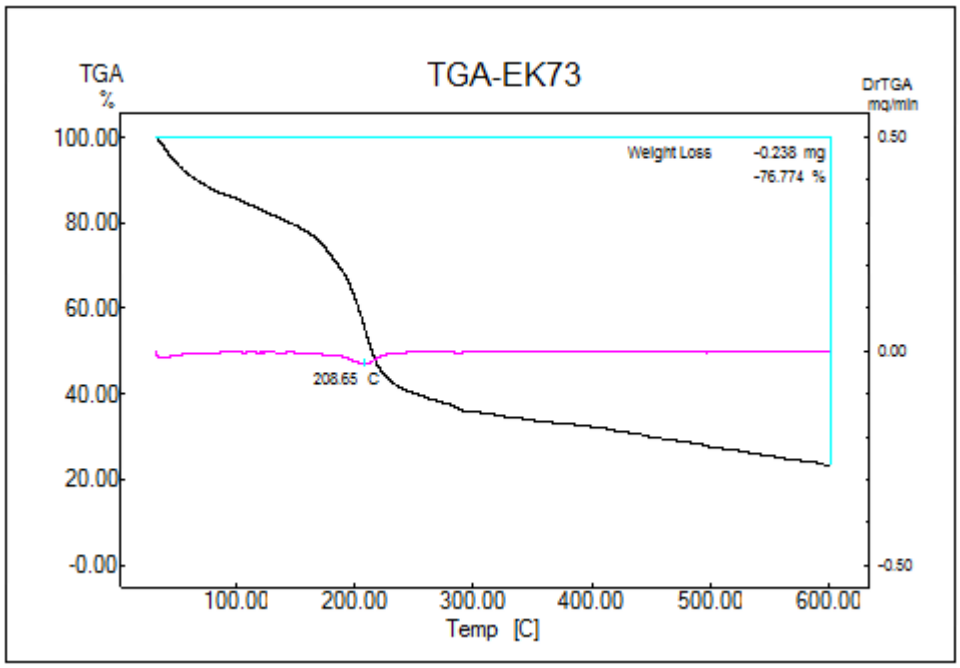

Figure B- 1 TGA Thermogram of GO

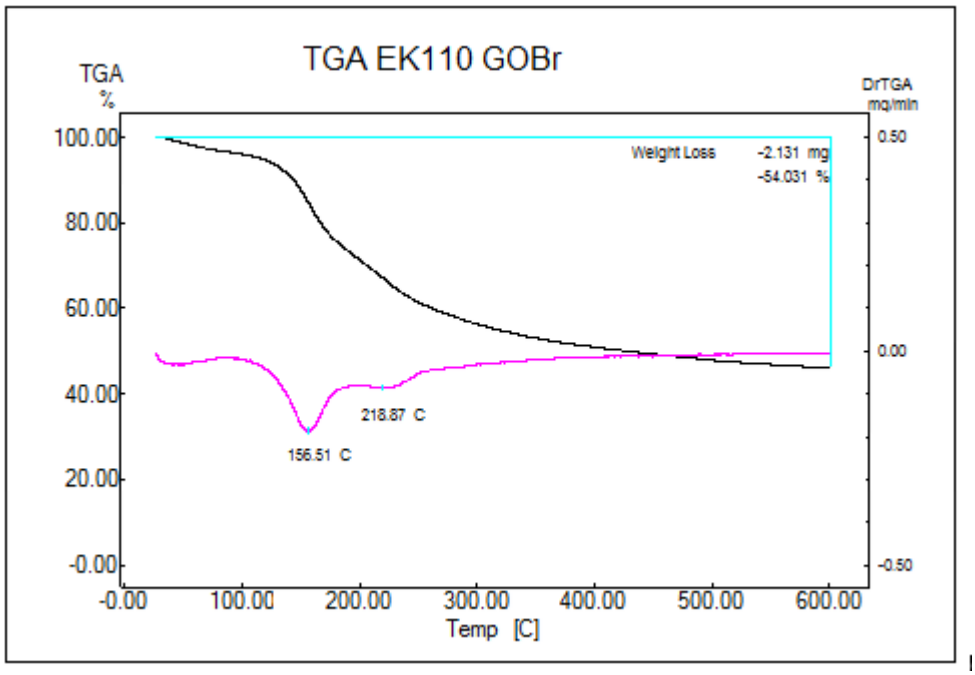

Figure B- 2 TGA Thermogram of GO-Br

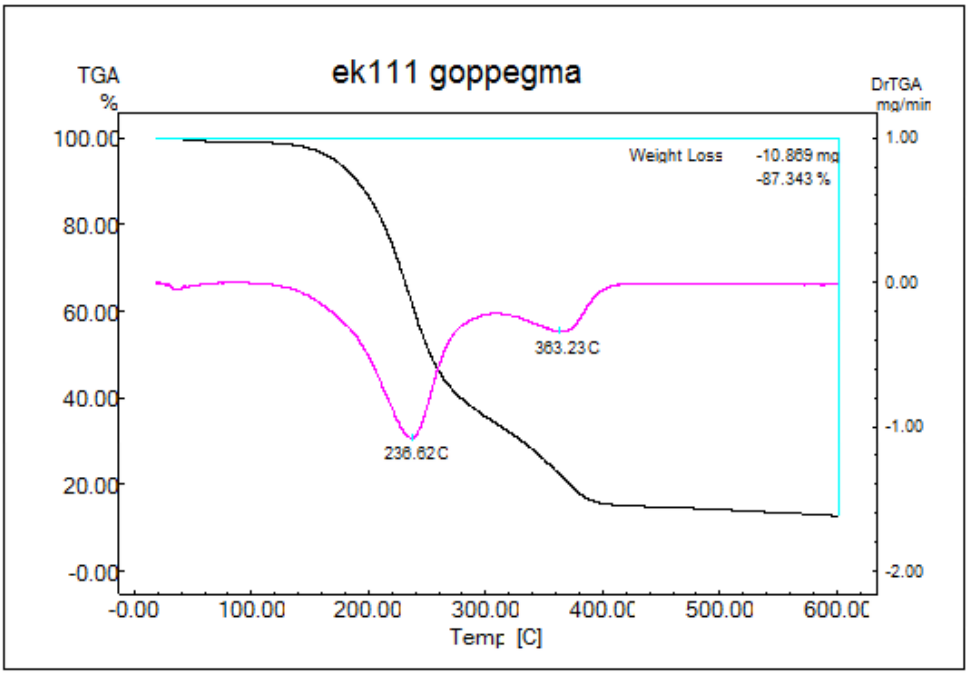

Figure B- 3 TGA Thermogram of GO-poly(PEGMA)